



DISSERTATION

First-principles simulations of tribologically relevant nanoscopic interfaces

Ausgeführt zum Zwecke der Erlangung des akademischen Grades eines Doktors der
technischen Wissenschaften unter der Leitung von

Ao.Univ.Prof. Univ.Prof. Dipl.-Ing. Dr.techn. Peter Mohn

und

Ao.Univ. Prof. Dipl.-Ing. Dr.techn. Josef Redinger

und

Privatdoz. Dr.rer.nat. András Vernes

E 134

Institut für Angewandte Physik

eingereicht an der Technischen Universität Wien

Fakultät für Physik

von

DI Gregor Feldbauer

0426070

Obere Weißgerberstraße 11/1/21, 1030 Wien

Wien, am 01. April 2015

Kurzfassung

In vielen modernen Anwendungen sind Grenzflächen auf atomarer Ebene von entscheidender Bedeutung. Prominente Beispiele hierfür reichen von experimentellen Methoden wie dem Rasterkraftmikroskop, über die Effizienz von Zusatzstoffen in Biotreibstoffen bis zu dem Einsatz von Nanotechnologien. Die detaillierte Untersuchung von Grenzflächen auf atomarer Ebene verspricht ein besseres Verständnis von nanotribologischen Vorgängen wie beispielsweise Nano-Verschleiß oder Schmierung. Aufgrund ihrer komplexen Natur ist das Ausmaß des Verständnisses für diese Prozesse noch immer unbefriedigend.

Das Ziel dieser Arbeit ist es zwei Grenzflächenphänomene, die sowohl in der Grundlagenforschung als auch in der praktischen Anwendung von großer Bedeutung sind, einer eingehenden Analyse zu unterziehen. Erstens wurde der Kontakt zwischen zwei glatten Oberflächen untersucht und zweitens die Adsorption von organischen Molekülen auf reinen und wasserbedeckten Eisenoberflächen überprüft. Die dazu erforderlichen Studien wurden mithilfe von ab initio Berechnungen im Rahmen der Dichtefunktionaltheorie durchgeführt.

Im ersten Themenblock wurden die Annäherung, der Kontakt und die anschließende Trennung zweier Oberflächen, die aus verschiedenen Materialien bestehen, behandelt. Die Metall-Keramik Grenzfläche zwischen Aluminium (Al) und Titanitrid (TiN) wurde als Modellsystem gewählt, weil diese eine Wechselwirkung zwischen weichen und harten Materialien aufweist. Um die Annäherung und Trennung der Materialien zu modellieren wurde einer der Partner in diskreten Schritten normal zu der Grenzfläche bewegt. Dabei wurde das System nach jedem Schritt elektronisch und atomar relaxiert. Um verschiedenste Konfigurationen untersuchen zu können, wurden unterschiedliche relative Anordnungen der Oberflächen zueinander für jede der drei untersuchten Oberflächenorientierung, (001), (011) und (111), gebildet. Darüber hinaus wurden der Aufbau des Modellsystems und die Einstellungen der Simulationen genau getestet. So wurden beispielsweise die Größe der betrachteten Systeme variiert und verschiedene Näherungen für das Austausch-Korrelations-Funktional untersucht. Die Verwendung verschiedener Konfigurationen, sowohl des

Modells als auch der Simulationsdetails, erlaubt die genaue Bestimmung der Einflüsse dieser Aspekte auf die Kontakteigenschaften der Oberflächen wie zum Beispiel der Adhäsionsenergie, des Gleichgewichtsabstands und eines möglichen Materialtransfers zwischen den Oberflächen. Es zeigte sich, dass diese Eigenschaften aufgrund unterschiedlicher Bindungsverhältnisse empfindlich von der geometrischen Konfiguration abhängen. Die Bindungen wurden mithilfe von Ladungs- und Zustandsdichten detailliert analysiert. Im Speziellen wurde Materialtransfer beobachtet, wenn der Absolutbetrag der Adhäsionsenergie bei einer gegebenen Konfiguration größer ist als der Aufwand atomare Schichten von einem Material zu entfernen. Dabei wurde auch festgestellt, dass dieser Aufwand um Material zu entfernen von der mechanischen Belastung abhängt. Außerdem wurde gezeigt, dass der einfache Vergleich zwischen den Oberflächenenergien der beteiligten Materialien nicht ausreicht um das Auftreten von Materialtransfer vorherzusagen. Die Überprüfung der Simulationsdetails zeigte, dass Gleichgewichtseigenschaften, zum Beispiel Adhäsionsenergie und Abstand der Oberflächen, zu einem kleinen Teil davon abhängen, aber das Auftreten und das Ausmaß des Materialtransfers unabhängig davon sind. Des Weiteren wurde der Einfluss von Sauerstoff auf das Verhalten an der Grenzfläche untersucht und gezeigt, dass dieses empfindlich von der Anordnung der Sauerstoffatome abhängt.

Der zweite Schwerpunkt dieser Arbeit beschäftigt sich mit der Adsorption der organischen Moleküle Ethanol und Isooktan (2,2,4-Trimethylpentan) auf Eisenoberflächen. Im Speziellen wurde die bcc Fe(100) Oberfläche untersucht. Zuerst wurde die Bedeutung der van der Waals (vdW) Wechselwirkungen erforscht, indem standard Dichtefunktionale mit erweiterten Funktionalen, die vdW Kräfte teilweise berücksichtigen, verglichen wurden. Im Detail wurde der Einfluss der verschiedenen Funktionalen auf Eigenschaften wie die Adsorptionsenergie, die Gleichgewichtsstruktur, Ladungsverteilung und die Bindungsmechanismen analysiert. Es zeigte sich, dass aufgrund der vdW Wechselwirkung die Adsorptionsenergien zu- und gleichzeitig die Gleichgewichtsabstände abnehmen. Diese Effekte sind stärker ausgeprägt für Isooktan als für Ethanol. Allerdings wird die räumliche Anordnung der Moleküle relativ zur Oberfläche, abgesehen vom Abstand, nicht signifikant verändert. In der Ladungsverteilung bewirken die vdW Kräfte eine nicht isotrope, delokalisierte Ansammlung von Ladung zwischen den Molekülen und der Oberfläche. Während

Isooktan beinahe ausschließlich über vdW Wechselwirkungen an die Eisenoberfläche bindet, spielt bei Ethanol auch eine schwache elektrostatische Anziehung zwischen der Hydroxygruppe und dem Eisen eine Rolle. VdW Wechselwirkungen sollten daher bei der Adsorption dieser Moleküle auf Eisen berücksichtigt werden. Auf diese ersten Ergebnisse aufbauend wurde eine die Eisenoberfläche bedeckende Wasserschicht analysiert. Im ersten Schritt wurde die Anordnung des Wassers auf der Oberfläche überprüft und anschließend der Einfluss der Wasserschicht auf den Adsorptionsprozess analysiert. Im Falle der untersuchten Moleküle zeigte die Wasserschicht eine abschirmende Wirkung, welche die Adsorptionsenergien verringert. Dieser Effekt scheint verstärkt bei Molekülen aufzutreten, die über eine polare funktionelle Gruppe verfügen, wie beispielsweise Ethanol. Im Falle von Ethanol ändert sich auch die geometrische Gleichgewichtsanordnung, während die Ausrichtung von Isooktan nur leicht beeinflusst wird. Daher scheint die Auswirkung der Wasserschicht auf Adsorptionsprozesse stark von der Bindung zwischen dem jeweiligen Molekül und der Oberfläche abzuhängen.

Abstract

Interfaces at the atomic length scale are crucial in many modern applications, from experimental techniques such as atomic force microscopy (AFM), via the efficiency of additives in biofuels to nanotechnologies applied, for example, in nanoelectromechanical-systems (NEMS). Furthermore, detailed insights into such interfaces are of fundamental interest for better understanding of tribological processes, like nanoscale wear and lubrication, for which there is still a lack of knowledge due to their highly complex nature. In this thesis two interfacial phenomena of high fundamental and technological interest are investigated in detail. First, the contact and interfacial properties between atomically flat surfaces and secondly, the adsorption of organic molecules on pristine and water-covered iron surface are discussed. To study these processes *ab initio* calculations were performed within the framework of density functional theory (DFT).

At first, the approach, contact and subsequent separation of two atomically flat surfaces consisting of different materials were investigated by performing DFT simulations. Aluminium (Al) and titanium nitride (TiN) slabs were chosen as a model system representing a metal-ceramic interface and the interaction between soft and hard materials. The approach and separation were simulated by moving one slab in discrete steps normal to the surfaces allowing for electronic and atomic relaxations after each step. Various configurations were analyzed by considering (001), (011) and (111) surface orientations as well as numerous lateral arrangements of these surfaces at the interface. Several tests were done, for example, by changing the system size or using different approximations for the exchange correlation functional. The atomistic simulations revealed the influences of all these factors on adhesion, equilibrium distance and material transfer and showed these to depend sensitively on the chosen configuration due to distinct bonding situations. Bonding between the slabs was investigated in detail by examining its effect on charge densities and densities of state. Material transfer, in particular, was observed if the absolute value of the adhesion energy for a given configuration is larger than the energy cost to remove surface layers. The removal energy for Al layers was found to depend on

tensile or compressive strain. Furthermore, it was shown that a simple comparison of the surface energies of the slabs is not sufficient to predict the occurrence of material transfer. Assessing the computational setup it was shown that properties such as the removal and adhesion energies depend on these settings to some degree, while the material transfer is not affected. Furthermore, the effect of oxygen at the interface was investigated, demonstrating the importance of the particular arrangement of oxygen atoms at the interface.

Secondly, the adsorption of the organic molecules ethanol and isooctane (2,2,4-trimethylpentane) on a bcc Fe(100) surface was studied. The importance of van der Waals (vdW) interactions in such systems was examined by comparing density functionals with and without vdW contributions. In particular, the impact of these functionals on the adsorption energies, equilibrium configurations, electronic charge distributions and the binding mechanism is discussed. According to the calculations, vdW interactions enhance the adsorption energies and decrease the equilibrium distances. In particular, these effects are more pronounced for isooctane than for ethanol. Nevertheless, vdW forces do not influence the spatial configurations of the adsorbed molecules, but effect the electronic densities via a non-isotropic, delocalized accumulation of charge between a selected molecule and the slab. Isooctane binds to the Fe(100) surface via dispersion forces primarily while for ethanol, in addition to the dispersion forces, a weak electrostatic interaction between the hydroxyl group and the iron surface also contributes to the bonding. Consequently, vdW forces are essential for the adsorption of the considered molecules on a bcc Fe(100) surface. Furthermore, a water mono-layer covering the iron surface was investigated with respect to its configuration on the iron slab as well as its influence on the adsorption of the considered organic molecules. For the studied molecules, where dispersion forces contribute significantly to the binding mechanism, the water layer has a strong screening effect. Thus, with the introduction of a water layer, the adsorption energy of isooctane and ethanol was reduced. This effect can be increased by the presence of polar functional groups such as in the ethanol molecule. The adsorption configuration of ethanol was changed, while for isooctane it was altered only very slightly. Thus, the effect of a water layer in the adsorption of organic molecules on an Fe(100) surface strongly depends on the type of bond.

Contents

1	Introduction	1
2	Tribology in a Nutshell	4
2.1	A brief History	4
2.2	Emerging Branches	13
2.2.1	Biotribology	13
2.2.2	Green tribology	14
2.2.3	Nanotribology	16
3	Theoretical Background and Computational Methods	21
3.1	Some Basics of Solid State Physics	21
3.2	Density Functional Theory (DFT)	24
3.3	Exchange-Correlation Functional	27
3.4	Van der Waals interactions	29
3.5	Numerical Implementations	32
4	Adhesion and material transfer between contacting surfaces	34
4.1	Interface: Aluminium - Titanium nitride	34
4.1.1	Introduction and Motivation	34
4.1.2	Computational Details	35
4.1.3	Results and Discussion	41
4.1.4	Conclusion and Outlook	63
4.2	Effect of oxygen on an Al - TiN interface	65

CONTENTS

4.2.1	Introduction	65
4.2.2	Computational Details	65
4.2.3	Results and Discussion	65
4.2.4	Conclusion	69
5	Adsorption of Organic Molecules on Iron Surfaces	73
5.1	Introduction and Motivation	73
5.2	Computational Details	76
5.3	Results and Discussion	79
5.3.1	Organic Molecules on a bare Fe(100) surface	80
5.3.2	Water mono-layer on Fe(100)	89
5.3.3	Organic Molecules on a water-covered Fe(100) surface	91
5.4	Conclusion	96
	List of Abbreviations	100
	Bibliography	102
	Acknowledgements	141
	Curriculum Vitae	143

Chapter 1

Introduction

Tribology is roughly spoken the science of friction, wear and lubrication. We encounter and have to deal with such phenomena on a daily basis. Sometimes their occurrence is wanted and beneficial or even crucial, but often problematic, unwanted or even harmful. Without friction we would not be able to walk on the earth or stop a moving car, however, friction also causes enormous energy losses, e.g., in engines. Wear enables us to write with a pencil, but also causes car tyres and shoes to loose their profiles or inflicts health issues when, e.g., a hip joint is severely affected. In general, wear often limits the life time of many industrial products as well as biological systems and thus is of great importance in engineering but also in economics as well as in health care. Lubrication is therefore commonly used to minimize the effects of friction and wear. On the other hand, lubrication can also turn into a problem, if for example we slip on a wet or icy spot or the braking distance of a car is drastically increased due to such slippery conditions. The usage of lubricants further raises ecological issues, since the commonly liquid substances are often released into the environment, where particularly water pollution is a risk. Moreover, the various additives contained in lubricants can be toxic to the fauna and flora. These few examples already show the wide range of topics tribology has to deal with. Due to the complexity of these issues there are, however, still many open questions, especially on a fundamental level. In particular, the nanoscale, where macroscopic models and laws often can not be readily applied, poses numerous challenges. Processes on the nanoscale

are of great importance because they allow to study fundamental questions from contributions to the frictional behaviour to the real size of a contact. Moreover, due to the ongoing miniaturization in many fields of modern technology, nanotribological aspects are receiving increasing attention. In particular, they often constitute a major limitation of the performance, reliability and life time, for example, of data storage devices or nanoelectromechanical systems (NEMS).

In this thesis tribologically relevant issues are investigated on the nanoscale using atomistic computer simulations. In the beginning, brief introductions to the field of tribology and the theoretical background are given. Next, contacts between flat surfaces of different materials are examined. In particular, the material transfer between these materials, which is a basic form of wear, is studied. This allows for new insights into fundamental wear and interface processes. Furthermore, oxidation effects are briefly discussed. Finally, the adsorption of organic molecules on iron surfaces is analyzed. This is important for a better understanding of the effectiveness of additives in fuels. Additionally, the lubricating effect of water in these systems is investigated.

Below two QR (Quick Response) codes are printed, which each contains a link to a movie presenting essential results of this work. The left one is displaying the approach and subsequent separation of an aluminium surface and a titanium nitride one yielding material transfer. The second movie presents the adsorption of an ethanol molecule on an iron (100) surface. In particular, the effect of the surface - molecule interaction on the charge density is depicted, which helps to analyze the binding mechanisms. Alternatively, the following links can be used: <https://www.youtube.com/watch?v=8Ui0cGv7x0E> and <https://www.youtube.com/watch?v=t-pJM2WGV7g> for the Al/TiN interface and the ethanol adsorption, respectively.



(a) Al/TiN interface



(b) Ethanol on Fe(100)

Figure 1.1: QR codes containing hyperlinks to two movies. (a) is showing the approach and separation of an Al(111) slab and a TiN(111) one for the Al/Ti(hcp) alignment. (b) is presenting the adsorption of an ethanol molecule on a Fe(100) surface and the effect of the molecule - surface interaction on the charge density. Alternatively, the following links <https://www.youtube.com/watch?v=8Ui0cGv7x0E> and <https://www.youtube.com/watch?v=t-pJM2WGV7g> can be used to directly reach the movies (a) and (b), respectively. These movies were created by Pedro O. Bedolla employing the programs VMD, POV-Ray, FFmpeg and VisIt using data obtained during the course of this thesis.

Chapter 2

Tribology in a Nutshell

2.1 A brief History

In the following a brief history of tribology is given, only including selected highlights. A comprehensive portrayal can be found, for example, in the book “History of Tribology” by D. Dowson [1]. Tribology is often referred to as the science of friction, wear and lubrication. However, in a more precise way tribology can be defined as “the science and technology of interacting surfaces in relative motion and of related subjects and particles” [2]. This includes the phenomena of friction, wear and lubrication as well as all corresponding interfacial interactions between a solid and a counter solid, liquid or gaseous body. Tribology is a multi-disciplinary research field involving branches of natural science and engineering such as chemistry, material science, metallurgy, physics as well as mechanical, chemical and electrical engineering. The word tribology was coined by H.P. Jost in 1966. It is a combination of the greek words “ $\tau\rho\iota\beta\omega$ (tribo)” (I rub or rubbing) and “ $\lambda\omicron\gamma\iota\alpha$ (logia)” (study of, knowledge of). The term tribology has spread after the Jost report [3] which was commissioned by the UK department of education and science. In this report H.P. Jost claimed that phenomena such as friction, wear and corrosion cost Britain huge amounts of money equivalent to over 1% of its gross domestic product. As a consequence numerous centres and societies for tribology have been founded since. In a more recent study K. Holmberg et al. [4] state that the frictional

2.1. A BRIEF HISTORY

losses in passenger cars are still 28% of the fuel energy. Those authors claim that new technology for friction reduction could reduce the losses by about 60% within the next 15–25 years. This improvement would save about half a billion euros per year in fuel spending (assuming current fuel prices) and reduce the annual CO₂ emission by about one billion tons. This example demonstrates the overall importance of tribology. However, the history of tribology starts quite some time earlier.

Already the early civilizations such as Mesopotamia and Egypt were studying and exploiting tribological phenomena [1]. For example, reliefs in Egyptian tombs, e.g., of the Monarch Djehutihotep and at Saqqara (see Fig. 2.1) from around 1800 B.C. and 2400 B.C., respectively, depict the use of a liquid lubricant (probably water) between sledges and sand to move stones and heavy statues weighing several tons.¹

Leonardo da Vinci (1452–1519) can be seen as the first tribologist. His unpublished notebooks are full of drawings of tribological experiments and devices such as ball bearings (see Fig. 2.2a) to minimize unwanted tribological effects. Furthermore, by performing experiments with sliding blocks (see Fig. 2.2b) he was able to give the first, still valid friction laws. Using modern terminology, these laws state that the frictional resistance is independent of the contact area and the force² needed to overcome friction doubles when the weight is doubled.

The two laws of L. da Vinci were only rediscovered and published by G. Amontons in 1699 [7]. In the late 18th century C.-A. de Coulomb verified and further developed the work of his tribological predecessors by distinguishing between static and kinetic friction as well as by claiming that the friction force is independent of the velocity [8]. These findings are considered to be the classical friction laws and particularly the proportionality between the friction force F_T and the normal load F_N is often referred to as Amontons-Coulomb law

$$F_T = \mu F_N \quad , \quad (2.1)$$

where μ is the dimensionless *coefficient of friction* (CoF). These laws are still used

¹The effect responsible for this lubrication was studied in detail only recently [5].

²The phenomenon of force was not well defined at the time of da Vinci. The term “forza” used by da Vinci seems to be related to the idea of necessary means to maintain a velocity against a resistance [1].

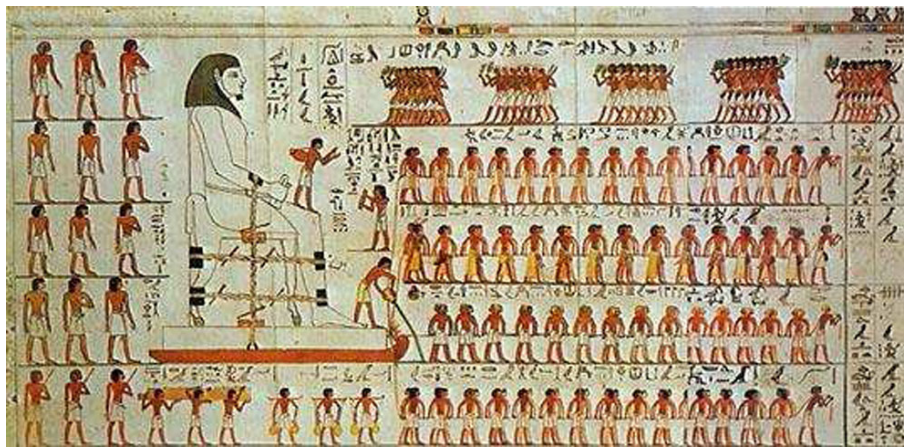
2.1. A BRIEF HISTORY



(a) Relief in a tomb at Saqqara from around 2400 B.C. Taken from D. Dowson [1].



(b) Zoom into Fig. 2.1a



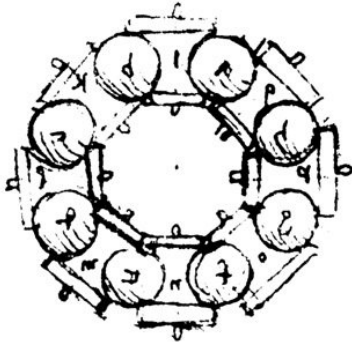
(c) Relief in the tomb of the Egyptian Monarch Djehutihotep from around 1800 B.C. Taken from A. Fall et al. [5].

Figure 2.1: Reliefs found in Egyptian tombs.

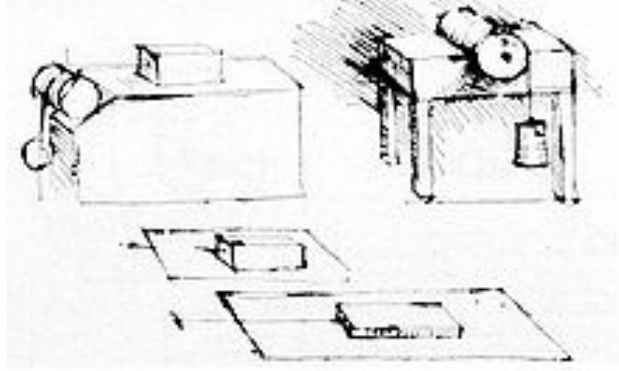
nowadays and have proven to be applicable to many systems. However, they are not generally valid. For lubricated surfaces in sliding contact Stribeck showed that the friction force depends on the velocity and proposed three distinct friction regimes [9, 10].³ For adhesive surfaces the friction force is not vanishing at zero load and an additive constant, the Derjaguin offset, has to be added to the Amontons-Coulomb law to account for that behaviour [13].

F.P. Bowden and D. Tabor investigated the importance of the surface roughness for bodies in dry contact [14]. They recognized that all bodies are rough. Even macroscopic bodies that seem to be smooth, actually exhibit roughness on the microscopic length

³Other researchers, e.g., R.H. Thurston observed a similar behaviour even before Stribeck [11, 12].



(a) Sketch of a ball bearing.



(b) Sketches of sliding experiments.

Figure 2.2: Sketches of tribological devices and experiments by Leonardo da Vinci. Taken from S. J. Shaffer [6].

scale. Thus, two bodies in contact are only touching on a few of their asperities and, consequently, the *real area of contact* A_{real} is orders of magnitude smaller than the apparent macroscopic one. This real area of contact was later shown to be linearly dependent on the normal load, if several different length scales of roughness are assumed [15, 16]. These essential findings about the contact area are the explanation for the stunning observation of the classic macroscopic friction laws that the friction force is independent of the *apparent area of contact*. Based on these findings F.P. Bowden and D. Tabor showed that the kinetic friction force for dry contacting conditions is proportional to the real area of contact

$$F_T = \tau A_{real}(F_N) \quad , \quad (2.2)$$

via the effective shear strength τ of the contacting bodies [17]. This relation is usually referred to as Bowden-Tabor law.

The first reliable experiments on wear were conducted by C. Hatchett (1760–1820) at the end of the 18th century [18]. The Privy Council⁴ had ordered for an investigation on the state of the gold coins in the United Kingdom (UK) because strong concerns had been expressed about possibly devastating consequences of massive wear of gold coins on the economy of the UK. Hatchett employed a simple reciprocating machine to examine

⁴The Privy Council, which is a short form of “Her Majesty’s Most Honourable Privy Council”, is a formal board of advisers to the sovereign of the UK. For more information see, for example, <http://privycouncil.independent.gov.uk/>.

2.1. A BRIEF HISTORY

the wear of gold coins and found that coins with grits between them wore at a faster rate compared to self-mated coins.

Various wear models and equations were developed during the 20th century. Already in 1860 T. Reye published a hypothesis that the volume of removed wear debris V_W is proportional to the work done by friction forces [19]. In 1927 F. Preston found empirically while he was studying the polishing of glass plates that the wear depth is proportional to the contact pressure, sliding velocity and time [20]. However, these early works are often forgotten and it took a few more years until wear models received a broader attention. In 1946 R. Holm formulated a wear law based on atomic encounters and plastic deformation of the contacting surfaces to discuss the conductivity of sliding electrical contacts [21]. Holm assumed that wear occurred due to the removal of single atoms and obtained a proportionality between the wear volume and the product of normal load F_N and sliding distance s

$$V_W = \frac{ZF_N s}{p_m} \quad , \quad (2.3)$$

with the flow pressure p_m . The material dependent proportionality factor Z denotes the number of abraded atoms per atomic encounter. Since the product of normal load and sliding distance is the work done by the friction force if multiplied with the coefficient of friction, the approaches of T. Reye and R. Holm yield similar expressions for the wear volume. Also Preston's equation describes in principle the same physics since the products of the apparent contact area with the wear depth and with the contact pressure give the wear volume and the normal load, respectively.

E. Rabinowicz and D. Tabor [22] performed a pioneering experimental work on wear using radioactive tracers. They observed that wear is proportional to the applied normal load as proposed by T. Reye and R. Holm, but independent of the sliding speed as well as of the apparent area of contact.

Based on the work of R. Holm, F.P. Bowden, D. Tabor and E. Rabinowicz, in 1953 J.F. Archard presented a wear law for adhesive contacts derived from contact mechanics [23]. While R. Holm assumed that atomic encounters and removal of single atoms determine the wear behaviour, J.F. Archard used the contact of asperities and the re-

2.1. A BRIEF HISTORY

removal of wear particles as basic processes explaining wear in the steady-state regime. Archard's wear equation reads

$$V_W = K \frac{F_N s}{H} \quad , \quad (2.4)$$

where H is the hardness of the softer material in dry contact and K the wear coefficient, which is often assumed to be the probability that an asperity contact yields a wear particle. Various alternative interpretations of this coefficient have been given over the years including that it represents: a) the fraction of plastically deformed asperity volume [24], b) number of necessary “events” to reach a critical value in, e.g., a fatigue process [25], c) the fraction of power contribution to the wear formation [26] or d) a complex of variables including, e.g., friction or surface film effects [27]. This variety of interpretations reflects the challenges in modelling wear which will be discussed in more detail below. Nevertheless, Archard's linear wear law is still commonly used and the basis for many other wear models. For example, E. Rabinowicz showed its validity for abrasive wear [28]. In addition, various derivatives of Archard's law exist using, for example, the contact pressure or dissipated energy as variables.

The complexity of wear processes was already shown in several experiments conducted by J.F. Archard. It was observed that most wear experiments feature a transition between a running-in phase and steady state behaviour which are accompanied by severe and mild wear, respectively [29]. Moreover, the strict proportionality between wear volume and load could not be found universally, not even for steady state conditions [30]. J.F. Archard concluded that most asperities in contact deform elastically and only rare damage yields wear particles.

A couple of decades later in 1995 H.C. Meng and K.C. Ludema performed an extensive review on existing wear models and equations [31]. In the course of that work they found over 300 wear equations in the literature. However, none of those equations was qualified to be suited for general use and most of them are only valid within a small range of parameters like working conditions or material properties. Nevertheless, they distinguished three stages of modelling:

- Empirical equations, e.g., by F.T. Barwell [32] or S.K. Rhee [33], which are typically

2.1. A BRIEF HISTORY

built on some experimental data. However, within the range, where they hold, they often show better agreement with the reality than common theoretical models.

- Contact mechanics based equations, e.g., by J.F. Archard [23], which mainly give simple phenomenological relations. Moreover, some of these models use information about the topography, the contact area and the material properties (e.g. hardness, Young’s modulus) of the contacting bodies.
- Equations based on material failure, e.g., the “Delamination Theory of Wear” by N.P. Suh [34] or the “Oxidational Wear Model” by T.F. Quinn [35], which include phenomena like dislocations, fatigue, fracture or oxidation and try to overcome limitations of contact mechanics based models.

So far wear has been mainly approached from the materials point of view using contact mechanics and failure mechanisms. However, wear is a very complex phenomenon including interdependences between different processes from chemical reactions to mechanical interactions. To analyze such a difficult situation H. Czichos [36] proposed a *systems approach* to wear, which accounts for the

- Functional aspect: The system is regarded as an operator transforming inputs $\{X\}$ into outputs $\{Y\}$
- Energy aspect: The exchange and the transformation between thermal and mechanical energies are considered. Additionally, entropy variations are studied.
- Material aspect: The exchange of materials between two contacting bodies and the interfacial volume is analyzed.

Generally, each aspect tends towards a balanced situation. Since, the different aspects typically influence each other, e.g., mechanical energy can affect the material properties, a very complex problem is the consequence. This also shows the interdisciplinary character of wear and tribology in general. For the reason of simplification most models do not account for all aspects, e.g., above mainly the material dimension has been stressed by

2.1. A BRIEF HISTORY

scientists such as J.F. Archard, F.T. Barwell, E. Rabinowicz and R. Holm. In the following several attempts for a more general description of wear phenomena are discussed.

One major shortcoming of many wear models is the assumption that wear particles immediately leave the contact area after being detached. Basically these particles just vanish. However, in reality, detached particles could be trapped between the contacting bodies for some time before they leave the contact. As long as they are inside the contact they can interact with the bodies or other detached particles, form new compounds or even be reattached to one of the bodies. The *third-body approach* by M. Godet tries to account for these behaviours [37]. The detached particles form an intermediate film, the *third-body*, whereas the contacting bodies are referred to as *first-* and *second-bodies*. This model describes wear as the loss of mass from the whole contact rather than from a single body. Furthermore, lubrication effects can be studied [38]. In the wake of Godet's formulation of the third-body, Y. Berthier introduced the *tribological circuit* [39], which considers wear as a problem of competing flows of particles. This model can be used to perform computational simulations [40–42] and to obtain analytical wear models [43], which show running-in and steady state behaviour in a similar form as the empirical Barwell laws [32].

As a first step to account for the energy aspect of wear, energy dissipation should be considered. In energy dissipation wear models the main assumption is that wear is the result of energy dissipation due to the friction between two contacting bodies [44]. Apart from the generation of wear particles, frictional energy can cause a rise in temperature and entropy changes connected to material transformations and transfers at the interface [45]. Several experiments on the wear of metals, for example, by S. Fouvry et al. [46, 47], M.Z. Huq and J.P. Celis [44] as well as A. Ramalho and J.C. Miranda [45] showed a linear relation between the wear volume and the dissipated energy. Based on the ideas of R.M. Matveesky [48], H. Mohrbacher et al. [49] as well as M.Z. Huq and J.P. Celis [50] on the energy dissipation in sliding contacts, A. Ramalho and J.C. Miranda [45] connected Archard's law and the frictional dissipation via the Amontons-Coulomb friction law

$$V_w = k F_N s = \frac{k}{\mu} F_T s = \frac{k}{\mu} E_d \quad . \quad (2.5)$$

2.1. A BRIEF HISTORY

In order to obtain a more rigorous description of the energy aspect it is necessary to consider the thermodynamic framework of wear. B.E. Klamecki was a pioneer in using thermodynamic methods for tribological analysis [51–54]. He showed the non-equilibrium nature of two bodies in contact sliding with a finite relative velocity. Because of the universality of friction and wear, he assumed that they are related to the fundamental nature of the materials and processes involved. Moreover, Klamecki argued that wear, which redistributes matter from some initial to a more random configuration, could be described via the thermodynamic entropy. However, H.A. Abdel-Aal [55] pointed out that no direct correlation between wear and entropy is apparent in the work of B.E. Klamecki.

Another pioneer in using thermodynamical methods in tribology was A. Zmitrowicz, who developed a complete mathematical framework for two contacting bodies including the third body [56–58]. He employed the axiomatic approach of rational thermodynamics⁵ to obtain constitutive equations for the state of the bodies in presence of friction, wear and frictional heat. The work of A. Zmitrowicz has been continued by researchers such as M. Dragon-Louiset [60] or C. Stolz [61], which led to thermodynamical interface models. However, M.D. Bryant [62] argued that the rigorous application of the laws of thermodynamics to tribo-systems only results in limited success because the resulting equations are highly complex and thus it is very difficult to solve them.

In the *degradation - entropy generation theorem*, M.D. Bryant et al. suggested that degradation in general occurs due to irreversible thermodynamical processes and it is a time-dependent phenomenon of increasing disorder [63]. Since entropy is interpreted as a measure of order, it should also reflect degradation. The degradation rate is then assumed to be determined by the entropy generation due to dissipative processes and it is describes by thermodynamical forces and fluxes.

First experimental results on the relationship between entropy and wear were obtained by K.L. Doelling et al. [64] followed by F.F. Ling et al. [65] and A.B. Aghdam et al. [66] who observed a linear relation between wear and entropy flows. However, M.D. Bryant et al. [67] and H.A. Abdel-Aal [55] pointed out that the entropy production rather than the entropy flow is a measure for degradation and only in steady state these two are equal.

⁵Details on rational thermodynamics can be found, for example, in [59].

2.2. EMERGING BRANCHES

Following the work of A.A. Feinberg and A. Widom [68], F.F. Ling et al. [65] described manufacturing as a process of creating a highly organized product out of raw materials. In the course of this process the entropy of the system describing the product is lowered. On the other hand, aging and degradation correspond to an increase in entropy and occur due to the “desire” of the product to reestablish its natural, unordered state.

In common, the main idea is to use the entropy production as a measure of irreversibility for the characterization of the degradation in a tribo-system. Furthermore, I.S. Gershman and N.A. Bushe pointed out that for a thermodynamical analysis of tribological problems not only the initial and final states are important but also the evolution in between [69]. Thus, non-equilibrium thermodynamics have to be used.

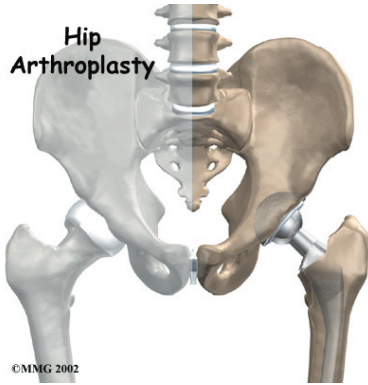
Nevertheless, all of the models presented above depend on some empirical coefficients, which, at least currently, cannot be derived from atomistic principles because “physical and chemical interactions at sliding interfaces are not fully understood” [70]. Thus, the predictive power of these models is limited [71, 72].

2.2 Emerging Branches

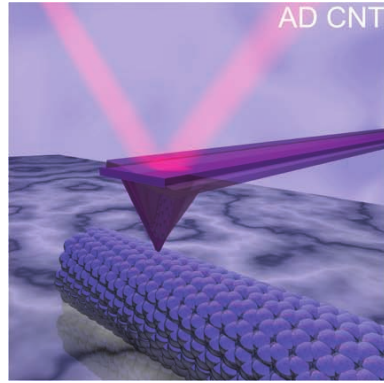
Since the 1990s new branches of tribology have emerged including biotribology [73], green tribology [74] and nanotribology [75–78]. Examples for these fields are displayed in Fig. 2.3. Especially during the last decade these areas have received increasing attention. Due to the further rising interest in biomedical devices, ecological aspects and the minimization of devices, to name three examples, the mentioned fields of tribology will continue to flourish.

2.2.1 Biotribology

Biotribology [73] deals with tribological phenomena occurring in biological systems such as the human body, animals, plants or single cells. Tribological contacts in nature are also investigated since biological systems comprise various interfaces of materials in relative motion such as the blood circuit, joints or teeth. On the other hand, the interaction



(a) Artificial hip joint. Taken from *eOrthopod* [79].



(b) Friction force microscope tip sliding over a carbon nanotube. Taken from H.-C. Chiu [80].



(c) Wind turbine. Taken from the *Global Wind Report 2013* [81].

Figure 2.3: Examples for applications from bio-, nano- and green tribology.

of biological and artificial components are separately considered. Examples range from biomedical devices and applications, like joint replacements (see Fig. 2.3a), prostheses, contact lenses or denture materials up to the clothing industry trying to obtain more comfortable fabrics by studying the skin and cloth contact.

2.2.2 Green tribology

In green tribology [74], ecological aspects of tribological phenomena are studied and negative impacts on the environment are tried to be minimized. M. Nosonovsky and B. Bhushan [74] defined three areas of green tribology: (a) biomimetics for tribological applications, (b) environment-friendly lubrication and (c) the tribology of renewable-energy

2.2. EMERGING BRANCHES

application.

The branch of renewable energy includes the generation of energy from renewable sources using, for example, wind turbines [82] (see Fig. 2.3c), tidal-wave turbines [83] or geothermal power plants [84, 85] and their specific tribological challenges. Furthermore, this area deals with tribological aspects of the use of renewable energy, for instance, in electro, biofuel or hydrogen powered cars.

Many standard lubricants contain compounds that are toxic to certain species [86]; therefore, more environment-friendly lubricants are desirable. This could be achieved by using, for example, natural biodegradable lubricants [87], which are, e.g., vegetable-oil-based or animal-fat-based, and powder lubricants [88]. In the case of biodegradable lubricants the entire process of degradation needs to be analyzed and its complete environmental impact should be assessed.

In biomimetics, biological systems and methods found in nature are used as models and sources of inspiration for design, engineering and technology solutions. By creating biomimetic or bioinspired materials scientists strive for the remarkable properties of certain biological materials by using, for example, composite structures and hierarchical multiscale organization with characteristic dimensions spanning from the nano- to the macroscale [89, 90]. Biological systems have the ability to heal or repair themselves, at least to some extent. Self-healing surfaces are able to repair minor damages such as cracks and voids [91–94]. Some examples for valuable abilities found in nature and their (potential) application in technology are presented in the following. The *lotus effect*, which is named after the lotus flower, is used to produce non-adhesive surfaces which are superhydrophobic and show self-cleaning abilities [95]. The skin of fishes inspired the construction of microstructured surfaces which are able to suppress turbulences (*shark-skin effect*, see Fig. 2.4) [96] and biofouling⁶ (*fish-scale effect*) [97]. Self-lubrication could be achieved by friction-induced self-organization [92]. Although these examples have the potential to be environmentally beneficial, their effect has to be further examined in detail. For example, L. Raibeck et al. [98] studied self-cleaning surfaces based on the lotus-effect and

⁶“Biofouling and biofilming are the undesirable accumulation of micro-organisms, plants and algae on structures that are immersed in water. Conventional antifouling coatings for ship hulls are often toxic and environmentally hazardous.” [74]

2.2. EMERGING BRANCHES

found that benefits from using such surfaces can be outweighed by environmental burdens during the production compared to other cleaning methods.

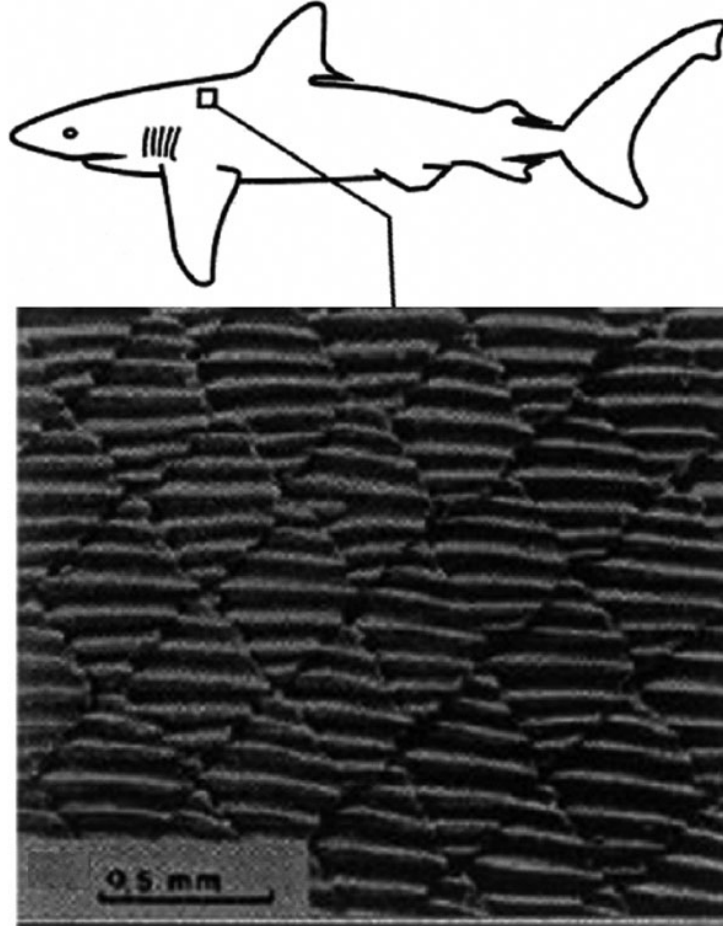


Figure 2.4: Scale structure on a Galapagos shark. Taken from W.-E. Reif [99].

2.2.3 Nanotribology

Nanotribology [75–77] deals with tribological phenomena on the nanometer length scale. Due to the ongoing miniaturization in many fields of modern technology, nanotribological aspects are receiving increasing attention. In particular, they often constitute a major limitation for the performance, reliability and life time, for example, of data storage devices or micro/nanoelectromechanical systems (MEMS/NEMS) [100–104]. These aspects are crucial for the usability of nanosystems and are strongly influenced by retardation forces like friction and adhesion because of the length scale and large surface-to-volume ratio.

2.2. EMERGING BRANCHES

In-depth studies in nanotribology only became possible after the advent of experimental techniques allowing to probe the nanoscale and the increasing computer power, which allows to simulate nanotribological systems large and accurate enough to be of interest and to be able to assist in the interpretation of experimental results [76]. Experimentally the development started with the surface force apparatus [105, 106], whereas currently the main player are electron microscopy techniques [107] as well as the atomic force microscope (AFM) [108]. In particular, the development of the AFM and its derivative the friction force microscope (FFM) [109], which both represent a single asperity contact, allowed for major advances in nanotribology [76, 110]. Computationally, since the 1980s classical molecular dynamics (MD) simulations have commonly been applied to nanotribological problems, examples can be found in the following references [76, 111–121] and still constitute a standard tool in numerical atomistic simulations. Nevertheless, during the last decade methods based on quantum mechanics such as density functional theory (DFT) calculations, which are employed in this work, have been increasingly used in this field, examples are presented in the following references [122–135] and should be seen as a valuable extension to the more common computational tools in tribology. DFT allows for parameter-free calculations as well as an accurate description of quantum mechanical systems and does not depend on empirical potentials. However, due to computational challenges, DFT calculations are currently limited to rather small systems of typically a few hundred atoms.

The goal of many macroscopic tribology studies is to determine the coefficient of friction or the wear rate. However, both quantities are not intrinsic physical properties and usually depend strongly on various influences such as the specific structure of the involved materials, environmental and ambient factors, elastic or plastic properties of the surfaces in contact and the history of the contact. To learn more about the fundamental interactions and dynamics involved in tribological phenomena, like friction, wear and lubrication, simulations on well-defined interfaces and contacts are necessary. Thus, studies on idealized situations such as single asperity contacts and interfaces between atomically flat surfaces are able to deliver valuable data and information. One should, however, always keep in mind that most real tribological systems are governed by rough, multi-asperity

2.2. EMERGING BRANCHES

contacts [136, 137].

Macroscopic tribological laws such as Amontons-Coulomb friction law and Archard's wear law (see section 2.1) do not seem to be generally applicable at the nanoscale [72, 136, 138]. For example, in the case of nanoscale wear [139] conflicting observations have been made. Various experiments have shown that Archard-type models are not valid at the atomic length scale [70, 140, 141]. These experiments typically investigate single asperity contacts established in AFM experiments. W. Maw et al. [140] as well as B. Gotsmann and M.A. Lantz [141] state a sub-linear dependence of the wear volume on the product of the load and sliding distance or time. T.D.B. Jacobs and R.W. Carpick [70] did not observe a trend in Archard-type plots at all, but an exponential relationship between atom-loss rate and the contact pressure. This AFM results by T.D.B. Jacobs and R.W. Carpick indicate an atom-by-atom attrition process. In contrast, R. Colaço [142] observed a linear dependence of the wear rate on the load in AFM abrasive wear tests, although only above a certain load threshold. In MD simulations on single asperity contacts M. Vargonen et al. [143] obtained a sub-linear dependence of the wear volume on load and sliding distance, whereas Z.-D. Sha et al. [144] found a linear Archard-type relationship. Z.-D. Sha et al. argue that the discrepancy with respect to experimental results occurs due to the several orders of magnitude higher sliding velocity in their simulations, which reduces the significance of thermal activation effects, or due to contamination of experimental surfaces. Based on AFM experiments, B. Bhushan and K.J. Kwak [145] proposed that the wear volume increases logarithmically with the sliding velocity up to a system-dependent critical value and then the increase levels off.

Similar to the case of nanoscale wear, also various dependencies of friction have been observed at the atomic length scale. One prominent example is the structural superlubricity [146–150], which describes the reduction of friction by several orders of magnitude and it was found for incommensurably aligned surfaces. However, the nature of the phenomenon is still a matter of debate and arguments have been presented that it is unstable [151, 152] or actually stems from thermal effects and the low effective mass of the nanocontact [153, 154]. The inclusion of a third body, further, hinders structural superlubricity and recovers a linear relationship between friction force and load [155, 156].

2.2. EMERGING BRANCHES

In general, various observations for the dependence of the friction force on load have been published including superlinear [157], sub-linear [136, 138, 158] as well as more complex relations [118, 159]. The dependence is influenced, for example, by the type of the contact, whether it is adhesive as well as single or multi-asperity [136]. Furthermore, frictional anisotropy has been shown on rather complex geometries [160, 161] as well as for a single-atom asperity [162]. While simulations on nanoscale friction are commonly done with classical MD [163, 164], as already mentioned DFT approaches are gaining increasing attention. Using DFT, for example, friction forces can be evaluated by using potential energy landscapes which are then fitted to mechanical models, like the Prandtl-Tomlinson one [165, 166] or employed to obtain the energy dissipation as it was done in the pioneering work by W. Zhong and D. Tománek [167, 168]. More recently, M. Wolloch et al. [135] found an exponential relationship between the friction force and load between copper surfaces employing DFT methods. For the low load regime those authors were able to retrieve the Derjaguin generalization of the Amontons-Coulomb kinetic friction law.

Another severely debated nanotribological topic is the definition and calculation of the real contact area [72, 138]. As already mentioned above, see section 2.1, the real contact area is always much smaller than the apparent one due to the ubiquitous roughness of surfaces. In classical contact mechanics the contact area can be evaluated by using the Hertz model [169] for non-adhesive surfaces and the JKR (Johnson, Kendall and Roberts) [170] or DMT (Derjaguin, Muller and Toporov) [171] approaches for adhesive surfaces. The latter two were unified by Tabor [172] and Maugis (Maugis-Dugdale model) [173]. However, probing nanoscale phenomena, the contact area approaches the size of the involved atoms. Thus, the application of continuum mechanics becomes at least problematic [138], if not impossible. Various methods have been presented to estimate the contact area on an atomic basis [120, 136, 138, 159, 174]. The challenge remains the definition of atomic contact, which, for example, has been proposed as the onset of repulsion [174] or via the distinction between chemical and van der Waals interaction [136]. M. Wolloch et al. [175] recently developed an ab-initio approach based on DFT calculations and Bader's *quantum theory of atoms in molecules* (QTAIM) [176].

2.2. *EMERGING BRANCHES*

The examples of wear, friction and contact area given above perfectly illustrate that nanotribology is a field involving numerous open questions and challenges. Thus, further detailed investigations are mandatory.

Chapter 3

Theoretical Background and Computational Methods

3.1 Some Basics of Solid State Physics

In the following some theoretical background is given, for a more comprehensive discussion see, for example, books on solid state physics such as [177, 178]. Materials consist of atomic nuclei and electrons. In an ideal solid the nuclei are arranged on a regular lattice. Such a many-body system can be described with a quantum mechanical Hamiltonian

$$\hat{H} = \hat{H}_N + \hat{H}_e + \hat{V}_{N-e} \quad , \quad (3.1)$$

which includes Hamiltonians for the nuclei \hat{H}_N , for the electrons \hat{H}_e as well as the potential between electrons and nuclei \hat{V}_{N-e} . The former Hamiltonians further consist of kinetic and potential energy contributions for the electrons and nuclei. Since Coulomb forces are considered to be dominant in the energy range of interest, gravitation, strong and weak interactions are disregarded. In a first approximation relativistic effects are usually neglected. However, for heavy elements, like gold, these effects often cause significant contributions and thus may need to be accounted for. Using the Hamiltonian (3.1), the

3.1. SOME BASICS OF SOLID STATE PHYSICS

time dependent Schrödinger equation in its most general form

$$\hat{H}\Psi = i\hbar \frac{\partial}{\partial t}\Psi \quad , \quad (3.2)$$

has to be solved to quantum mechanically describe a solid. This Schrödinger equation simplifies to

$$\hat{H}\Psi = E\Psi \quad , \quad (3.3)$$

in case the Hamiltonian does not explicitly depend on time. In this equation Ψ is the many-body wave function given by

$$\Psi = \Psi(\mathbf{r}_1, s_1, \dots, \mathbf{r}_n, s_n, \mathbf{R}_1, I_1, \dots, \mathbf{R}_m, I_m) \quad , \quad (3.4)$$

i.e., Ψ is a function of the electron and nuclear coordinates \mathbf{r}_i and \mathbf{R}_j as well as the spins s_i and I_j , respectively. In the following the spatial coordinate and the spin degree of freedom will be combined into \mathbf{r} and \mathbf{R} for electrons and nuclei, respectively. For a many-body problem the Schrödinger equation can not be solved analytically. Approximations are therefore needed for most problems in solid state physics.

The first step is usually the separation of the motion of electrons and ions (nuclei), which is called Born-Oppenheimer approximation. Due to the large mass and velocity difference between the ions and electrons, it is assumed that the electrons follow the ionic motion almost instantaneously. Mathematically, the wave function can be written as a product of an electronic and an ionic contribution resulting in two Schrödinger equations where the ionic motion is often treated classically. The electronic Hamiltonian \hat{H}_e then reads

$$\hat{H}_e = \hat{T}_e + \hat{V}_{e-e} + \hat{V}_{N-N} + \hat{V}_{N-e} \quad , \quad (3.5)$$

with the kinetic \hat{T} and potential \hat{V} energy contributions.

Due to the vast number of particles in a solid (about 10^{23}), further approximations are necessary to handle the electronic Schrödinger equation. Since the introduction of quantum mechanics various approaches were used to describe the electronic structure of

3.1. SOME BASICS OF SOLID STATE PHYSICS

solids. The *free-electron* or *Drude-Sommerfeld model* was obtained by A. Sommerfeld in 1927 by combining the classical Drude model and quantum mechanical Fermi-Dirac statistics. In this model electron-electron interactions are not taken into account, the crystal lattice is neglected and the valence electrons are completely detached from the ions. The resulting Schrödinger equation is solved by plane waves. Despite these rather crude assumptions the model is able to describe many experimental findings to some extent such as the temperature dependence of the heat capacity and electrical conductivities. However, it cannot explain, for example, the existence of insulators. Thus, in the *nearly-free electron model* the interactions between the ions of the crystal and the electrons are modelled by a weak periodic potential. Because of the periodicity of the potential, the solution to the Schrödinger equation is then given by Bloch waves, which are the product of plane waves and a periodic function representing the crystal lattice. The inclusion of this interactions allows for the existence of band gaps at the Brillouin zone boundaries and thus is able to describe insulators.

While the two models above are limiting cases for almost free electrons, the *tight-binding model* forms the opposing limit, where the particular atomic solution is approximated by the wave functions of the isolated, constituent atoms. The entire solution to the Schrödinger equation is therefore given by a linear combination of atomic single-electron orbitals. This model allows for a good description of materials with a small or modest overlap between the atomic orbitals and potentials of neighbouring atoms, which is, e.g., the case for silicon or diamond.

The Hartree method [179] is a different approach to solve the time-independent electronic Schrödinger equation (3.2). The Rayleigh-Ritz variational principle is used to obtain *Hartree equations* which have the form of effective one-particle Schrödinger equations. Since the single-particle solutions enter the effective one-particle Hamiltonian, the Hartree equations can only be solved iteratively and interactions between the particles are included to some extent. To fully include the Pauli principle, the anti-symmetry of the wave functions has to be accounted for, which is achieved in the Hartree-Fock (HF) method [180]. In its simplest form, Slater determinants are used to construct the wave functions for the *Hartree-Fock equations*. This approach includes the Coulomb part of the

3.2. DENSITY FUNCTIONAL THEORY (DFT)

electron-electron interaction as well as the *exchange energy*, which is a quantum mechanical effect based on the exchange symmetry of indistinguishable particles [181, 182]. Electrons of the same spin are repelled by an additional Coulomb-like interaction. This effect is called *exchange hole* and decreases the total energy. However, *electron correlation*, which describes the correlated interaction between electrons of different spins, is not included within the HF method. This additional contribution, which keeps the electrons apart, would further reduce the total energy by the *correlation energy*. Due to the lack of correlation, HF fails to describe metals correctly because of problems with a vanishing density of states at the Fermi level. Furthermore, relativistic effects are usually neglected in HF.

To overcome the shortcomings of HF, various *Post-Hartree-Fock* methods have been suggested mainly dealing with the incorporation of electron correlation. Examples for such methods are the *configuration interaction* (CI) [183, 184] and *coupled cluster* (CC) [184–186] methods, which add electronic excitations to the HF wave functions. Presently, the “gold-standard” for quantum chemistry reference calculations is the *CCSD(T)* method, where triple excitations are accounted for perturbatively. A different approach is the *Møller-Plesset perturbation theory* [187], where the difference between the many-body Hamiltonian and the HF one is treated perturbatively. If only the second order terms are added, this is referred to as *MP2 method* which is cheaper but less accurate than CCSD(T) calculations. Post-Hartree-Fock methods are computationally cumbersome and thus typically only feasible for rather small systems. Thus, methods are needed to treat larger systems efficiently and with the required accuracy. Over several decades *density functional theory* (DFT) has proven to be a well-suited choice to achieve these requirements. Thus, DFT is currently the most common method for electronic structure calculations in solid state physics and chemistry [188, 189].

3.2 Density Functional Theory (DFT)

Since a many-body wave function is a rather complicated object, it would be convenient to have another quantity which is easier to handle but still contains the information

3.2. DENSITY FUNCTIONAL THEORY (DFT)

of the full system. This can be achieved by using the electron density $\rho(\mathbf{r})$. In 1927 L. Thomas and E. Fermi have already proposed that the electron density can be used in electronic structure calculations [190, 191]. However, the *Thomas-Fermi model* is not based on a solid theory which relates electron density to the corresponding many-body wave function [192]; therefore, its application to real systems yields poor quantitative results.

The *Hohenberg-Kohn theorems* [193] are the foundation of density functional theory (DFT). P. Hohenberg and W. Kohn postulated that the ground state electron density $\rho(\mathbf{r})$ of a system of N interacting electrons in an external potential, which is here the field of the nuclei, uniquely determines the potential $V_{\text{ion}}(\mathbf{r})$ apart from an additive constant¹. The number of electrons $N = \int \rho(\mathbf{r}) d\mathbf{r}$ is also determined by the electron density. The total energy $E[\rho]$ of the system is then expressed as a functional of the electron density $\rho(\mathbf{r})$

$$E[\rho] = T[\rho] + V_{\text{ion}}[\rho] + E_{\text{H}}[\rho] + E_{\text{xc}}[\rho] \quad . \quad (3.6)$$

The variational principle of Hohenberg and Kohn states that the ground state density minimizes this energy functional and consequently gives the ground state energy. However, all terms of the energy functional (3.6) have to be expressed through the electron density first. This is easily achieved for the external potential $V_{\text{ion}}[\rho]$ and the classical electron Coulomb interaction, which corresponds to the Hartree energy $E_{\text{H}}[\rho]$,

$$V_{\text{ion}}[\rho] = \int d\mathbf{r} V_{\text{ion}}(\mathbf{r}) \rho(\mathbf{r}) \quad , \quad (3.7)$$

$$E_{\text{H}}[\rho] = \frac{1}{2} \int d\mathbf{r}' \int d\mathbf{r} \frac{\rho(\mathbf{r}') \rho(\mathbf{r})}{|\mathbf{r} - \mathbf{r}'|} \quad . \quad (3.8)$$

All quantum mechanical many-body effects are handled by the *exchange-correlation energy functional* $E_{\text{xc}}[\rho]$. This as well as the kinetic energy functionals are universal because they do not depend on the external potential. Unfortunately, no exact expression for the exchange-correlation functional is known. Thus, approximations are necessary, which will be discussed below, see section 3.3. To avoid difficulties in expressing the kinetic energy

¹The proof of this theorem can be found, for example, in [192].

3.2. DENSITY FUNCTIONAL THEORY (DFT)

functional $T[\rho]$, W. Kohn and L.J. Sham [194] introduced auxiliary single-electron orbitals $\varphi_i(\mathbf{r})$, which give exactly the same charge density

$$\rho(\mathbf{r}) = \sum_{i=1}^N |\varphi_i(\mathbf{r})|^2 \quad . \quad (3.9)$$

The kinetic energy can be written as sum of the single-electron and correlation contributions

$$T = T_0[\rho] + T_{corr}[\rho] \quad , \quad (3.10)$$

where the first term T_0 is determined by the single-electron orbitals

$$T_0 = \sum_i \int d\mathbf{r} \frac{\hbar^2}{2m} (\nabla \varphi_i(\mathbf{r}))^2 \quad . \quad (3.11)$$

The Kohn-Sham theorem [194] states that for every system of interacting electrons in an external potential $V_{\text{ion}}(\mathbf{r})$ there exists a unique local potential $V_{\text{ion},l}(\mathbf{r})$ such that the non-interacting electron exposed to $V_{\text{ion},l}(\mathbf{r})$ exhibit the same ground-state density as the interacting system. The uniqueness of this local potential is given by the Hohenberg-Kohn theorem and its existence follows from the *V-representability theorem* [195]. This theorem states that on a lattice any normalizable positive function $\rho(\mathbf{r})$, that is compatible with the Pauli principle, is ensemble-V-representable. Similar to the Hartree method the variational principle can be used to obtain single-particle equations, the *Kohn-Sham equations*,

$$\left\{ -\frac{\hbar^2}{2m_e} \Delta + v_{\text{ion}}(\mathbf{r}) + v_{\text{H}}(\mathbf{r}) + v_{\text{xc}}(\mathbf{r}) \right\} \varphi_i(\mathbf{r}) = \varepsilon_i \varphi_i(\mathbf{r}) \quad , \quad (3.12)$$

which are Schrödinger equations for non-interacting particles in an effective potential

$$v_{\text{eff}}(\mathbf{r}) = v_{\text{ion}}(\mathbf{r}) + v_{\text{H}}(\mathbf{r}) + v_{\text{xc}}(\mathbf{r}) \quad . \quad (3.13)$$

The exchange-correlation potential $v_{\text{xc}}(\mathbf{r})$ can be expressed by a functional derivative of the exchange-correlation energy $E_{\text{xc}}[\rho]$, i.e.,

$$v_{\text{xc}}(\mathbf{r}) = \frac{\delta E_{\text{xc}}[\rho]}{\delta \rho(\mathbf{r})} \quad , \quad (3.14)$$

3.3. EXCHANGE-CORRELATION FUNCTIONAL

which also includes $T_{corr}[\rho]$. If all contributions were known, the Kohn-Sham equations could be solved self-consistently now and, in principle, the ground-state energy could be determined exactly. However, approximations are necessary, since the true exchange-correlation term is not available. Possible approximations are discussed in the following section. So far the electron spin has not been accounted for, however, this can be achieved by using electron densities for spin up and down states instead of the total density. This is described by the Kohn-Sham spin density functional theory [194]. Furthermore, the Hohenberg-Kohn theorem can be extended to the relativistic treatment of electrons [196], which is, for example, often necessary to reasonably treat heavy elements, like gold [197].

3.3 Exchange-Correlation Functional

As already mentioned in the previous section the exchange-correlation energy functional $E_{xc}[\rho]$ is not known in general. This functional can be expressed as

$$E_{xc}[\rho] = \int d\mathbf{r} \rho(\mathbf{r}) \epsilon_{xc}[\rho] \quad , \quad (3.15)$$

where ϵ_{xc} is the exchange-correlation energy density, which depends on the electron density. As a first approximation the *homogeneous electron gas*, which is often referred to as *jellium*, is commonly used. In the *Local-Density Approximation* (LDA), a common parametrization can be found in [198], the exchange-correlation energy of jellium is evaluated for the local densities of non-homogeneous systems, namely

$$\epsilon_{xc}^{\text{LDA}}[\rho(\mathbf{r})] := \epsilon_{xc}^{\text{hom}}(\rho_0)|_{\rho_0 \rightarrow \rho(\mathbf{r})} \quad . \quad (3.16)$$

The exchange-energy density ϵ_x^{LDA} can be obtained by applying the Hartree-Fock method to jellium using plane waves. More details can be found, for example, in [199]. Then, the exchange-energy density reads as

$$\epsilon_x^{\text{LDA}}(\rho_0) = -\frac{N}{V} \frac{3}{4} \frac{e^2 k_F}{\pi} = -\frac{3}{4} \left(\frac{3}{\pi}\right)^{\frac{1}{3}} e^2 \rho_0^{\frac{4}{3}} = -C_x \rho_0^{\frac{4}{3}} \quad , \quad (3.17)$$

3.3. EXCHANGE-CORRELATION FUNCTIONAL

where V is the reference volume of the system, N the number of electrons and k_F the Fermi wave vector. The correlation term ϵ_c^{LDA} can be calculated with advanced many-body techniques such as *Quantum Monte Carlo* simulations [200]. The sum of both terms yields the exchange-correlation energy density within LDA and is obtained via integration of the exchange-correlation energy functional, i.e.,

$$E_{\text{xc}}^{\text{LDA}}[\rho] = \int d\mathbf{r} \rho(\mathbf{r}) \epsilon_{\text{xc}}^{\text{LDA}}(\rho(\mathbf{r})) \quad . \quad (3.18)$$

In turn this can be used to solve the Kohn-Sham equations self-consistently. LDA was conceived to be a good approximation for systems with slowly varying charge densities, which is typically observed for s- and p-states. However, rather surprisingly LDA yields acceptable results for many other systems as well [201]. One reason for this flexibility is that not an exact modelling of the exchange-correlation hole is necessary but already a reasonable approximation of its spherical average and the fulfilling of the sum rules are sufficient to obtain good results [202]. Nevertheless, LDA also shows many limitations like the poor treatment of systems with rapidly changing electron densities. Moreover, LDA often gives larger binding and cohesive energies than found in experiments [203].

These limitations are commonly tried to be overcome by adjusting the exchange-correlation functional. One possibility is to add information on the semi-local neighbourhood. This is achieved within the *Generalized Gradient Approximation* (GGA) by considering not only the local density but also its gradient in the exchange-correlation functional

$$E_{\text{xc}}^{\text{GGA}}[\rho, \nabla\rho] = \int d\mathbf{r} \rho(\mathbf{r}) \epsilon_{\text{xc}}^{\text{GGA}}(\rho(\mathbf{r}), |\nabla\rho(\mathbf{r})|) \quad . \quad (3.19)$$

There are various parametrizations of GGA functionals², but one of the most commonly used flavor is currently the *Perdew-Burke-Ernzerhof* (PBE) functional [204, 205]. For many systems GGA improves total and atomization energies compared to LDA [206]. Furthermore, bonds are softened by GGA [207], which often results in an under-binding [208, 209] compared to experiments.

²There are also different functionals within LDA, however, the variations in the parameters are much smaller than for GGA. A commonly used parametrization can be found in [198].

3.4. VAN DER WAALS INTERACTIONS

While DFT on the level of LDA and GGA works well for many systems, they have several drawbacks such as: (a) the over- and under-binding of LDA and GGA, respectively, (b) the poor treatment of strongly correlated systems, (c) the underestimation of band gaps and (d) the missing description of non-local interactions like van der Waals (vdW) forces. Consequently, various approaches have been proposed to overcome these weaknesses. For example, in *meta-GGA* functionals [210] higher-order powers of the density gradient or the local kinetic energy are included. On the other hand, in *hybrid functionals* a portion of exact exchange obtained with the Hartree-Fock method is combined with DFT exchange-correlation contributions. Commonly used hybrid functionals are HSE [211] and B3LYP [212, 213]. These methods give accurate results, e.g., for band gaps, however, they are computationally cumbersome. Possibilities to include van der Waals interactions in DFT are discussed in the following section.

3.4 Van der Waals interactions

The long-range van der Waals (vdW) interactions are, in principle, present between all atoms and thus in all molecules as well as solids; therefore, they should be considered [214–216]. Long-range is meant here in comparison with typical chemical bond lengths. The vdW interactions are named after J.D. van der Waals who first described these intermolecular forces [217]. Nowadays, vdW forces are commonly divided into three contributions [218]: (a) the *Keesom forces* between permanent dipoles, (b) the *Debye forces* between a permanent and a induced dipole and (c) the *London dispersion forces* between a quantum-induced spontaneous dipole and an induced dipole. In the DFT community the latter are often meant when the term vdW forces is in use.

In a simple picture, the London dispersion forces can be seen as the attractive interaction between particles due to the induction of a dynamic multipole in one particle by quantum fluctuations within an adjacent particle. Its first quantum mechanical description was given by London [219–221] using second order perturbation theory. This approach yields an approximation for the dispersion interaction which becomes proportional to r^{-6} , if r is the distance between the dipoles. For atoms and small molecules this

3.4. VAN DER WAALS INTERACTIONS

approximation gives good results, however, for macroscopic objects their geometry has to be accounted for [222]. In the case of extended systems the pairwise additivity of vdW contributions is assumed commonly, which is only a good approximation if many-body effects are neglected.

VdW interactions are usually weak compared to chemical bonds; therefore, their contributions are negligible in many systems. This also explains the success of many methods that do not include vdW forces such as standard DFT. However, vdW interactions play important roles in several systems due to their long-range nature and their collective effect as well as when stronger forces are missing. Examples for such cases are systems including noble gas atoms, the physisorption of molecules on surfaces [223–226], layered materials, like graphite [227], and even some ionic as well as semiconducting solids [228]. Consequently, there is an increasing demand for methods that are capable of properly treating vdW interactions.

Standard DFT methods using local or semi-local exchange-correlation functionals such as LDA or GGA, obviously, can not treat non-local vdW interactions correctly. Moreover, they do not account for instantaneous fluctuations of the density. As a rough approximation, LDA is still often used to describe systems where vdW forces are essential, because due to its over-binding behaviour, LDA is often fairly close to experimental results, e.g., for graphite. However, the long-range polynomial behaviour of vdW interactions can not be described by the exponential decay of the LDA interactions [229–231]. Thus, the agreement is for a wrong physical reason. Consequently, over the past decade various approaches have been proposed to incorporate vdW interactions into DFT.³

In the *force-field correction* methods, which are often referred to as DFT-D approaches, a semi-empirical vdW term E_{vdW} is added to the Kohn-Sham DFT energy E_{DFT} . The attractive vdW contribution is modelled by a pairwise interatomic term of the form $C_6 r^{-6}$ and includes a damping term to eliminate the divergence for small distances. Various types of such a correction have been proposed, which basically differ only in the coefficient C_6 [233–242]. While the coefficients are kept constant for each pair of elements in the basic methods, more advanced approaches try to account for changes due to the bonding

³An overview of the currently used methods can be found in [232].

3.4. VAN DER WAALS INTERACTIONS

situation or hybridization. These methods, especially the simple ones, are computationally very efficient but exhibit several weaknesses [243] such as that these corrections are not derived from the electron density or the necessity of a damping function.

Currently, the most sophisticated approaches try to go beyond the pairwise approximation. This is done, for example, in the *many-body dispersion approach* [244–247] which employs coupled dipoles. Within this method, harmonic oscillators are placed at the atomic position and the vdW interaction is obtained from frequency shifts due to their interaction. One major difficulty of this approach is the necessity for accurate relations between atoms and oscillator models [232]. Another approach that yields very accurate vdW energies is the *random phase approximation* (RPA) [248–251] combined with the *adiabatic-connection fluctuation-dissipation theorem* (ACFDT) [252, 253]. Since this method is computationally very demanding, it is currently limited in its application to rather small systems [254].

As an intermediate option several models have been proposed that assume vdW interactions to be pairwise additive, but do not need any external input parameters. Some examples are *VV10* [255], the *local dispersion approach* [256, 257] and the *van der Waals density functionals* (vdW-DF) [258]. Since vdW-DFs are used in this thesis, these will be explained in more detail here. In the original version devised by Dion et al. [258] the exchange-correlation energy is expressed as

$$E_{\text{xc}}^{\text{vdW-DF}}[\rho] = E_{\text{revPBE(x)}}[\rho] + E_{\text{LDA(c)}}[\rho] + E_{\text{nl(c)}}[\rho] \quad . \quad (3.20)$$

In this form the exchange term $E_{\text{revPBE(x)}}$ is obtained from the revised PBE (revPBE) functional [259] and the correlation is split into a local $E_{\text{LDA(c)}}$ and a non-local $E_{\text{nl(c)}}$ contribution. The local one is calculated with LDA, whereas the non-local correlation is obtained based on electron densities that interact via a model response function. Originally, the non-local term was derived from the correlation energy within the ACFDT formalism, but the particular form of $E_{\text{nl(c)}}$ is still under debate [231, 260]. This provides the non-local correlation as a double space integral of the density weighted interaction

3.5. NUMERICAL IMPLEMENTATIONS

kernel $\varphi(r_1, r_2)$ that captures the correct $O(1/|r_1 - r_2|^6)$ asymptotic behaviour

$$E_{\text{nl(c)}} = \iint d\mathbf{r}_1 d\mathbf{r}_2 \rho(\mathbf{r}_1) \varphi(\mathbf{r}_1, \mathbf{r}_2) \rho(\mathbf{r}_2) \quad . \quad (3.21)$$

Since first calculations using the vdW-DF method showed rather large errors [261], improvements were necessary. One possibility was to find a better approximation for the exchange part. This was, for example, done by Klimeš et al. [262, 263] who conceived three new functionals (optPBE, optB88 and optB86b) which significantly reduce the initial errors. The optB86b functional will be presented in the following because it is used in this thesis. To obtain this functional a re-parametrised form of the Becke86 exchange term [264] is employed

$$E_{\text{xc}}^{\text{optB86b}}[\rho] = E_{\text{optB86b(x)}}[\rho] + E_{\text{LDA(c)}}[\rho] + E_{\text{nl(c)}}[\rho] \quad . \quad (3.22)$$

The “opt” functionals have been applied to a wide range of systems such as layered materials [230, 265], dimers [262], solids [266–268], the adsorption of organic molecules on surfaces [269–278] as well as graphene, thin films and noble gases on metals [229, 279–283]. These studies show the capabilities of the “opt” functionals and that they are among the most accurate in this class of models. Computationally, the demand of calculations with vdW-DF is comparable to standard GGA.

3.5 Numerical Implementations

All DFT calculations in this thesis are performed by employing the Vienna Ab initio Simulation Package (VASP) [284–287]. This “computer program for atomic scale materials modelling, . . . , from first principles”⁴ is very versatile, accurate and highly efficient. According to its citation numbers, it is currently the most widely used DFT code. Using VASP, solutions to the many-body Schrödinger equation can be obtained within DFT or HF approximations [288]. Hybrid functionals [211, 289], which combine both approaches, are also available. VASP offers various approximations to the DFT exchange correla-

⁴Visit www.vasp.at for more details.

3.5. NUMERICAL IMPLEMENTATIONS

tion energy such as LDA, GGA (see section 3.3) and vdW-corrected [231, 263, 290, 291] functionals. Moreover, Green’s function methods [251, 254, 292–296], many-body perturbation theory [297, 298] and quantum-mechanical molecular dynamics schemes [284, 285] are implemented. VASP employs periodic boundary conditions and expresses its central quantities in plane wave basis sets. The electronic-ionic interactions are modeled by norm-conserving or ultrasoft pseudopotentials [299, 300] or the projector augmented-wave (PAW) method [301, 302]. Throughout this thesis the PAW method is employed. VASP allows to compute the quantum mechanical forces and the full stress tensor. These quantities can be used in relaxations to obtain equilibrium structures. Additionally, VASP offers possibilities to investigate, for example, magnetic and optical properties as well as the linear response of systems to electric fields or ionic displacements.

For analyzing the data, created with VASP, several visualization tools have been used throughout this work, like GNUPLOT, P4VASP, VESTA [303] (Visualization for Electronic and Structural Analysis), VisIT [304] and VMD [305] (Visual Molecular Dynamics).

Chapter 4

Adhesion and material transfer between contacting surfaces

4.1 Interface: Aluminium - Titanium nitride

4.1.1 Introduction and Motivation

Contacts of surfaces at the atomic length scale are crucial in many modern applications, from experimental techniques such as nanoindentation [306–308] and atomic/friction force microscopy (AFM/FFM) [108–110] to nanotechnologies applied, for example, in nano-/microelectromechanical-systems (NEMS/MEMS) [100–104]. The reliability, performance and life time of such systems, for example, depends sensitively on the interactions between contacting materials. Furthermore, detailed insights into such contacts are of fundamental interest for better comprehension of tribological processes, such as nano-scale wear [70, 75, 141, 309–313], for which there is still a lack of understanding due to its highly complex nature [139]. More information can be found in section 2.3b.

Metal-ceramic interfaces [314] are of fundamental and technological interest because they exhibit advantages of both types of materials such as valuable mechanical properties, high thermal stability, and degradation resistance [315]. Hence, such interfaces are important in numerous applications such as communication devices and nanoelectronics [316]. In this thesis, the interface between the metal Al (aluminium) and the

transition-metal nitride TiN (titanium nitride) is investigated. This interface consists of a soft material and a hard material, which simplifies wear processes because the softer material is primarily affected.

Although classical molecular dynamics (MD) simulations currently constitute the most common computational tool in nanotribological, density functional theory (DFT) calculations have been increasingly used in this field during the last decade and should be seen as a valuable extension. Further information can be found in section 2.3b. Since DFT has proven to yield reliable results for this class of systems [317–319], it is also employed in this work to analyze the electronic and atomic structure of the Al/TiN interfaces and to determine properties such as adhesion energies. Results obtained with DFT, such as potential-energy curves, can be used as an input, e.g., for large-scale classical MD simulations [320, 321]. Furthermore, the combination of approaches such as DFT and MD as well as the continuously increasing available computer power and advances in software tools promise the possibility to investigate even larger and more realistic systems in the near future.

Al/TiN and similar interfaces have already been investigated by various researchers with experimental [322, 323] and theoretical [324–332] methods. Here, however, the emphasis lies on a realistic way to simulate the separation of the interfaces as well as on a comprehensive discussion of interfaces between Al and TiN low-index surfaces. To assess this problem, the effects of various configurations at the interface as well as approach and subsequent separation of Al and TiN slabs are analyzed. Various tests on, e.g., the effect of adjusted lattice parameters, the simulation cell size and various approximations for the exchange correlation functional in DFT are carried out.

4.1.2 Computational Details

Density Functional Theory Calculations

To study the interfacial properties of Al and TiN slabs upon approach and subsequent separation, first-principles calculations within the framework of DFT were performed employing the Vienna Ab initio Simulation Package (VASP), for more information see

section 3.5. Unless explicitly mentioned otherwise, the generalized gradient approximation (GGA) in the Perdew, Burke, and Ernzerhof (PBE) parametrization was applied in this chapter to describe the exchange and correlation functional. More details on such functionals can be found in section 3.3. Since GGAs often underestimate binding and adhesion energies, the local-density approximation (LDA), which usually overestimates these quantities, was also employed for comparison. Additionally, the van der Waals (vdW) density functional (DF) optB86b was used, which includes a nonlocal correlation term approximating vdW interactions. A more detailed discussion of the treatment of vdW interactions within DFT can be found in section 3.4. Although vdW interactions should not play a major role in the investigated systems, the calculations are included for comparison and clarification. The calculation parameters were carefully chosen to obtain accurate total energies. An energy cutoff of 800 eV was used for the plane-wave basis. Unless noted otherwise, the Brillouin zone sampling was performed using a Γ -centred $15 \times 15 \times 1$ Monkhorst-Pack mesh [333]. Both settings allow for total energies accurate to 1 meV/atom. While the tetrahedron method with Blöchl corrections [334] was utilized for static calculations, for relaxations a smearing of 0.11 eV using the first-order method of Methfessel and Paxton [335] was selected. In order to relax the structures a damped molecular dynamics¹ (MD) algorithm was employed to update and move the ions according to the Hellman-Feynman forces. This is achieved by employing a second order equation of motion which includes a damping factor. Atomic movements were allowed until an energy convergence criterion of 10^{-5} eV was fulfilled. This damped MD scheme was chosen instead of the widely used quasi-Newton or conjugate-gradient algorithms, because these caused convergence problems as well as the tendency to remain stuck in local minima. Each converged relaxation was followed up by a static calculation to obtain more accurate total energies. For electronic self-consistency cycles a convergence criterion of 10^{-6} eV was used. All simulations were performed at 0 K.

¹The term quenched MD is often used instead.

Simulation Model

To model Al/TiN interfaces, simulation cells were built from a face-centred-cubic (fcc) Al slab at the bottom and a rock salt TiN slab above (see Fig. 4.1). Such cells were constructed for the low-index surface orientations (001), (011) and (111) of both slabs. Only configurations with slabs of the same surface orientations at the interface and without any relative rotations were considered. The two slabs were separated by a gap which is given by the vertical distance between the top Al and bottom TiN layers and will be referred to as the “interface distance”. The vertical distance between the bottom Al and top TiN layers, which is the sum of the interface distance and the heights of the two slabs, is called “slab height”. In the case of (111) slabs this height is measured up to the top Ti and N layer for Ti and N termination, respectively. Unless otherwise stated, 1×1 surface cells were used, which represent an infinitely extended surface due to the periodic boundary conditions. The Al slab consisted of at least seven layers, and the TiN consisted slab of a minimum of six Ti and six N layers. These thicknesses were found to be sufficient to converge the surface energies and to mimic bulk-like features in the centre of the respective slab. These system dimensions are in good agreement with other published work [325, 328, 332, 336].

The TiN (111) slab can be terminated with either Ti or N atoms. To investigate the stability of these terminations a thermodynamic analysis [337, 338] was performed to calculate the surface Gibbs free energy for the off-stoichiometric slabs [339]. The surface Gibbs free energy Ω for surface termination i without vibrational contributions is given by

$$\Omega^i = \frac{1}{2} \left(E_{slab}^i - N_{Ti}^i E_{TiN}^{bulk} \right) - \Gamma_{Ti,N}^i E_N - \Gamma_{Ti,N}^i \Delta\mu_N, \quad (4.1)$$

where E_{slab}^i is the total energy of the slab with termination i , N_{Ti}^i is the number of Ti atoms in the slab, E_{TiN}^{bulk} is the total energy of bulk TiN and E_N is the total energy of a nitrogen atom. The two latter terms in Eq. (4.1) are necessary to calculate the surface energy of off-stoichiometric slabs. The number of off-stoichiometric atoms $\Gamma_{Ti,N}^i$ is defined

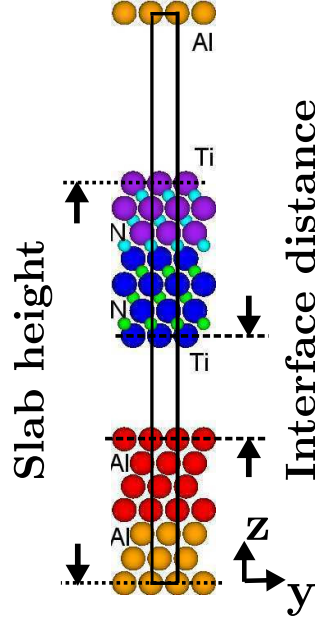


Figure 4.1: Side view of an Al (111) and Ti-terminated TiN (111) interface. The simulation interface cell is indicated by the solid black lines. During relaxations the orange Al, cyan N and purple Ti atoms were kept rigid, while the red Al, green N and blue Ti ones were allowed to relax.

as

$$\Gamma_{Ti,N}^i = \frac{1}{2} \left(N_N^i - N_{Ti}^i \frac{N_N^{bulk}}{N_{Ti}^{bulk}} \right), \quad (4.2)$$

where N_j^i and N_j^{bulk} are the number of atoms of type j in the slab and in bulk, respectively. For rock-salt bulk TiN the fraction N_N^{bulk}/N_{Ti}^{bulk} in Eq. (4.2) is equal to 1. $\Delta\mu_N$ is the deviation of the nitrogen chemical potential μ_N from the molecular reference $\frac{1}{2}E_{N_2}$,

$$\Delta\mu_N = \mu_N - \frac{1}{2}E_{N_2}. \quad (4.3)$$

In Fig. 4.2 the calculated surface Gibbs free energy is plotted for the N- and Ti-terminated TiN (111) slabs in the stability range of nitrogen in TiN obtained from the heat of formation of bulk TiN [340] at 0 K, $\Delta H_{f,(TiN)}^0 = -3.461$ eV, and the chemical potential of gas phase nitrogen, i.e., $\Delta H_f^0 \leq \Delta\mu_N \leq 0$. Fig. 4.2 shows that the favourable termination of a (111) TiN slab depends on the chemical potential of nitrogen, in agreement with the references [325, 341]. Since both cases are found in reasonable nitrogen concentration ranges, both terminations are investigated.

4.1. INTERFACE: ALUMINIUM - TITANIUM NITRIDE

Dipole corrections [342] perpendicular to the interface (z-direction) were tested for the systems but were found to be negligible. Atop the TiN slab a vacuum spacing of at least 10 Å was included to decouple periodically repeated cells in z-direction. The lattice parameters of the single slabs, 4.040 Å and 4.254 Å for Al and TiN, respectively, were obtained from bulk calculations. These values are in very good agreement with the experimental lattice constants of 4.05 Å and 4.265 Å for Al and TiN, respectively [343]. The relative error between calculated and experimental values is below 0.5%. For the simulation cells combining Al and TiN slabs, unless otherwise stated, an intermediate lattice parameter of 4.144 Å was used for the lateral xy lattice vectors to equalize the relative error of about 2.6% for both materials. For the z-direction the material-specific values were kept assuming a pseudomorphic interface. In reality such a combination of stretching and compression of thick slabs does not usually occur, but dislocations at the interface or an incommensurate contact are possible. Thus, some of the atoms on both sides of the interface would not be aligned perfectly, but rather sample slightly different local environments. For computational reasons, these different local arrangements are assessed here by considering various orientations at the interface as limiting cases.

The approach of the two slabs was simulated by moving the upper slab in discrete steps along the negative z-direction and allowing for electronic and atomic relaxations after each step. Alternatively, moving the bottom slab toward the upper slab or both toward each other would not affect the results. For the atomic relaxations the top TiN (three Ti and three N) as well as the bottom three Al layers were kept fixed at bulk-like distances, whereas the intermediate “free” ones were allowed to fully relax. This is depicted in Fig. 4.1 for the Ti-terminated (111) surface orientation. For the approaching movement a step size of 0.2 Å was used for all configurations. Before the slabs were brought into contact, the free layers were allowed to relax in order to simulate surfaces in their equilibrium for the chosen lattice parameters. The separation of the slabs was started from the equilibrium structure, i.e., the structure with the lowest energy determined during the approach. To simulate a realistic separation of the slabs only the topmost, rigid TiN layers were moved in discrete steps in the positive z-direction, again allowing for electronic and atomic relaxations after each step. The choice of the step size is crucial

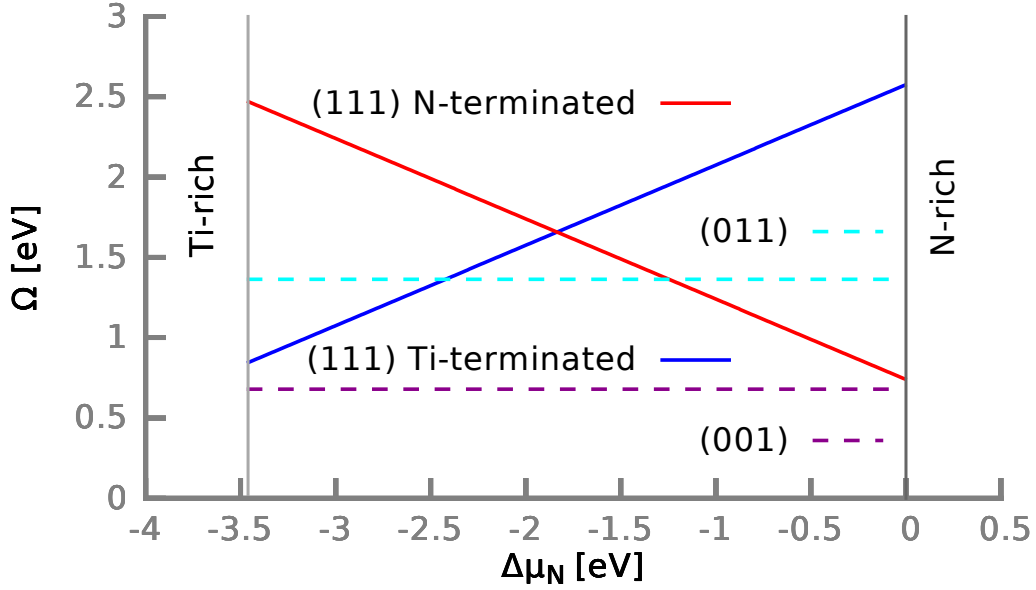


Figure 4.2: Surface phase diagram for TiN. The surface Gibbs free energy Ω [see Eq. (4.1)] referenced to a 1×1 surface cell of the (111) orientation is plotted versus the deviation $\Delta\mu_N$ of the nitrogen chemical potential from its molecular reference [see Eq. (4.3)] for N- and Ti-terminated (111) TiN slabs (solid lines) as well as for (001) and (011) orientations (dashed lines).

for the separation process. Separation velocities allowing for an adiabatic behaviour of the system were assumed, meaning that the system continuously fully adjusts during the separation at each step. However, this assumption should also be valid for velocities up to several hundreds m/s but still be considerably lower than the material-specific speed of sound, which is above 6000 m/s for Al and TiN [344]. It is evident that the step size has to be small enough to mimic the adiabatic relaxation, but on the other hand, a smaller step size leads to increased computational costs. For the investigated systems a step size of 0.1 Å was found to be a practical trade-off because calculations showed this value to be necessary to converge the final results of the simulated separation processes. Smaller step sizes down to 0.01 Å were also considered for approach and separation but did not yield qualitatively different results. Of course, the distance between the slabs where material transfer takes place can be determined more accurately, but the process itself did not change.

4.1. INTERFACE: ALUMINIUM - TITANIUM NITRIDE

In order to study the effects of different alignments of the slabs at the interface, the upper slab was also laterally placed on various sites with respect to the surface of the lower slab. The definitions of the configurations are depicted in Fig. 4.3 by marking the high-symmetry points on the low index TiN surfaces where the next Al atom can be placed. In this context the interaction energy $E_I(z)$ is an important quantity, which is defined as the difference of the total energy of the interacting slabs $E_{(Al/TiN)}(z)$ at slab height z and the reference energies of the independent slabs, $E_{(Al)}$ and $E_{(TiN)}$,

$$E_I(z) = E_{(Al/TiN)}(z) - E_{(Al)} - E_{(TiN)}. \quad (4.4)$$

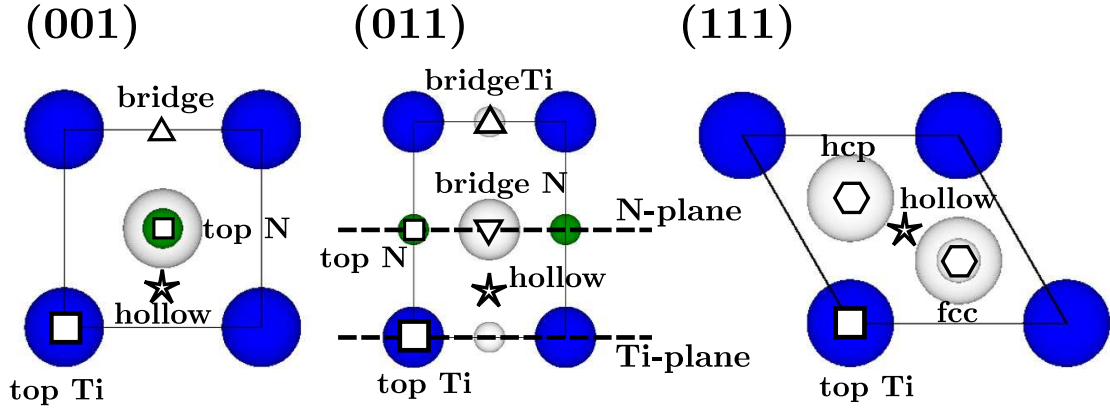


Figure 4.3: Top view of (001), (011) and Ti-terminated (111) TiN surfaces. For each orientation the 1×1 surface cell is presented. Filled circles indicate atoms in the top surface layer (Ti and N are given by large blue and small green circles, respectively), while empty circles label atoms below the top surface layer. To obtain a N-terminated (111) TiN surface the Ti and N atoms of the Ti-terminated surface have to be exchanged. High-symmetry points are highlighted. For the TiN (011) surface the “Ti plane” and “N plane” are marked by dashed lines.

4.1.3 Results and Discussion

Removal of Layers from an Al Slab

As a first step the energy cost for removing layers from an Al slab was examined for all three low-index surface orientations. The removal of selected layers was simulated by

4.1. INTERFACE: ALUMINIUM - TITANIUM NITRIDE

placing these layers at a large distance from the slab, which does not allow for interactions between the slab and the separated layers. The TiN slab is not investigated here because the Al slab is assumed to be mainly affected by deformations or material transfer within an Al/TiN interface since TiN forms a much more rigid lattice. This assumption is validated by simulations presented in section 4.1.3. The energetical results for the removal of the top Al layer are given in Tab. 4.1. These removal energies are calculated for simulation cells using the bulk lateral lattice parameters as well as the modified ones used for the Al/TiN simulation cell. For the modified lattice parameters the removal energies are typically overestimated by about 5–10%, meaning that it is actually easier to remove layers from the equilibrium structure. The increased removal energy for the modified Al slab occurs because the lateral stretching causes a vertical compression of the slab if relaxations are allowed. This compression occurs to minimize the volume change and locally strengthens the bonding of the surface layers. This effect is strongest for the top surface layer, which moves about 0.24 Å towards the rigid part and becomes weaker for the subsurface layers; for example, the fourth layer is only shifted by about 0.08 Å.

The influence of compressive and tensile stress on the removal energies of the top Al layer is illustrated in Fig. 4.4 for the three low-index surface orientations. The data points for the (001) and (111) surfaces follow a similar trend, whereas the behaviour of the (011) surface clearly deviates. This difference occurs probably due to the openness of the (011) surface and the significant impact of relaxations. The influence of stress, found for all surfaces, supports the notion of stress-assisted wear [70, 141], which states the possibility of a reduction of the activation barriers for the detachment of atoms from a structure due to stress. Furthermore, different approximations for the exchange correlation functional were tested. As expected it was found that LDA and the vdW-DF optB86b yield larger removal energies by about 15–20%, where LDA typically gives values larger by a few percent than the vdW-DF (see Tab. 4.1).

Lateral Alignments at the Al/TiN Interface

Effects of various lateral alignments of the slabs at the interface (see Fig. 4.3) were investigated for the different surface orientations. These studies revealed the strong dependence

4.1. INTERFACE: ALUMINIUM - TITANIUM NITRIDE

	(001)	(011)	(111)
PBE (a_{Al})	1.08	1.78	0.78
PBE ($a_{Al/TiN}$)	1.16	1.79	0.87
LDA ($a_{Al/TiN}$)	1.33	2.02	1.02
vdW ($a_{Al/TiN}$)	1.27	1.89	1.00

Table 4.1: Energy costs to remove the top layer from an Al slab for the (001), (011) and (111) surface orientations using PBE, LDA and vdW-DF optB86b. The removal energies are given in eV per 1×1 surface cell. a_{Al} is the Al bulk lattice parameter, whereas $a_{Al/TiN}$ corresponds to the modified Al/TiN interface.

of equilibrium properties such as adhesion energies and the equilibrium distances on the chosen configuration. The calculated interaction energies [Eq. (4.4)] of relaxed interfaces are shown in Figs. 4.5a – d for slab heights around the energy minima, which are equivalent to the adhesion energies for each alignment. In general, the top Al atoms prefer the proximity of N atoms over Ti. The bonding situation will be discussed in more detail in the following paragraphs. From an energetical point of view material transfer between the slabs should be possible only if the energy cost to remove layers is compensated for. Thus, the energy gain due to adhesion has to be larger than the energy cost to remove one or more layers. This argument is sketched in Figs. 4.5a – d by including a horizontal line at the negative value of the Al removal energy for each surface orientation. It has been observed experimentally that metal-ceramic interfaces with weak and strong interfacial adhesion break upon stress at the interface and in bulk areas, respectively [345, 346]. We find that the four surfaces investigated exhibit essentially different behaviour. The adhesion energies and the equilibrium distances, i.e., the slab heights at the minimum of each energy curve, depend strongly on the surface orientation as well as on the alignment at the interface. In the case of the (111) surfaces all configurations should lead to the removal of at least one Al layer. For the (011) surfaces this is the case only for three alignments, Al/N (top), Al/TiN (hollow) and Al/N (bridge) (see Fig. 4.3). In contrast, for the (001) surfaces no material transfer should occur since for all cases studied the energy to remove one Al layer is larger than the adhesion energy.

As mentioned above, in reality, surfaces with a bulk lattice mismatch are usually not perfectly aligned at an interface. Consequently, not all atoms are placed on the same

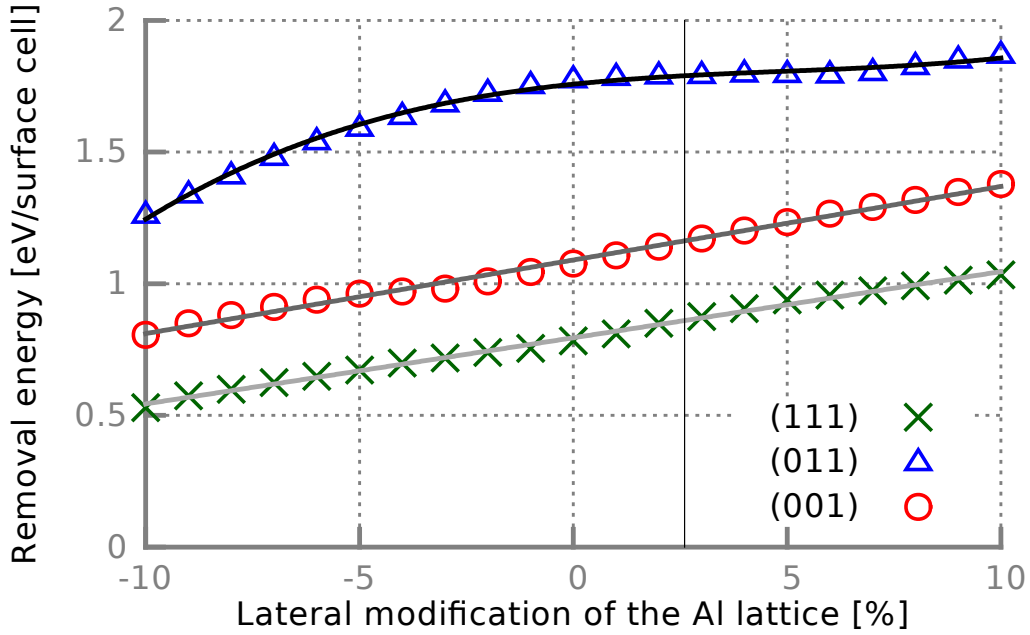


Figure 4.4: PBE energy costs to remove the top Al layer for the (001), (011) and (111) surface orientations. The lateral effects of stretching and compression of the 1×1 surface cell on the removal energies are shown. The Al bulk lattice constant is used as a reference value at 0%. The vertical line indicates the intermediate Al/TiN interface lattice parameter, while the other solid lines are given to guide the eye.

contact site, i.e., some would be placed close to favourable fcc sites, while others closer to more unfavourable top sites. Thus, the interfacial properties such as the adhesion energy are an average of the actually occupied sites. The configurations presented here, however, constitute limiting cases of perfectly aligned systems, such that the properties of real interfaces should be found within these boundaries.

Generally, relaxation effects have to be accounted for to obtain the correct equilibrium values of the adhesion energy and the interface distance as well as to predict the occurrence of material transfer. A comparison between the relaxed and static results is shown in Fig. 4.6 for the studied surfaces. For rather closed TiN surfaces, such as the (001) and Ti-terminated (111) orientations (see Fig. 4.6a), relaxations typically cause only small changes in the equilibrium quantities of the interface. Hence, computationally “cheap” static calculations give good estimates, unless pronounced changes in the structure of the Al slab occur. This is, for example, the case for the Al/Ti (hollow) alignment of the

4.1. INTERFACE: ALUMINIUM - TITANIUM NITRIDE

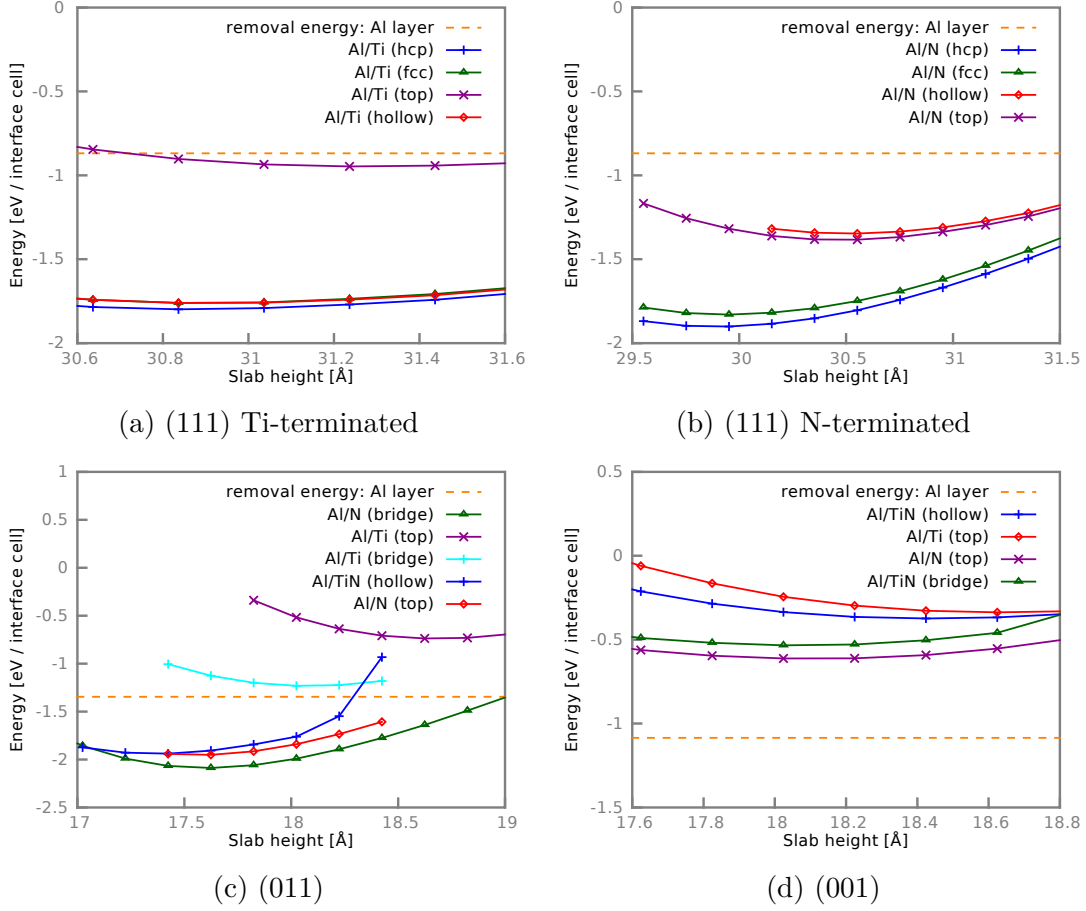


Figure 4.5: Calculated PBE interaction energies of the relaxed Al/TiN interface for the (111) Ti-terminated, (111) N-terminated, (011) and (001) surface orientations. Various lateral alignments of the two slabs are considered, see Fig. 4.3. The horizontal dashed orange lines give the energy costs to remove at least one layer from an Al slab of the corresponding surface orientation.

(111) Al/TiN (Ti-terminated) interface since the interfacial Al atom relaxes towards the energetically more favourable fcc contact site. In the case of the more open (011) surface, relaxations show more pronounced effects for all alignments and should be taken into account. Nevertheless, the energy hierarchy and the prediction of the occurrence of material transfer are not affected for all alignments with the exception of the Al/TiN (hollow) case. Again, the Al/TiN (hollow) interface behaves differently because the relaxed structure of the Al slab is modified by the approaching TiN slab. In more detail the interfacial Al layer is moved to the Al/N (bridge) site, which is the most favourable alignment. This movement of about 0.8 Å occurs mainly in the lateral plane. The free subinterface layers

4.1. INTERFACE: ALUMINIUM - TITANIUM NITRIDE

are shifted to gradually compensate the change in the stacking between the fixed layers at the bottom of the slab and the interfacial layer. These shifts range approximately between 0.2 Å and 0.6 Å. For the cases discussed so far, except for the hollow alignments, relaxations showed rather small effects on the equilibrium quantities. In contrast, all alignments of the (111) Al/TiN (N-terminated) interface are crucially affected by relaxations (see Fig. 4.6b). The adhesion energies are strongly increased, and the energetical hierarchy of the alignments is altered. Furthermore, while static calculations suggest the absence of material transfer, relaxations predict its occurrence for all tested alignments.

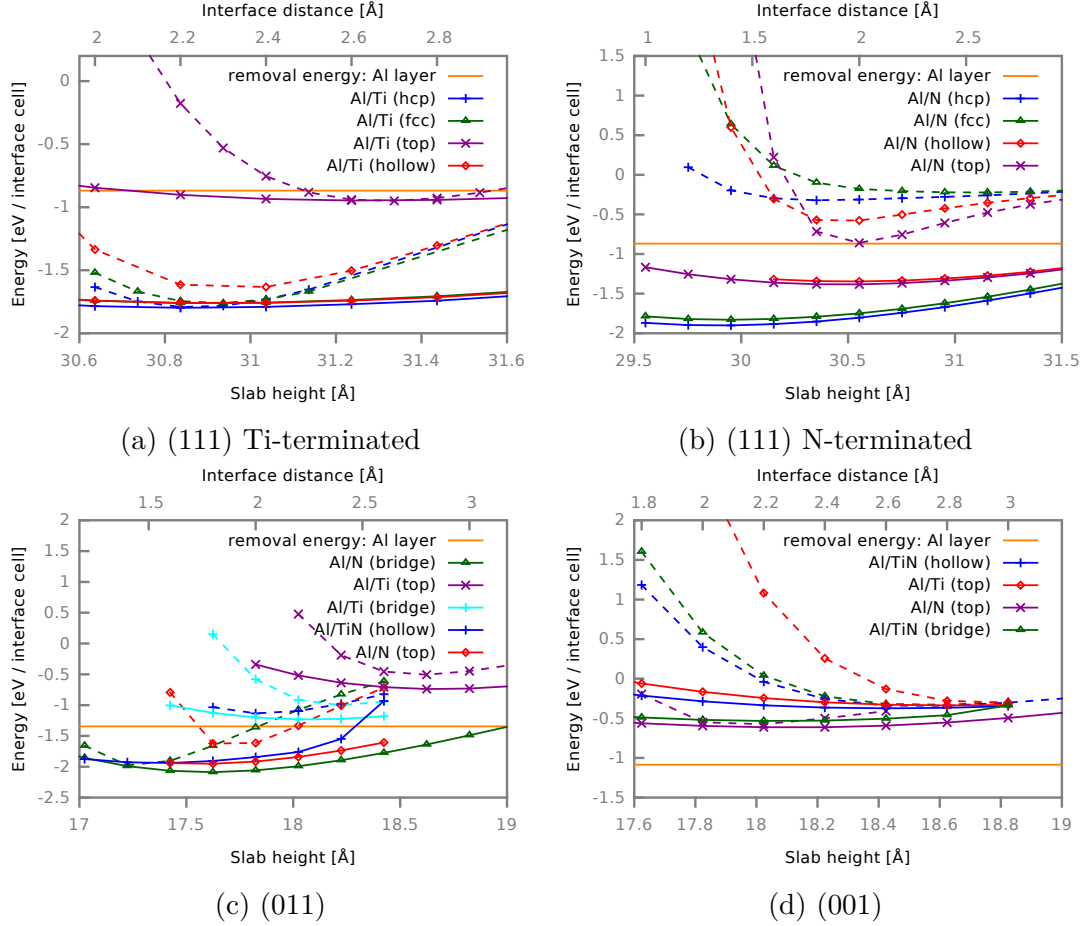


Figure 4.6: Calculated PBE interaction energies of the Al/TiN interface for the (111) Ti- and N-terminated surfaces. Solid and dashed lines indicate results of relaxed and static calculations, respectively. The slab heights on the lower x-axis are valid for static and relaxed calculations, whereas the interface distances on the upper x-axis refer only to the static calculations. Various lateral alignments of the two slabs are considered, see Fig. 4.3. The horizontal solid orange lines give the energy costs to remove at least one layer from an Al slab of the corresponding surface orientation.

4.1. INTERFACE: ALUMINIUM - TITANIUM NITRIDE

For a better understanding of the energetically preferred configurations at the interface, layer-projected densities of state (DOSs) and differences in charge densities are examined. Layer-projected DOSs are displayed in Fig. 4.7 for the two alignments Al/N (bridge) and Al/Ti (top) as well as the isolated slabs of the (011) surface orientation. This surface orientation has been chosen because it exhibits a large spread in adhesion energies for different alignments. Additionally, the occurrence of material transfer should depend on the alignment. In Fig. 4.7 “interface (surface) layers” indicate the first layers of Al, Ti and N immediately at the interface (surface), whereas “subinterface (subsurface) layers” mean the next layers of Al, Ti and N moving deeper into both materials. Further layers are not presented because they exhibit only minor differences with respect to the subinterface layers. The DOSs of the shown alignments display distinct features. For the Al/Ti (top) case, where Ti is the next interfacial neighbour of the top Al atom, the Al DOS is almost not affected by the interface. Only a small accumulation of sp states just below the Fermi energy and a depletion of s states at the edges of the DOS are found for the interface layers with respect to the other layers. The N sp states are shifted closer to the Fermi energy for the interfacial layer, and in particular, the Ti d states exhibit more occupied states at the Fermi energy. These changes indicate a weakly covalent bonding between the Al sp states and the Ti d states. Furthermore, the DOS is very similar to the case of the isolated Al and TiN slabs. This also shows the weak interaction for the Al/Ti (top) interface. On the other hand, for the Al/N (bridge) configuration, where the uppermost Al atoms are closer to N across the interface, the Al DOS is changed in a more pronounced way. The sp states in the interface layers are partially shifted to lower energies, resulting in a pronounced peak at about -8 eV and a few minor ones around -7 eV. The N p states around -5 eV are broadened in the interfacial layer resulting in common peaks with Al states roughly between -6 eV and -8 eV. These effects at the interface indicate a hybridization of Al and N sp states and explain the stronger adhesion due to covalent interaction. The interfacial Ti states are only slightly affected, exhibiting a few more occupied states at the Fermi level.

In addition to the DOS, charge densities at the interfaces are investigated and presented for the same alignments of the (011) surface. For a better visualization the differences

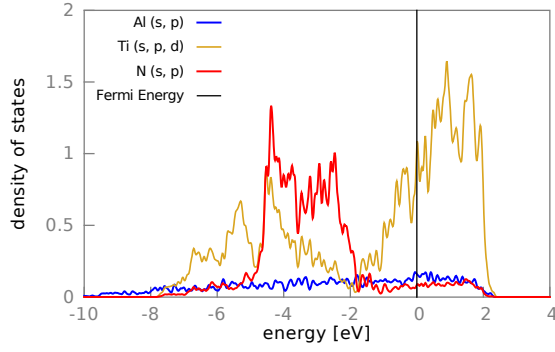
4.1. INTERFACE: ALUMINIUM - TITANIUM NITRIDE

of charge densities ρ_{diff} between the Al/TiN interface and the isolated, independent Al and TiN slabs are presented in Fig. 4.8. The charge-density difference ρ_{diff} is defined as

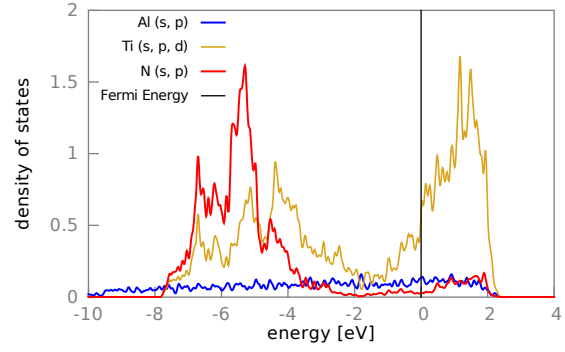
$$\rho_{diff} = \rho_{Al/TiN} - (\rho_{Al} + \rho_{TiN}), \quad (4.5)$$

where $\rho_{Al/TiN}$ is the charge density of the interface, while ρ_{Al} and ρ_{TiN} represent the charge densities of the isolated slabs. Both displayed alignments result in a rather continuous charge accumulation between Al and Ti at the interface suggesting a bonding (see Fig. 4.8a and Fig. 4.8c). For the Al/N (bridge) configuration an additional charge buildup occurs between the interfacial Al and N atoms, which indicates covalent contributions to the bonding due to the more localized and directional character of the accumulation (see Fig. 4.8d). These findings support the DOS arguments made in the previous paragraph.

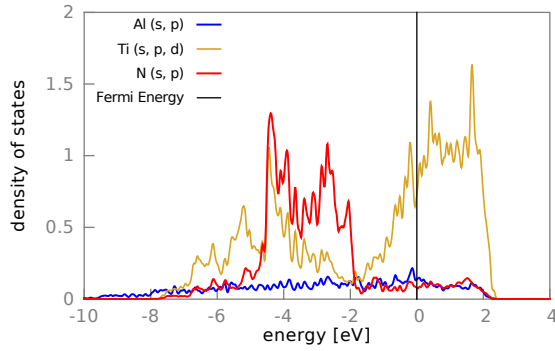
4.1. INTERFACE: ALUMINIUM - TITANIUM NITRIDE



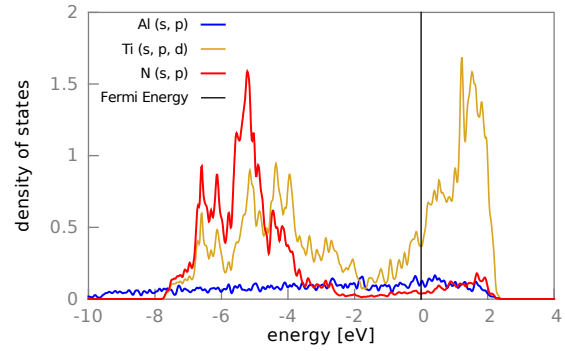
(a) Al & TiN (isolated): surface layers



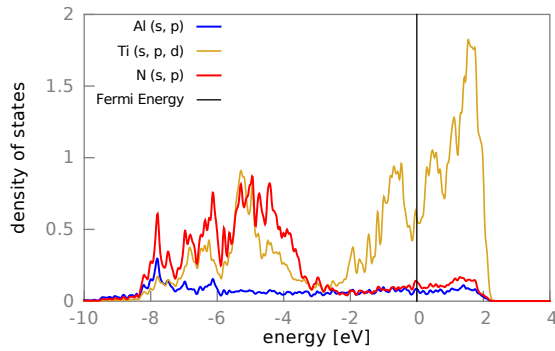
(b) Al & TiN (isolated): subsurface layers



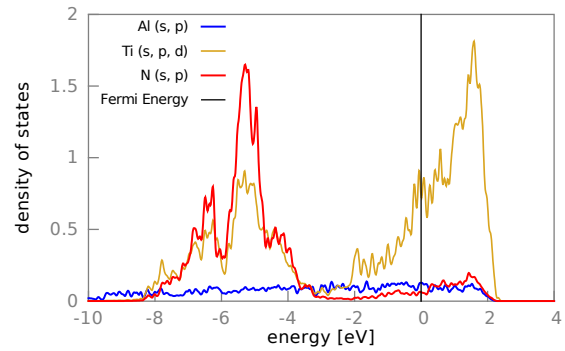
(c) Al/Ti (top): interface layers



(d) Al/Ti (top): subinterface layers



(e) Al/N (bridge): interface layers



(f) Al/N (bridge): subinterface layers

Figure 4.7: Layer-projected DOSs from PBE calculations of the isolated Al and TiN slabs as well as of the Al/TiN (011) interface for the Al/Ti (top) and Al/N (bridge) alignments. The Fermi energy is shifted to 0 eV.

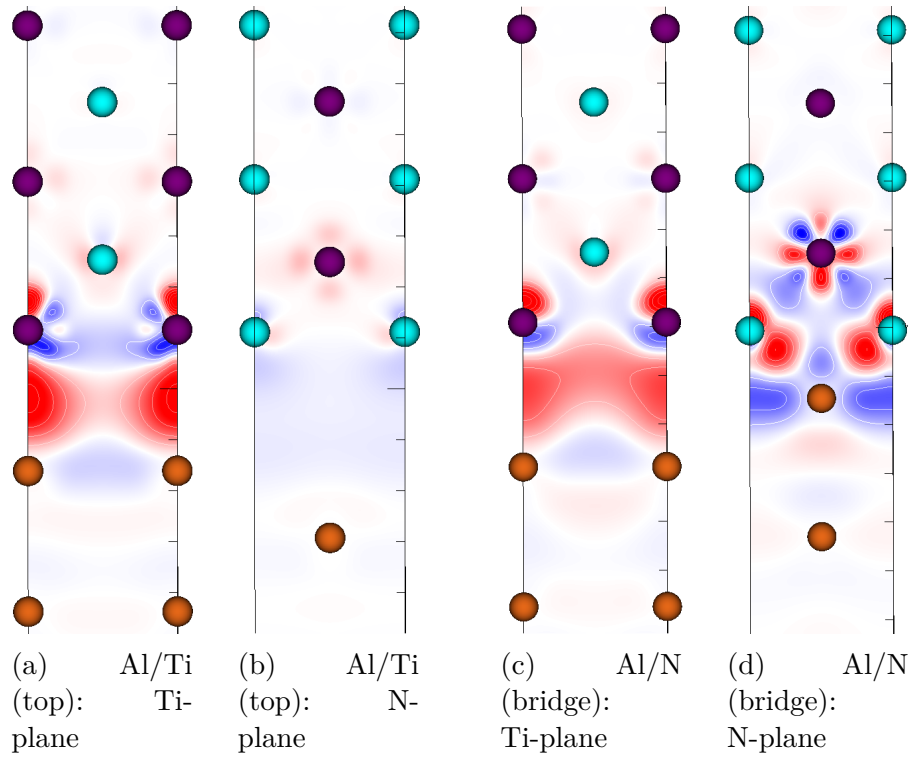


Figure 4.8: Charge-density differences (ρ_{diff}) [see Eq. (4.5)] of the Al/TiN (011) interface. ρ_{diff} was obtained from PBE calculations for the relaxed equilibrium configurations of the Al/Ti (top) alignment (subfigures (a) and (b)) as well as of the Al/N (bridge) alignment (subfigures (c) and (d)). The charge-density difference of each alignment is plotted for the “Ti plane” and the “N plane” (recall Fig. 4.3) for values from -0.2 (solid blue, deficit) to 0.2 (solid red, accumulation) electrons/Å³. Colour code: Al (orange), Ti (violet) and N (cyan).

Approach and Separation of Al and TiN Slabs

The energetical argument on material transfer presented above can be tested by “slowly”, i.e., using small discrete steps, approaching and subsequently separating the slabs. The energetical results of such loops are depicted in Figs. 4.9a – d for different configurations, the respective energies are presented in Tab. 4.2. The green curves with their data points indicated by pluses in Figs. 4.9a – d give static potential-energy curves, where all atoms were kept rigid for each selected interface distance. For large interface distances this curve shows the limiting case of separated, independent slabs. For ever-shorter distances the effect of relaxation becomes important, and the actual energies deviate from the green curves. The blue curves with their data points marked by crosses show the interaction energies of the approaching slabs including atomic relaxations after each discrete step. For some of these cases we find rather large jumps which are either due to material transfer between the slabs, namely, from Al to TiN, or due to the Al slab expanding into the space between the slabs. The initial material transfer always occurred during a single relaxation like a binary event. However, during this single relaxation the layer(s) do not jump across the gap at once, but are moving rather slowly towards the other slab. Typically up to several hundreds of atomic steps are necessary to converge the relaxation, when material transfer occurs. In that sense during one relaxation many intermediate states are tested, but since they are energetically unfavourable, the relaxation continues. Finally, the red curves with their data points displayed by circles indicate the interaction energies of the subsequent separation of the slabs, again including atomic relaxations after each step. These curves are also not completely smooth but display some kinks or smaller jumps mainly due to the breaking apart of the Al/TiN slab into two separated ones. When material transfer takes place, these curves, of course, do not approach the green ones, even at large slab separations.

To obtain reliable results especially the atomic relaxations after each discrete step are crucial. At first commonly used quasi-Newton and conjugate-gradient algorithms were employed to relax the structures. Both approaches, however, ran into problems. Performing calculations using the quasi-Newton method hardly yielded any converged

4.1. INTERFACE: ALUMINIUM - TITANIUM NITRIDE

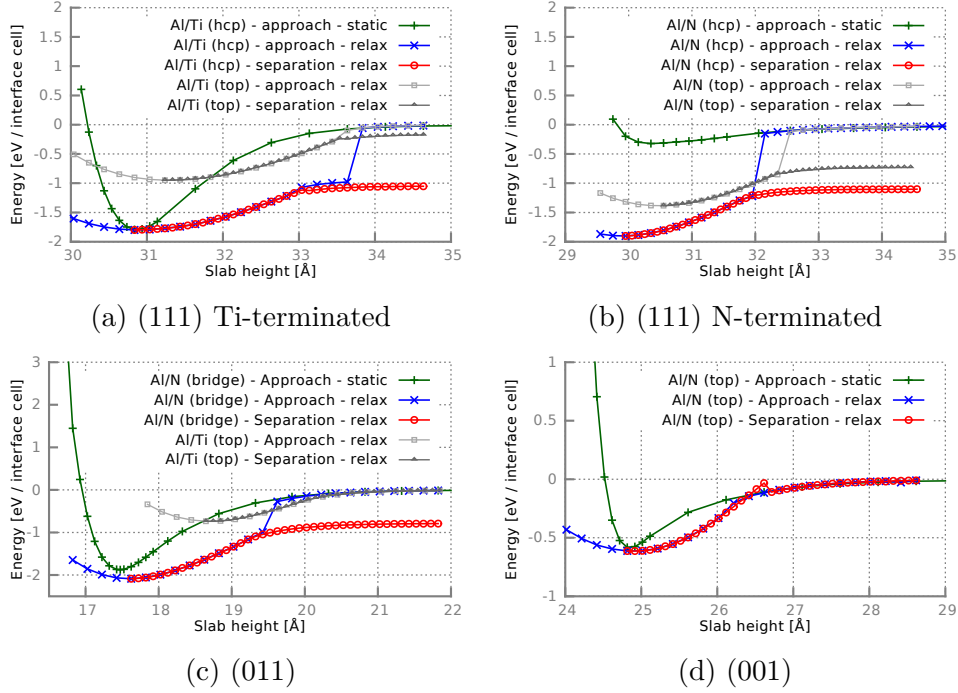


Figure 4.9: Calculated PBE interaction energies, see Eq. 4.4, for the approach and subsequent separation of Al and TiN slabs for (111) Ti-terminated, (111) N-terminated, (011) and (001) surface orientations. The alignments follow the definitions in Fig. 4.3.

results. The conjugate-gradient algorithm showed no convergence problems and produced energy curves (see Fig. 4.10a) similar to the ones presented above using damped MD (see Fig. 4.9a). However, the energy gain after separation was significantly smaller and the examination of the structural results revealed nonphysical results such as floating separated Al layers (see Fig. 4.10b). These findings indicate problems with local minima, which can be avoided usually by using a damped MD scheme.

For the Ti-terminated (111) surface orientation potential-energy curves are presented in Fig. 4.9a for the two extremal alignments, Al/Ti (hcp) and Al/Ti (top), which show the highest and lowest adhesion energies. As expected from the energetics, material transfer occurs during separation, and both systems end up in an energetically more favourable configuration compared to the initial setup. In particular, two and one Al layer(s) for Al/Ti (hcp) and Al/Ti (top), respectively, are transferred (see Figs. 4.11h and 4.12d). This discrepancy in the number of transferred layers cannot be explained from the energetics but could stem from the different equilibrium interface distances. Compared

4.1. INTERFACE: ALUMINIUM - TITANIUM NITRIDE

	Equilibrium interface distance [Å]	Adhesion energy [eV]	Removal energies [eV]	Material transfer [Al layers]
(001) Al/N (top)	2.06	-0.61	1.16	0
(011) Al/N (bridge)	1.39	-2.09	1.35	2
(011) Al/Ti (top)	2.77	-0.73	1.35	0
(111) Al/Ti (hcp)	2.22	-1.78	0.80	2
(111) Al/Ti (top)	2.67	-0.94	0.80	1
(111) Al/N (hcp)	1.04	-1.90	0.80	2
(111) Al/N (top)	1.87	-1.38	0.80	1

Table 4.2: Equilibrium interface distances, adhesion energies, energy costs to remove layers from the Al slab, and number of transferred Al layers for various interface configurations. For the (111) orientation Al/Ti and Al/N denote the Ti- and N-terminated surfaces, respectively. All energies are given per interface cell.

to that of the hcp alignment, this distance is significantly increased by almost 20% for the top configuration, hindering the interaction between TiN and the subinterface Al layer. For the Al/Ti (hcp) configuration snapshots of the structures during approach and separation are presented in Fig. 4.11. Furthermore, in the introduction (see section 1) a link is provided in Fig. 1.1a which leads to a movie showing the approach and subsequent separation of this alignment. For the Al/Ti (top) configuration images of the separation are presented in Fig. 4.12. During the approach at a slab height of about 33.6 Å a large drop in interaction energy occurs for the Al/Ti (hcp) alignment (see Fig. 4.9a) due to material transfer of the topmost Al layer to the TiN slab (see Fig. 4.11b). This is not the ground state since a transfer of two layers would yield an even lower total energy. At this distance, the transfer of the second Al layer is hindered by an energy barrier of about $E_{b2} \approx 324$ meV, which is significantly larger than for the first layer alone, $E_{b1} \approx 122$ meV. Upon further approaching, at a slab height of about 32.8 Å, a slight kink occurs (see Fig. 4.9a) because the Al slab is expanded into the space between the slabs (see Fig. 4.11c). For a further approach, the interaction energy follows an essentially parabolic curve until the minimum energy is reached (see Figs. 4.9a and 4.11d). The subsequent separation is started from the equilibrium structure at the interaction energy minimum. At first the red interaction energy curve lies on top of the blue one (see Fig. 4.9a), meaning that the

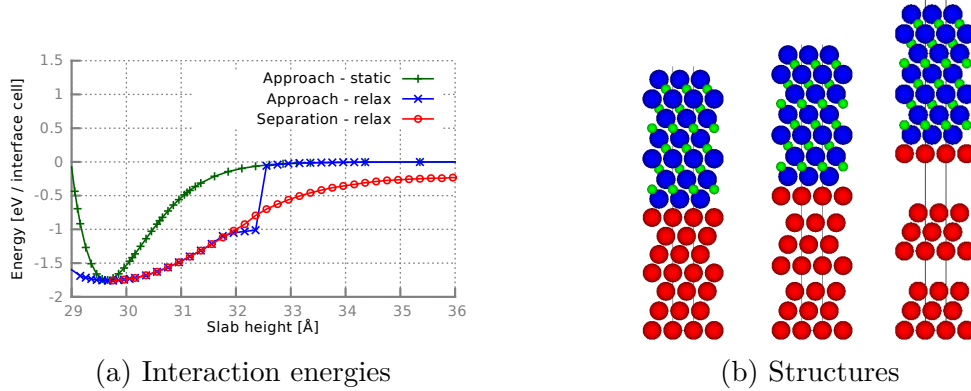


Figure 4.10: Results of calculations using the conjugate-gradient algorithm for the interface between Al and Ti-terminated TiN slabs in the Al/Ti (hcp) alignment. Subfigure (a) gives the calculated PBE interaction energies for the approach and subsequent separation of the slabs. In Subfigure (b) three snapshots of the interface during the separation are displayed. These images are taken at the slab heights of 29.56, 32.56 and 37.36 Å (from the left).

Al slab becomes extended again (see Fig. 4.11f). At a slab height of about 33.1 Å the two curves for approach and separation start to deviate (see Fig. 4.9a) when the Al/TiN compound separates (see Fig. 4.11g). Two Al layers stick to the TiN slab and form a stable configuration. This behaviour during the complete loop is typical for all cases exhibiting material transfer. While the Al slab is strongly affected by the approach of the TiN slab, almost no changes in the TiN structure are observed. The more pronounced impact on the Al slab is not surprising when considering that TiN forms a much more rigid lattice than Al. This claim is not entirely valid for the N-terminated (111) TiN slab, which will be discussed in the following paragraph. Using the finally stable state (TiN plus two Al layers) as a starting configuration for a new loop of approach and separation versus an Al slab yields a reversible cycle. This should be kept in mind when one is interpreting, for example, AFM experiments. However, it should be stressed that the simulations here are a very crude model for a real AFM. Even considering a rather blunt AFM tip roughness is important. The more an ideal sharp tip is approached, the larger the differences between an AFM and current simulations will become. A sharp tip would probably detach only a few or a single atom(s) from the investigated surface and not an entire layer or a “large” cluster. In addition, depending on the materials

4.1. INTERFACE: ALUMINIUM - TITANIUM NITRIDE

also material transfer in the other direction should be possible. Thus, it seems likely that the surface is only damaged/alterd in a minor way and will change (reconstruct) due to the missing/additional atoms. Consequently, the tip would not see exactly the same surface upon another approach. Furthermore, at finite temperatures thermal effects might be important, which could further change the surfaces as well as the tip after material transfer. Of course, these considerations are important for the reproducibility of experiments, but at this point they are merely speculations. From the work done here it can be stated that upon the first contact between the tip and a particular spot on a surface material transfer might occur, which in turn changes the contact properties and forces between the tip and the surface. However, further encounters on the same spot should then be within the reversible cycle and lead to the same response.

The N-terminated (111) orientation is, in some respects, very similar to the Ti-terminated one. As predicted, both configurations yield material transfer for all tested alignments (see Fig. 4.9). For the Al/N (hcp) configuration snapshots of the structures during approach and separation are presented in Fig. 4.13. In contrast to the Ti-terminated surface, as explained above, static calculations however completely fail to describe the equilibrium quantities of the N-terminated case. This discrepancy is due to the behaviour of the interfacial N layer for N-terminated (111) TiN. In the absence of the counter Al slab, the surface N layer is closely bound to the next Ti layer at a distance of 0.84 Å, while in contact with an Al slab the distance grows to 1.47 Å at the equilibrium configuration. This behaviour is crucial for the energetics and can be captured only when relaxations are included. The interfacial N layer is actually closer to the next Al layer with a distance of 1.11 Å than to the next Ti one. Due to this result the possibility of a diffusion of the interfacial N layer into the Al slab was investigated. For all but the Al/N (top) alignments no energetically favourable configurations were found. However, for the Al/N (top) alignment the exchange of the interfacial Al and N layers and a subsequent relaxation of the system yield a favourable state by about 683 meV, which is also about 235 meV lower than the previously found minimum for the Al/N (hcp) alignment. In this favourable configuration an Al-N-Al tri-layer is formed showing the wurtzite structure, which is typically observed in aluminium nitride crystals. From the thermodynamical

4.1. INTERFACE: ALUMINIUM - TITANIUM NITRIDE

point of view diffusion seems to be possible. Of course, for the full picture reaction paths and energy barriers have to be considered.

The (011) surface orientation also presents an interesting case because due to the energetic results (see Fig. 4.5c), material transfer is expected for only the alignments Al/N (bridge), Al/N (top) and Al/TiN (hollow). As an example, one can see from the loops given in Fig. 4.9c that Al/N (bridge) shows an favourable configuration after separation corresponding to the transfer of two Al layers, whereas the Al/Ti (top) case is reversible upon approach and separation without any material transfer.

Finally, for the (001) surface orientation material transfer is not expected for any of the alignments. Among all cases Al/N (top) has the largest adhesion energy; therefore, if a material transfer occurs, it will happen for this case. However, since the energy cost for the removal of an Al layer exceeds the adhesion energy, no material transfer is observed (Fig. 4.9d). The deviation of the curves for approach and separation around 26.5 Å slab height occurs due to the expansion of the Al slab upon separation until the interface breaks apart and relaxes into the initial Al and TiN slabs. Snapshots of the structures during separation are presented in Fig. 4.14.

In the literature some publications on tensile test simulations of Al/TiN interfaces can be found, where the separation is achieved by increasing the size of the whole simulation cell in one direction in discrete steps including interim relaxations. Liu et al. [326] and Zhang et al. [328] investigated the Al/TiN (111) and (001) interfaces, respectively. Liu et al. obtained similar results with respect to material transfer for the hcp alignment at the (111) surface for both terminations but did not examine any further alignments of Al and TiN slabs at the interface. Zhang et al. studied the Al/N (top) configuration of the (001) interface and, in contrast to our work, found a material transfer of the top Al layer. This discrepancy could stem from the different simulation approaches and computational details. However, the calculations presented above were repeated using a setup for the separation of the slabs similar to that of Zhang et al. and did not result in any material transfer. Additional simulations for the different setups used by Zhang et al. and in the present investigation testing the influence of varying step sizes also did not lead to a material transfer.

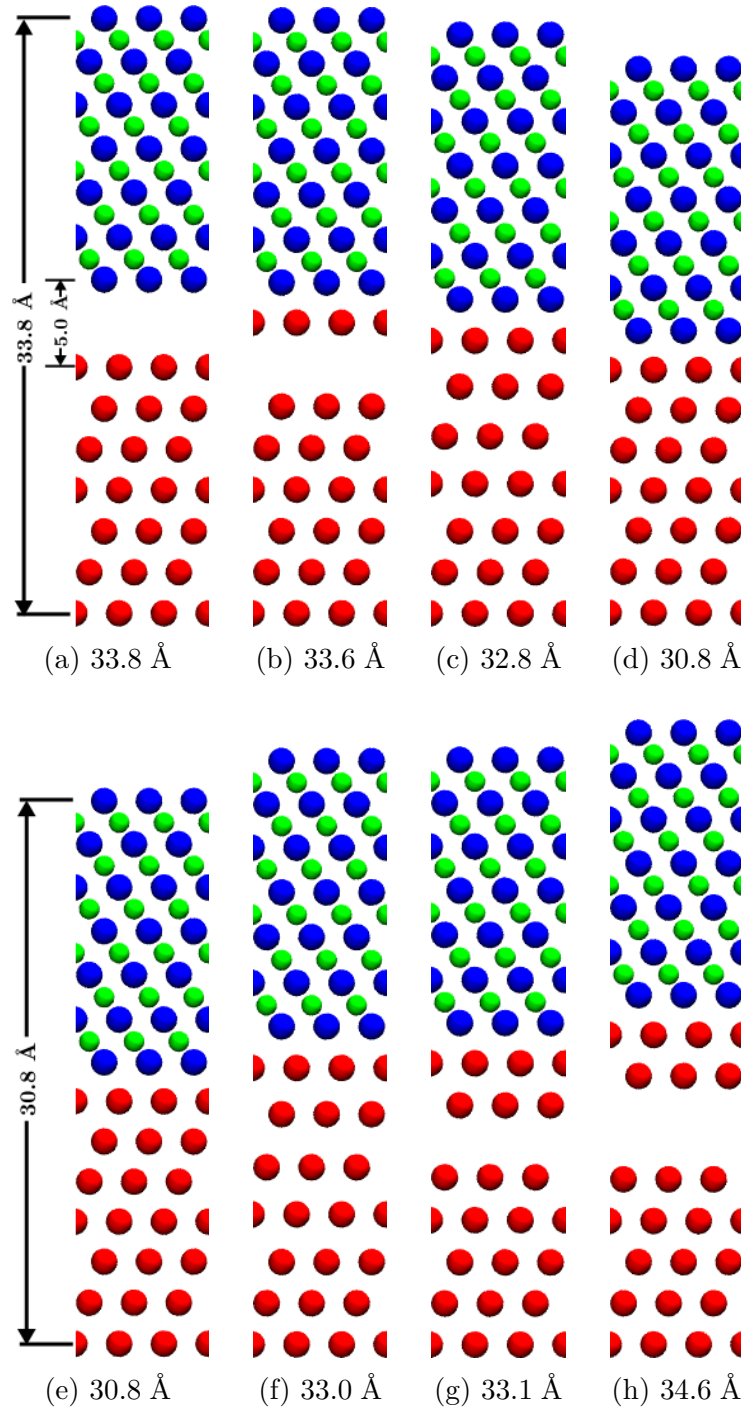


Figure 4.11: Approach (a–d) and separation (e–h) of Al/Ti (hcp) aligned Al (111) and Ti-terminated TiN (111) slabs. Al, Ti and N are coloured in red, blue and green, respectively. Subfigures (d) and (e) show the structure at the relaxed equilibrium distance. The steps are defined by the slab height.

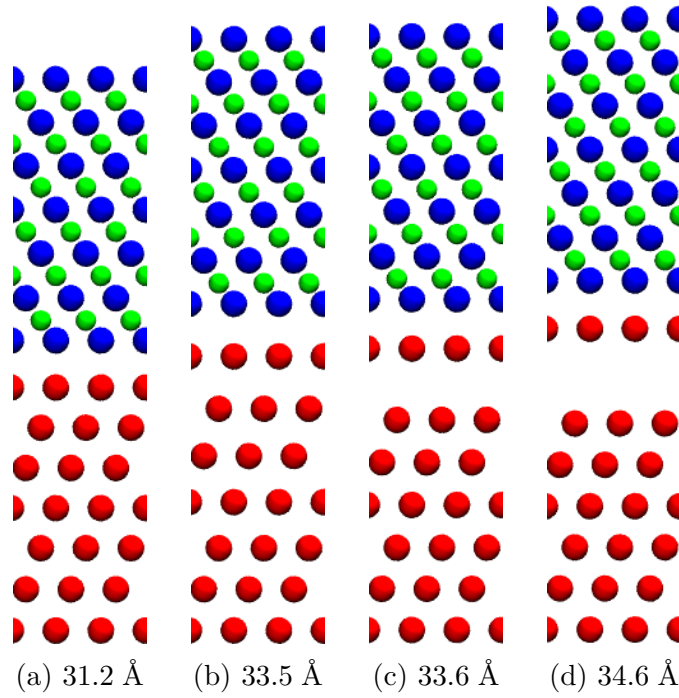


Figure 4.12: Separation (a–d) of Al/Ti (top) aligned Al (111) and Ti-terminated TiN (111) slabs. Al, Ti and N are coloured in red, blue and green, respectively. Subfigure (a) shows the structure at the relaxed equilibrium distance. The steps are defined by the slab height.

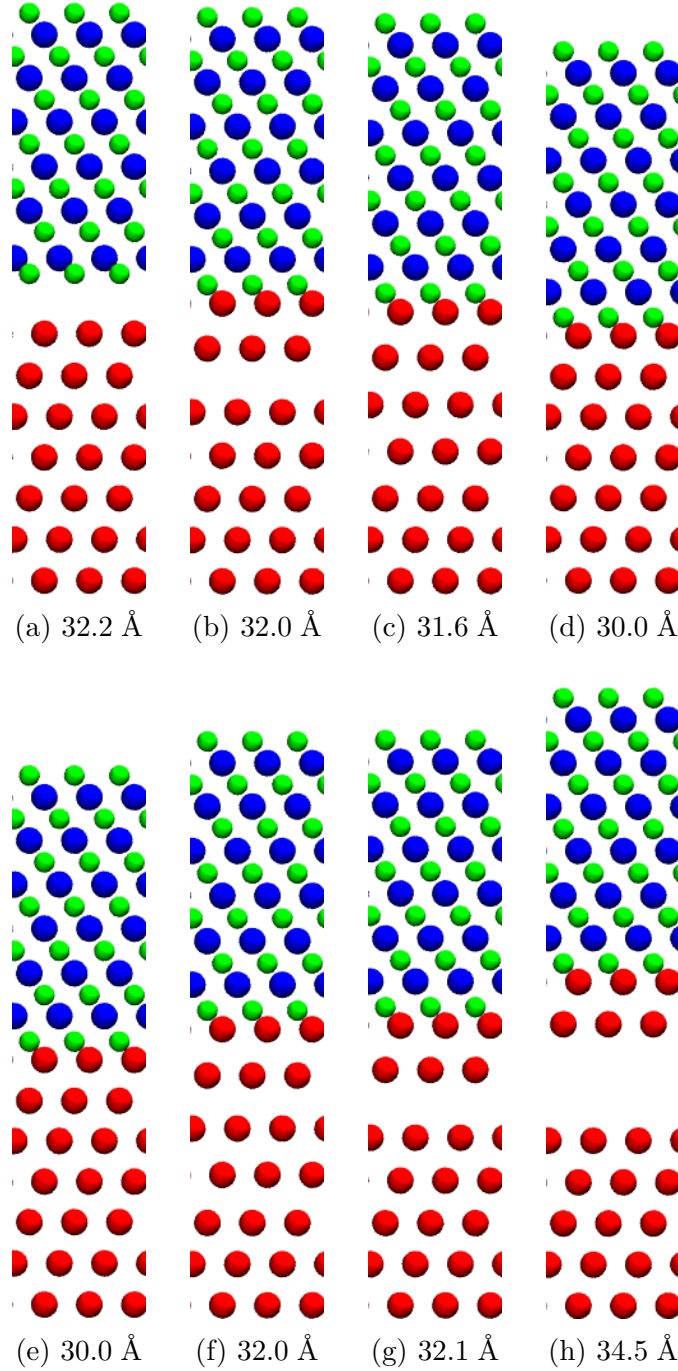


Figure 4.13: Approach (a–d) and separation (e–h) of Al/N (hcp) aligned Al (111) and N-terminated TiN (111) slabs. Al, Ti and N are coloured in red, blue and green, respectively. Subfigures (d) and (e) show the structure at the relaxed equilibrium distance. The steps are defined by the slab height.

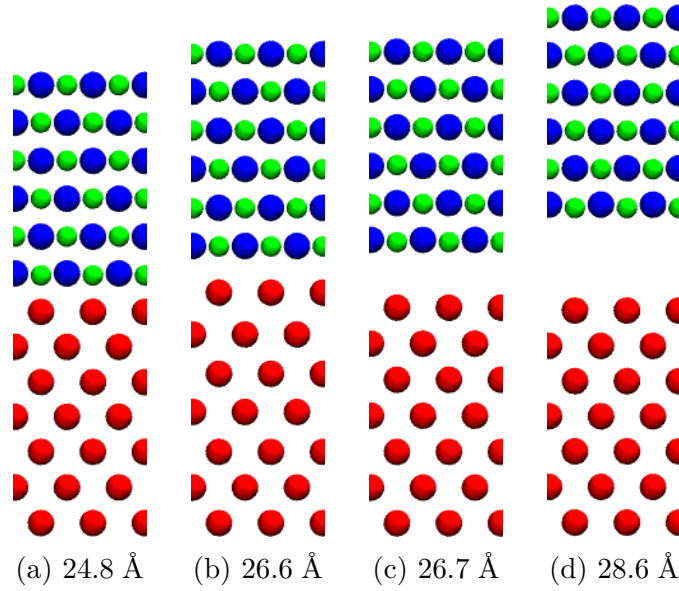


Figure 4.14: Separation (a–d) of Al/N (top) aligned Al (001) and TiN (001) slabs. Al, Ti and N are coloured in red, blue and green, respectively. Subfigure (a) shows the structure at the relaxed equilibrium distance. The steps are defined by the slab height.

Comparison of Surface Energies

The behaviour of the different surface orientations can also be discussed from the surface energy's point of view. The surface energies for Al and TiN slabs are presented in Tab. 4.3. It has to be noted that for (111) TiN the surface energy depends on the termination and the chemical potential of nitrogen. Here the lowest possible value for the surface energy is used, which is achieved by the N-terminated surface at $\Delta\mu_N = 0$ (see Fig. 4.2). The value of the surface energy for the Ti-terminated surface at $\Delta\mu_N = 0$ is about three times larger, but its minimum is comparable to that of the N-terminated case. For the (001) and (011) orientations the surface energy is independent of the chemical potential [341]. As shown in Tab. 4.3, the Al surfaces always exhibit a smaller surface energy than the TiN ones. The differences between Al and TiN are pronounced for the (011) and (111) orientations. For (001), however, the surface energies are rather comparable. Material transfer can be seen as a measure of surface-energy minimization by creating a new energetically cheap surface and covering an expensive one with it. This argument provides a hint about which surface orientations may favour material transfer. However, for the full picture other contributions such as the interaction energy, influenced additionally by the alignment of the slabs, also have to be considered. For example, the surface-energy argument would suggest the possibility of material transfer for (001) and cannot explain why only some (011) configurations exhibit this feature.

	(001)	(011)	(111)
Al	0.058	0.064	0.052
TiN	0.087	0.174	0.094

Table 4.3: Surface energies in $\text{eV}/\text{\AA}^2$ of the Al and TiN slabs for the (001), (011) and (111) surface orientations. In the case of the (111) TiN surface the N-terminated one at $\Delta\mu_N = 0$ is given here because it exhibits the lowest surface energy of all (111) TiN surfaces (see Fig. 4.2).

Assessment of Computed Results

To validate the information presented above various additional tests were performed. The results will be presented for the Ti-terminated (111) Al/Ti (hcp) configuration. First of all, finite-size effects are a major concern. Thus, the size of the simulation cell was increased laterally up to a 3×3 surface cell and vertically up to a 19-layer Al slab. Also, intermediate Al slab thicknesses were examined. The TiN slab was not extended vertically because it is almost not affected by the approach of the Al slab. In the case of laterally magnified simulation cells the number of \mathbf{k} points was decreased accordingly, e.g., for a 3×3 surface cell, a $5\times 5\times 1$ mesh was used. For all tested systems the equilibrium interface distances, adhesion energies and energy costs to remove Al layers were found within about 2% of the values given above. The energies are referenced to 1×1 surface cells. Particularly, the results on material transfer were not affected, meaning that the number of transferred Al layers was not altered. For the 3×3 surface cell the effect of fluctuations at the surface was tested by moving one atom out of the surface plane at several interface distances before material transfer occurs. These tests resulted in the transfer of entire layers too, since the shifted atom either relaxed back into its originating slab or was transferred together with the rest of the layer.

Furthermore, the effect of the chosen lattice parameters was investigated. The simulations were repeated using the lattice constants of pure Al and TiN for the lateral lattice parameters of the simulation cell. The equilibrium interface distance again changed by only about 2%. Although the adhesion energies were altered by about 4%, the removal energies were affected in a similar way, resulting in the same material transfer. Moreover, the influence of other approximations for the exchange-correlation functional was tested as already discussed for the removal energies above. The results are presented in Fig. 4.15. The adhesion energies were enhanced similar to the removal energies, again producing the same results for material transfer. Using the vdW functional, the interaction between the slabs started at larger interface distances. This behaviour is expected because of the nonlocal correction added in the vdW functional.

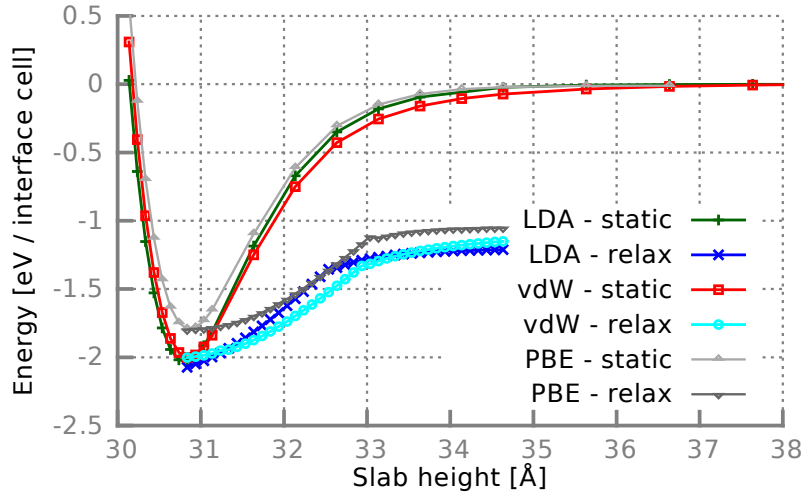


Figure 4.15: Comparison of calculated interaction energies for the Ti-terminated (111) Al/Ti (hcp) configuration and various exchange-correlation functionals, namely, PBE, LDA and opbB86b. The relaxed energies represent the separation of the slabs starting from the equilibrium configuration. The differences between static and relaxed curves at large heights occur due to material transfer.

4.1.4 Conclusion and Outlook

Al/TiN interfaces were examined in detail by investigating the contact between Al and TiN slabs showing low-index surface orientations within the framework of density functional theory. Moreover, these contacts were established for various lateral alignments of the slabs at the interface. It was shown that interfacial properties such as the adhesion energy and the equilibrium structure sensitively depend on the given configuration. This behaviour can be qualitatively explained by comparing the densities of state and the charge densities of different configurations, because distinct bond situations are revealed at the interface. Furthermore, the approach and subsequent separation of Al and TiN slabs was simulated to study the effect on the slabs, especially the possibility of material transfer. The transfer of material from an Al toward a TiN slab was observed for interfacial configurations, which exhibited a larger adhesion energy than the energy cost to remove layers from the Al slab. This is in agreement with the observation that metal-ceramic interfaces break at the interface or in bulk areas according to their interfacial adhesion [345, 346]. The removal energy for Al layers was found to depend on tensile

4.1. INTERFACE: ALUMINIUM - TITANIUM NITRIDE

or compressive stress. In all systems showing material transfer one or two layers of Al stick to the TiN slab after the separation and form an energetically favourable compound with respect to the initial configuration. The differences in surface energies between the slabs are not sufficient to explain the occurrence of material transfer because the given alignment at the interface has to be considered as well. All results were tested for various computational setups such as different sizes of the investigated system or several approximations for the exchange-correlation functional. While properties such as the removal and adhesion energies depend on these settings to some degree, the results for material transfer are not affected.

The method used in this work can be, in principle, applied to any pair of materials. However, complex materials or pairs with an unfavorable bulk lattice mismatch may need very large simulation cells to be considered, which means high computational demands, in order to preserve the translational symmetry and to keep the distortions at an acceptable level. Furthermore, larger cells also allow the inclusion of additional features. For example, the distortions due to the lattice mismatch can be minimized, dislocations as well as quasi-incommensurate contacts can be modeled. Such complex models can be achieved in simulations by using larger and/or rotated surface cells of different size for the slabs in contact, e.g., a 5×5 Al and a 4×4 TiN slab. Furthermore, even roughness could be included to some degree, e.g., by using stepped surfaces or a regular grid of small asperities.

The main results presented in this chapter are accepted for publication in Physical Review B [347].

A closely related topic of high interest, particularly from a technological point of view, is the effect of interfacial species. This will be discussed in the following section for the eminent example of oxygen.

4.2 Effect of oxygen on an Al - TiN interface

4.2.1 Introduction

In the previous section (4.1) investigations on idealized interfaces between pristine aluminium and titanium nitride have been presented. However, when aluminium is exposed to air a thin film of aluminium oxide is formed at the Al surface. This oxide film prevents further oxidation and results in excellent corrosion resistance [348]. The typical thickness of such a film is up to 50 nm. Consequently, interfaces between oxidized Al and TiN are of high interest and will be discussed in the following. L.M. Li et al. [326] and H.Z. Wang et al. [329] showed that Al/TiN interfaces contaminated with hydrogen and zinc as well as magnesium, respectively, exhibit a lower interfacial adhesion than a clean interface. A similar behaviour is expected in the case oxygen is introduced at the interface.

4.2.2 Computational Details

To study an interface between oxidized Al and TiN the same methods and, in particular, the same VASP settings were used as for the pristine Al/TiN contact (see section 4.1.2). As a prototype the (111) surface orientation of Al and TiN (Ti-terminated) were chosen to examine the effects of interfacial oxygen. Since it is currently computationally impossible with DFT methods to treat an Al surface coated with a 50 nm aluminium oxide layer, here only one or a few atomic layer(s) incorporating oxygen are placed above an Al slab.

4.2.3 Results and Discussion

An aluminium oxide coated Al slab: simple models

At first the effect of a single oxygen layer terminating an Al slab was investigated. This setup represents the simplest model of an aluminium oxide (AlO) film and was achieved by placing one oxygen atom on top of each 1×1 Al surface cell. Preliminary calculations (see Fig. 4.16) showed that the energy of an O-Al system is minimized if the atoms in the oxygen layer follow the fcc stacking of the Al slab (see Figs. 4.17a and 4.17c) (the definition

4.2. EFFECT OF OXYGEN ON AN AL - TIN INTERFACE

of the adsorption sites on an Al (111) slab is depicted in Fig. 4.3). An oxygen strongly adsorbs on an Al slab with an adsorption energy of about 8.5 eV at a vertical distance of only about 0.7 Å above the top Al layer. While an oxygen adsorbs similarly on the hcp adsorption site and the adsorption energy is only reduced by 0.2 eV, the adsorption on hollow and top sites are much weaker by 1 eV and 5 eV, respectively.

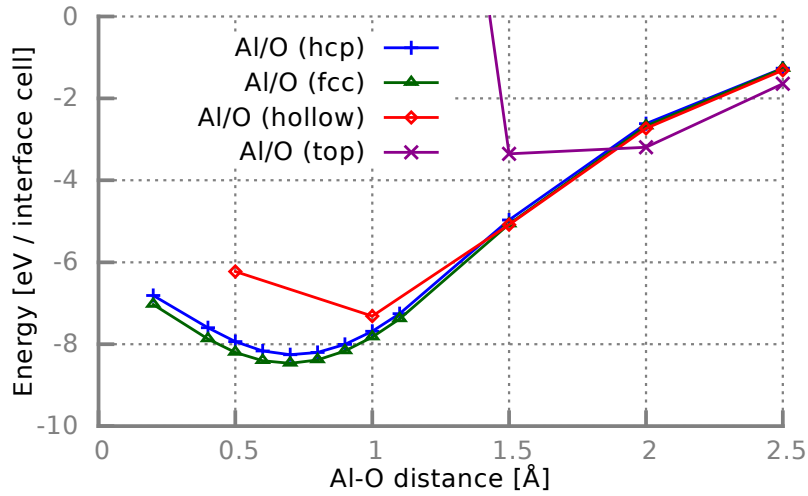


Figure 4.16: Calculated PBE adsorption energies of a 1×1 oxygen layer on an Al (111) surface. Various lateral alignments of the oxygen layer on the Al slab are considered (see Fig. 4.3).

Placing two oxygen atoms above each 1×1 Al surface cell results in a rather unstable system. The O atoms were initially placed above the fcc and hcp adsorption sites. During the relaxation of the system the fcc O diffused into the Al slab between the top and second Al layers, while the hcp O stayed above the Al surface. Additionally, the six bottom Al layers coated with the diffused O layer formed a new slab, whereas the top Al and O were almost detached from the rest with a distance of about 4.2 Å. An analysis of the potential-energy curve revealed that this top two-layered O-Al compound was only bound to the lower slab by about 10 meV, which is a very small adsorption energy, for example, compared to the thermal energy at room temperature of 25 meV. Thus, an Al slab covered with a 1×1 oxygen layer was chosen to be the first model system.

Moreover, a model for an ultrathin two O-layers aluminium oxide (Al_2O_3) film covering an Al slab was studied (see Figs. 4.17b and 4.17d). This model was suggested by

4.2. EFFECT OF OXYGEN ON AN AL - TIN INTERFACE

D.R. Jennison et al. [349], who described this film as “tetrahedral Al ions atop oxygens in fcc hollows of the Al(111) surface, with a stacking fault at second oxygen layer”. In this setup the Al surface is first covered by a chemisorbed 1×1 oxygen layer placed at a vertical distance of 0.7 \AA following the Al fcc stacking. Then an almost coplanar layer of Al and O atoms, forming an Al_2O_3 film, is placed above the first oxygen layer. This Al-O ratio can not be achieved within an 1×1 Al surface cell; therefore, a $\sqrt{3} \times \sqrt{3}$ cell is used. The vertical distance between the oxygen and the Al_2O_3 layer is about 2.3 \AA , while the non-coplanarity within the Al_2O_3 film is less than 0.1 \AA .

A single oxygen layer at an Al/TiN interface

Such as in the case of the pristine Al/TiN interface also for the oxidized Al different alignments of the slabs at the interface are possible. In the following two contact situations will be discussed. While for the “top” alignment the bottom Ti atom of the TiN slab is placed directly above the interfacial O atom, the “fcc” alignment is established by Ti atoms continuing the fcc stacking of the oxygen coated Al slab. Allowing for relaxations both configurations exhibit a very similar, but rather weak adhesion energy. The energy difference is at the accuracy limit of the calculations; therefore, it is not possible to determine the more favourable alignment and both are investigated.

To examine the properties of the Al/O/TiN interface, at first the oxygen layer plus x ($x = 1,2,3$) Al layers were manually shifted from the Al/O slab towards the TiN slab, which was placed at a large distance to the Al slab to minimize unwanted interactions. The energetics revealed that these shifts are unfavourable (see Tab. 4.4); therefore, no material transfer should occur between the slabs from a thermodynamical point of view. Next, the slabs were brought into contact and separated (see Fig. 4.18) again using the same method as described for the pristine Al/TiN interfaces (see section 4.1.2). These calculations showed the importance of relaxations at the interface because particularly for the fcc configuration the distance between the oxygen and Al layers is growing in the vicinity of the TiN slab. However, in contrast to the energetical argument presented above these loops of approach and separation result in the material transfer of the oxygen and two Al layers toward the TiN slab, although the final configurations are energetically less

4.2. EFFECT OF OXYGEN ON AN AL - TIN INTERFACE

favourable than the initial ones (see Fig. 4.18). Further calculations showed that these results are not affected by an increased number of Al layers. During the separation the Al slab expands before it breaks apart. Keeping more layers of the Al slab rigid clearly shows that this expansion is necessary for the occurrence of material transfer in the simulations. At least the oxygen layer as well as the two uppermost Al layers have to be able to relax to allow for material transfer. This suggests that a weakening of the bonds between the Al layers could be responsible for this effect. However, the material transfer could also be a computational artefact and based on the presented results no unambiguous conclusion can be drawn. Assuming an artefact and following the energetical argument the oxygen layer would be able to passivate the Al slab with respect to material transfer towards a TiN slab.

shifted layers	top	fcc
O + 1 Al	0.4292	0.2555
O + 2 Al	0.1717	0.2134
O + 3 Al	0.1774	0.2486

Table 4.4: PBE energy costs to shift the oxygen layer plus one to three of the following Al layers from an Al (111) slab toward a TiN (111) slab. The energies are given in eV per 1×1 surface cell. The two slabs are separated by a gap of 10 Å. “top” and “fcc” describe the lateral alignment of two slabs via the relative positions of the top O and bottom Ti atoms.

Ultrathin aluminium oxide layer at an Al/TiN interface

An Al slab terminated with the ultrathin aluminium oxide was brought into contact with a TiN slab. In this section the lateral alignments at the interface are defined relative to the Al atoms in the top Al_2O_3 layer. Probing possible contact sites showed that it is crucial to allow for relaxations. Static calculations suggest that only the hcp alignment results in strong adhesion while the other configurations only yield weaker interactions comparable to the single O layer case (see Fig. 4.19a). However, including relaxations all alignments yield strong adhesion. Since the hcp alignment is the strongest, it was investigated further. The approach and separation of the hcp-aligned slabs resulted again in a material transfer of several layers (see Fig. 4.19b). Snapshots of the structures during

4.2. EFFECT OF OXYGEN ON AN AL - TIN INTERFACE

approach and separation are presented in Fig. 4.20. During the approach at first the single Al_2O_3 layer was transferred towards the TiN slab without a significant change in the structure of the involved layers. Upon further approach the Al atoms of the Al_2O_3 layer were slightly shifted towards the Al slab. The non-coplanarity was increased to about 0.6 Å, which did not significantly change when the slabs were separated. During the separation the oxide film as well as additional Al layers were transferred toward the TiN slab. While two Al layers were completely transferred, the third layer breaks up and partially stayed at the Al slab. Contrary to the single oxygen layer, the final configuration obtained from this material transfer is however more favourable than the initial one. Consequently, this ultrathin oxide film does not seem to be able to passivate the Al slab against material transfer towards TiN.

4.2.4 Conclusion

The occurrence of oxygen atoms at an Al/TiN interface has a strong effect on the interfacial properties. However, this influence depends on the arrangement of the oxygen atoms. A single oxygen layer weakens the interfacial adhesion by about a factor two. The energetical differences between the alignments studied are diminished. Thermodynamics suggest that material transfer is hindered by the presence of an oxygen layer. This is in line with the expected passivation of an aluminium slab by oxygen atoms. The occurrence of material transfer in the simulations can not unambiguously be determined as an artefact or a real effect. On the other hand, the ultrathin aluminium oxide layer exhibits an opposite effect on the Al/TiN interface. The interfacial adhesion is increased by about a factor two and the differences between the alignments persist. This behaviour occurs probably due to the rather unstable nature of this oxide film. Material transfer is observed between the slabs. For a better assessment of these effects thicker and more realistic oxide films should be investigated in the future.

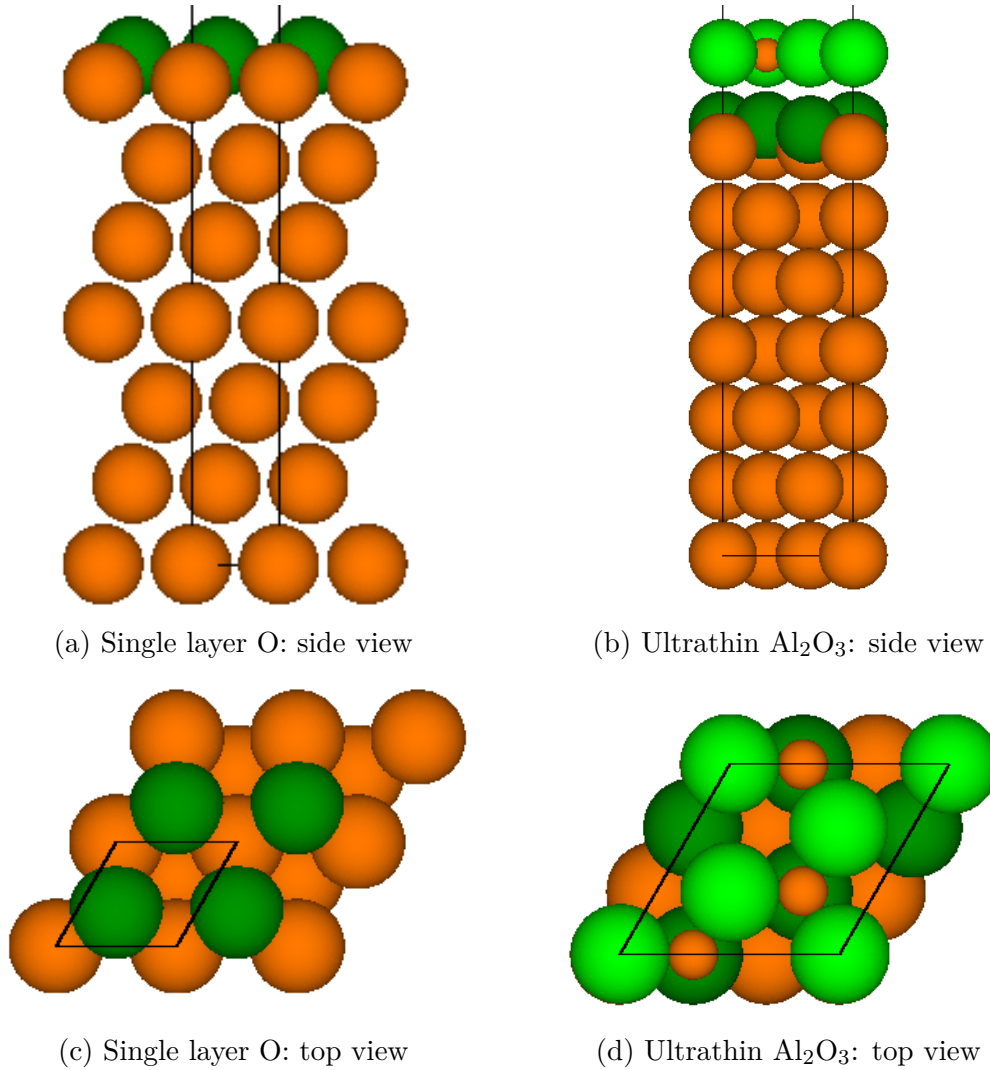


Figure 4.17: Side and top view of two oxide coated Al (111) slabs. On the left the single O layer terminated Al slab is shown, while the ultrathin aluminium oxide coating is presented on the right. The simulation cells are indicated by the solid black lines. Orange and green label Al and O atoms, respectively. For the ultrathin aluminium oxide layer light green indicates the O atoms in the top layer, while dark green marks the O atoms in the second layer.

4.2. EFFECT OF OXYGEN ON AN AL - TIN INTERFACE

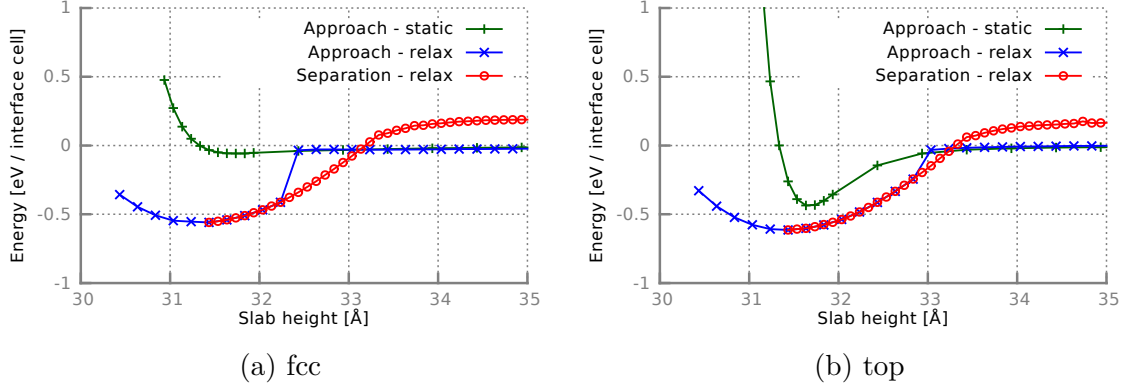


Figure 4.18: Calculated PBE interaction energies, see Eq. 4.4, for the approach and subsequent separation of a single oxygen layer coated Al slab and a Ti-terminated TiN slab for the (111) surface orientation. The labels “fcc” and “top” refer to the alignment of the O and bottom Ti layers.

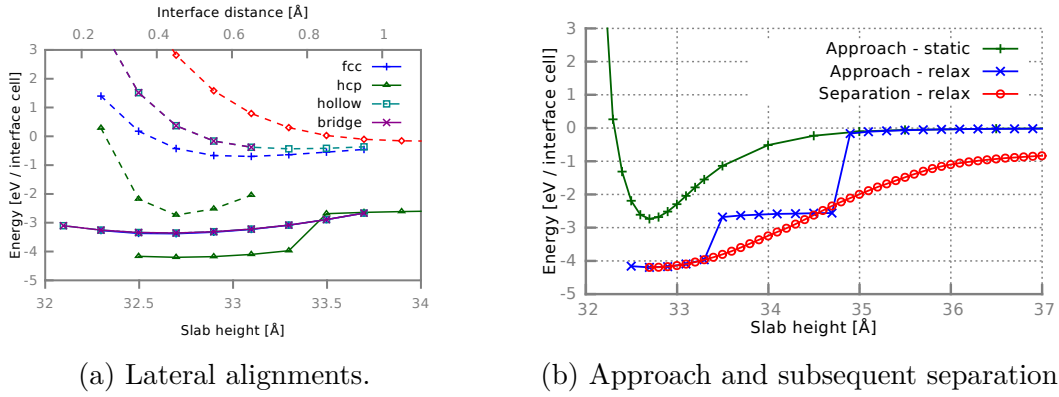


Figure 4.19: Calculated PBE interaction energies, see Eq. 4.4, of an ultrathin aluminium oxide coated Al slab and a Ti-terminated TiN slab for the (111) surface orientation. In subfigure (a) the static (dashed) and relaxed (solid) energies are shown for various lateral alignments (the axes are explained in Fig. 4.6), while in subfigure (b) only the approach and subsequent separation of the hcp alignment is displayed.

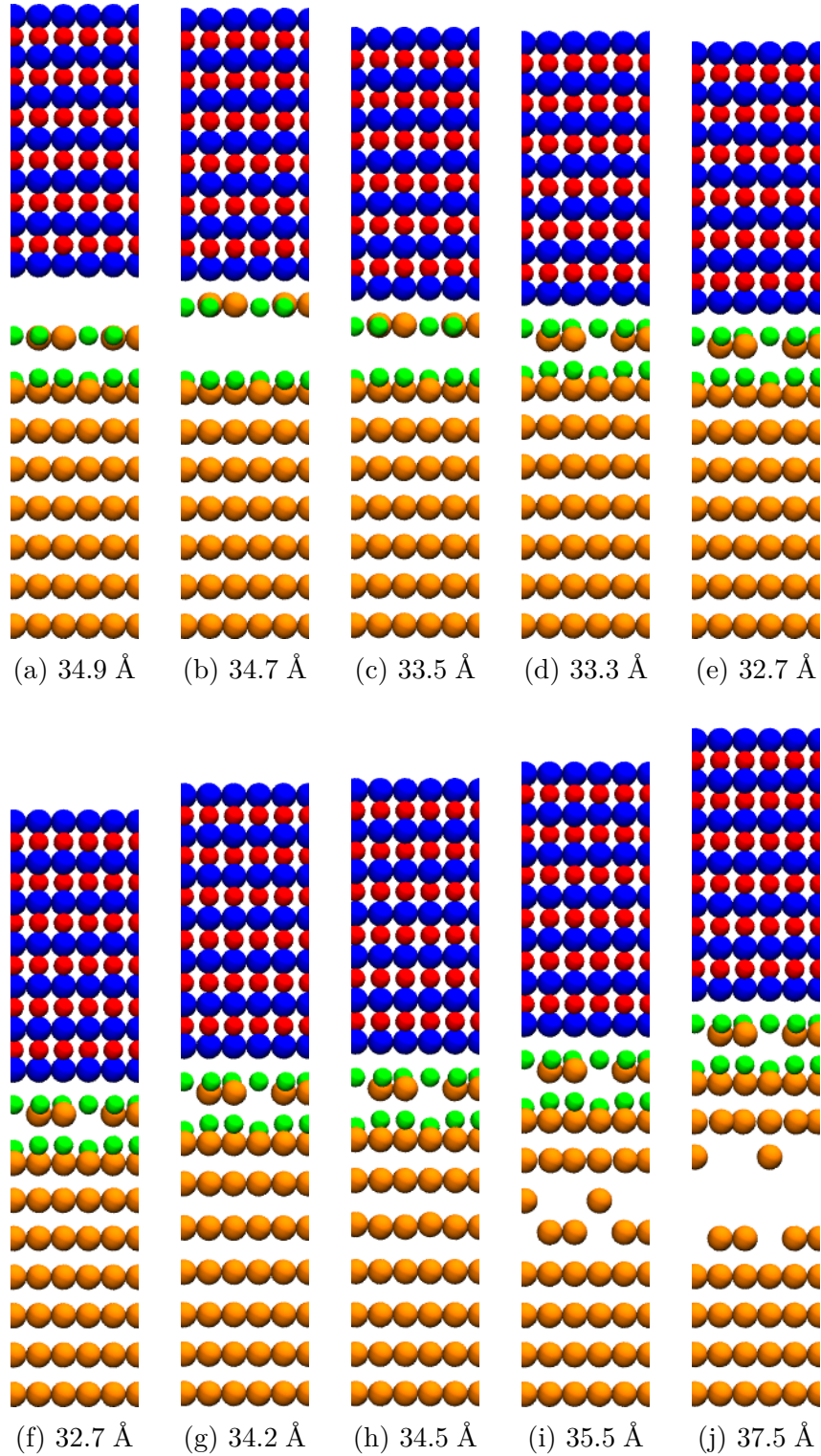


Figure 4.20: Approach (a–e) and separation (f–j) of $\text{Al}_2\text{O}_3/\text{Ti}$ (hcp) aligned ultrathin Al_2O_3 covered Al (111) and Ti-terminated TiN (111) slabs. Al, O, Ti and N are coloured in orange, green, blue and red, respectively. Subfigures (e) and (f) show the structure at the relaxed equilibrium distance. The steps are defined by the slab height.

Chapter 5

Adsorption of Organic Molecules on Iron Surfaces

5.1 Introduction and Motivation

The adsorption of molecules and especially organic molecules on metallic surfaces is of high interest from a theoretical point of view as well as for technological purposes. Due to their diverse technological applications, a wide range of systems has been investigated, for example, promising candidates for optoelectronic devices [274, 350–352] or materials with catalytic potential [353–356]. The research in the field of catalysis has proven to be of interest in the synthesis of biofuels. During the last decade the production of biofuels, of which ethanol is the most common one, has surpassed 100 billion litres per year and will continue to rise (see figure 5.1) [357]. Thus, biofuels are becoming a more and more important part of the world wide fuel consumption. Ethanol is seen as a very promising renewable resource because of its high energy density, and the steam reforming process [358] ($\text{C}_2\text{H}_5\text{OH} + 3\text{H}_2\text{O} \longrightarrow 2\text{CO}_2 + 6\text{H}_2$) is considered an important mechanism to produce hydrogen [359–362]. The search for catalysts such as Pt surfaces is currently the main research focus in that field. The interactions of fuels and lubricants as well as their base fluids and additives with metallic surfaces or other chemical constituents, such as water, are another matter of high technological importance. In particular, the

5.1. INTRODUCTION AND MOTIVATION

increasing use of biofuels, such as ethanol, poses many new questions; therefore, this will be the main focus here. In this regard, one question of high relevance is how the effectiveness of additives in fuels is influenced by the contact with metallic surfaces and the presence of additional chemical constituents.

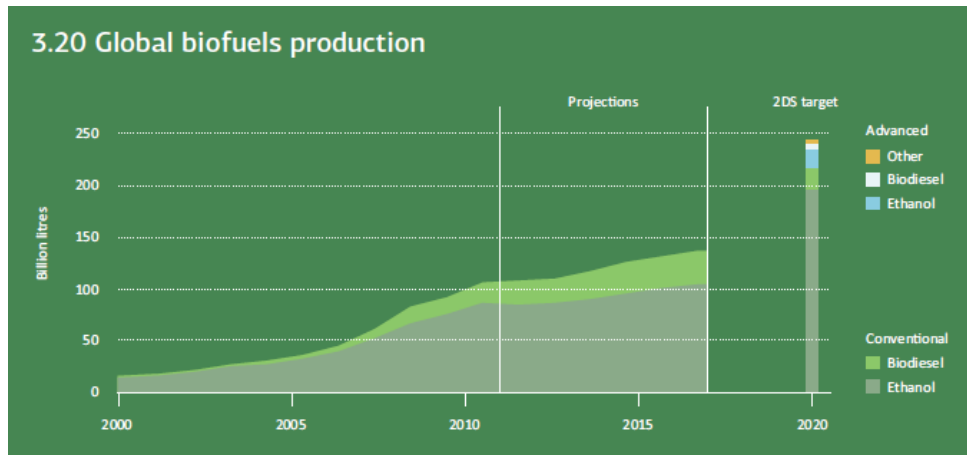


Figure 5.1: World wide biofuel production. Taken from IEA [357].

Recently various approaches were used to perform nano- and microtribological simulations in the field of fuel tribology. Classical molecular dynamics (MD) was employed to study the frictional performance of additives [118, 119] as well as the stability of monolayers of stearic acid adsorbed on iron surfaces during shearing [120, 159]. On the microscale, wear processes in a diesel-fuel lubricated sliding contact were investigated using a combination of finite-element and boundary-element methods [363]. However, none of these approaches explicitly considered the adsorption process as an initial step towards the lubricity of surface-active species. The adsorption of ethanol on several transition metal surfaces, including Fe(110), was studied by P. Tereshchuk and J.L.F. Da Silva [364] using DFT methods including corrections for van der Waals (vdW) interactions. This study was performed using the *DFT-D3* empirical vdW correction approach by S. Grimme [241], which is computationally efficient but overall less accurate than other available methods [232] (for more information on vdW corrections in DFT see section 3.4). Thus, a validation of the results with an approach independent of external input parameters is desirable. Additionally, a more detailed knowledge of the adsorption process is necessary for better understanding of the above mentioned systems.

5.1. INTRODUCTION AND MOTIVATION

A better understanding of the interactions between all the different constituents is crucial for approaching these questions. A fuel contains various organic compounds such as branched alkanes, alcohols and acids. Further, the fuel will be stored, transported and used in metallic components, typically made from iron alloys such as steel. Additionally, there may be other chemical constituents present, for example, water adsorbed on the metallic surfaces. All of these components form a very complex system including processes on a broad range of length and time scales, from atomic to macroscopic scales. As a first step the interaction of selected parts of the whole system will be simulated and analyzed on the atomic length scale. From these simulations, potential-energy curves (PEC), information on the relevant interactions and the influence of additional chemical constituents can be obtained. Such results can be used as an input for approaches working on larger scales. Due to its complexity, the system has to be broken down into manageable units (see figure 5.2). Thus, only the adsorption of single organic molecules on an iron surface is investigated here. The organic molecules studied are isooctane (2,2,4-trimethylpentane) and ethanol with the chemical formulas $(\text{CH}_3)_3\text{CCH}_2\text{CH}(\text{CH}_3)_2$ and $\text{CH}_3\text{CH}_2\text{OH}$, respectively. Isooctane is a representative aliphatic gasoline compound, and ethanol is the currently most common bio-component in fuels. Furthermore, some properties differ remarkably in these molecules, such as the chemical polarity, polarizability and chemical reactivity; therefore, it is possible to investigate their influence on the adsorption process. Additionally, a water mono-layer covering the metallic surface is introduced into the system. Only few theoretical studies including vdW interactions have investigated the effects of water on the adsorption of organic molecules. On an ab initio level P. Błóński and N. López [355] examined these effects for methanol and formaldehyde, while P. Tereshchuk and J.L.F. Da Silva [356] investigated the adsorption of a water-ethanol mixture. Both studies dealt with the adsorption on a platinum (111) surface due to its catalytic potential. Here, the iron (100) surface orientation has been chosen because it is present in systems of industrial interest, and it was used in several previous studies on the adsorption of water on iron [365–370]. In particular, in the case of isooctane, vdW forces (see section 3.4) are expected to be essential in the adsorption process. The analysis of their impact on adsorption energies and geometries as well as on

charge densities is, therefore, one of the major goals of the presented work. Moreover, the effect of a water mono-layer on the adsorption process is examined in detail.

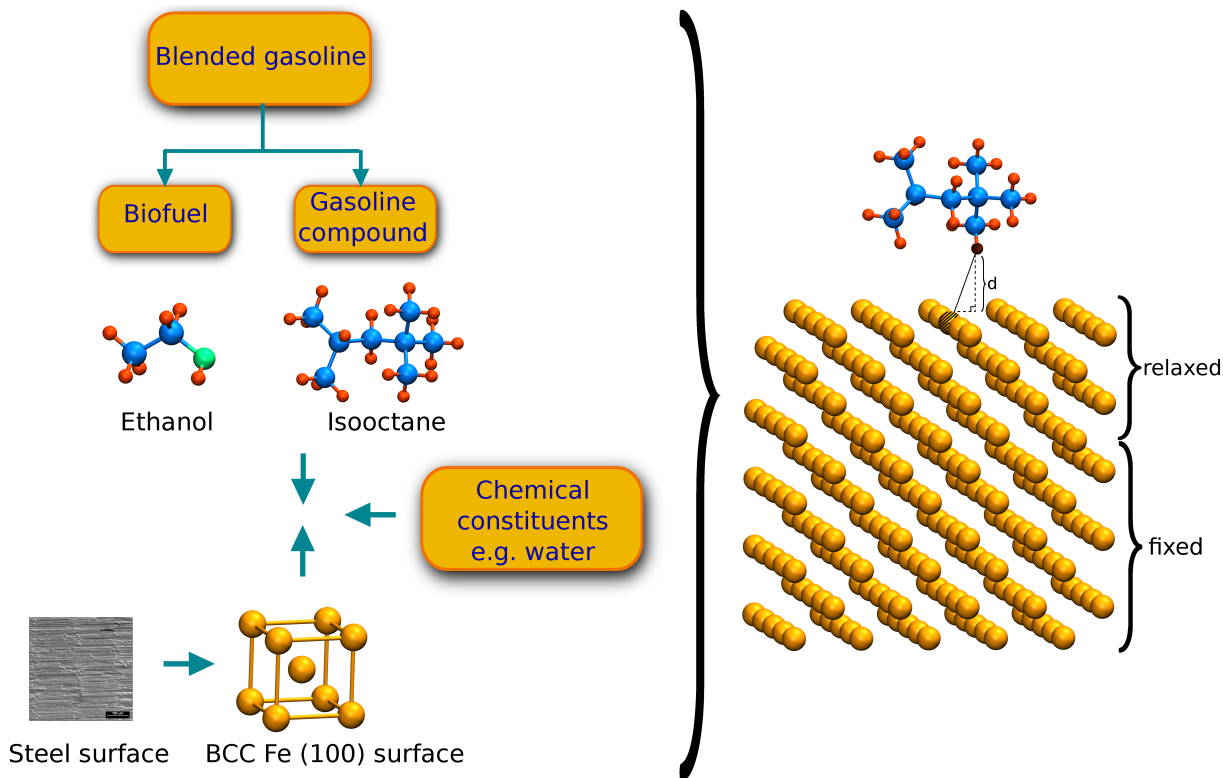


Figure 5.2: Strategy to obtain computationally manageable systems starting from the complex interaction between a steel surface and blended gasoline.

5.2 Computational Details

To study adsorption processes of organic molecules on iron surfaces, calculations within the framework of DFT (see section 3.2) were carried out using the VASP code (see section 3.5). In this chapter spin polarized calculations were performed to account for the magnetic moment of iron. In order to investigate the binding mechanisms and the effect of vdW forces in the adsorption process, various exchange-correlation functionals (see section 3.3) were compared. At first, two GGA functionals were used, PBE and its revised version (revPBE) [259]. These functionals differ only in one parameter of the exchange term, κ , changed from 0.804 in PBE to 1.245 in revPBE. Both have been widely applied in physics and chemistry. Secondly, two van der Waals density functionals (vdW-DF)

5.2. COMPUTATIONAL DETAILS

(see section 3.4) were used. These vdW functionals intend to take long-range interactions into account by means of adding a non-local term to the correlation energy. The original vdW-DF was proposed by Dion et al. [258],

$$E_{\text{xc}}^{\text{vdW-DF}}[n] = E_{\text{revPBE(x)}}[n] + E_{\text{LDA(c)}}[n] + E_{\text{nl(c)}}[n] \quad (5.1)$$

where n is the electronic density in the ground state, $E_{\text{revPBE(x)}}[n]$ is the exchange energy calculated with the revPBE functional, $E_{\text{LDA(c)}}[n]$ is an LDA correlation and $E_{\text{nl(c)}}[n]$ is a non-local correlation term that approximates the vdW interactions. The optimised Becke86 [264] van der Waals (optB86b) functional was introduced by Klimeš et al. [262, 263],

$$E_{\text{xc}}^{\text{optB86b}}[n] = E_{\text{optB86b(x)}}[n] + E_{\text{LDA(c)}}[n] + E_{\text{nl(c)}}[n] \quad (5.2)$$

where a reparametrised version of the Becke86 exchange functional replaces the revPBE exchange in equation (5.1). This second vdW functional is generally more accurate than the original vdW-DF [263]. Thus, results achieved with the optB86b functional should be used as reference. Here, the original vdW-DF is applied to analyse the effects of non-local correlation. The contributions of the other terms can be easily subtracted by introducing a revPBE+LDA functional,

$$E_{\text{xc}}^{\text{revPBE+LDA}}[n] = E_{\text{revPBE(x)}}[n] + E_{\text{LDA(c)}}[n] \quad (5.3)$$

which involves terms that have been tested and applied in a wide range of materials.

To model the adsorption of ethanol and isooctane on an Fe(100) surface, a simulation cell was constructed. This cell consisted of a slab of 10 layers body-centred cubic (bcc) Fe and a single molecule placed on one side of the slab at a distance d above it. Additionally, the adsorption of a water mono-layer on the Fe surface was considered in some calculations. The distance d was defined as the vertical distance between the atom of the molecule which was the lowest in z direction and the closest atom of the Fe surface or the water layer, if present. Unless stated otherwise, a 5×5 Fe surface cell was used. Typically, for calculations including a water layer, a 4×4 surface cell was used for structural reasons

5.2. COMPUTATIONAL DETAILS

which will be explained in more detail below (see section 5.3.2). A vacuum spacing of 29.73 Å was included in z-direction, which is perpendicular to the Fe surface, to decouple the periodically repeated slabs. This setup accurately models a bcc Fe(100) surface and avoids slab-slab interactions as well as intermolecular interactions, if single molecules are placed above the slab. The last statement may not be valid for molecules larger than the investigated ethanol and isooctane. Dipole corrections were tested but found to be negligible for this setup. The Fe slab was constructed using a lattice constant of 2.83 Å, which was obtained from bulk calculations employing the PBE functional. The computational parameters were chosen to be consistent with the accuracy of the surface calculations, and the obtained value is in good agreement with the experimental lattice constant of 2.86 Å [343].

The calculation parameters were carefully chosen and tested to ensure a sufficient accuracy of total energies and forces. A convergence criterion of 10^{-6} eV on the total energy in the self-consistency cycle was employed. An energy cut-off of 400 eV was applied for the plane-wave basis set. For calculations using the 5×5 surface cell, the Brillouin zone sampling was performed on a $2 \times 2 \times 1$ Monkhorst-Pack mesh [333, 335]. For smaller surface cells the mesh was adjusted to keep the k-point density constant. Static calculations were performed employing the tetrahedron method with Blöchl corrections [334] to obtain accurate total energies, whereas relaxations were done with a Gaussian smearing of 0.2 eV. Smaller smearing widths were tested to ensure that the selected value leads to the ground-state geometry. Most structures were relaxed within the conjugate gradient algorithm allowing the atoms to move until the convergence criterion of 10^{-5} eV in total energy was fulfilled. A damped molecular dynamics algorithm was preferred for ill-defined starting positions or systems showing convergence problems. During relaxations the atoms of the top four layers of the Fe slab as well of the molecule and of the water layer were allowed to move in all directions, while the remaining atoms in the six bottom layers of the slab were kept rigid at bulk-like positions.

A main goal of this work was to obtain accurate potential-energy curves (PEC) for the molecule-surface interaction. These can be used to shed light on the adsorption process, and these will aid in the fitting of potentials necessary for classical molecular dynamics

5.3. RESULTS AND DISCUSSION

simulations. Such MD simulations will allow to study the system on larger length and time scales. To obtain accurate PECs, the distance d was varied in discrete steps for various orientations of the molecules above the slab, and the total energy was computed for each resulting system. At first, this was done with static calculations to find an estimate for the equilibrium distance and geometry, which were considered to be the ones that minimize the total energy. Of course, the accuracy of these estimates depends on the step size Δd between the distances and the number of tested orientations. Additional relaxations were performed to verify the equilibrium structures. For most distances these relaxations resulted in small geometrical deviations. The relaxed geometries significantly differed only at very short molecule slab distances. The adsorption energies E_{ads} were calculated via

$$E_{ads} = E_{tot}^{mol+Fe(100)} - (E_{tot}^{Fe(100)} + E_{tot}^{mol}) \quad (5.4)$$

where $E_{tot}^{mol+Fe(100)}$ is the total energy of products adsorbed on the Fe(100) slab at the equilibrium distance, $E_{tot}^{Fe(100)}$ is the total energy of the clean Fe(100) slab and E_{tot}^{mol} is the total energy of the isolated molecule calculated using a box with 15 Å edge length. The following equation was used in the presence of water

$$E_{ads} = E_{tot}^{mol+H_2O+Fe(100)} - (E_{tot}^{Fe(100)+H_2O} + E_{tot}^{mol}) \quad (5.5)$$

where $E_{tot}^{mol+H_2O+Fe(100)}$ is the total energy of products adsorbed on the water-covered Fe(100) slab at the equilibrium distance, $E_{tot}^{mol+H_2O}$ is the total energy of the water-covered Fe(100) slab and E_{tot}^{mol} is the total energy of the isolated molecule as above.

5.3 Results and Discussion

In the following section the adsorption of isooctane and ethanol on a bare Fe(100) surface is presented. The effects of different orientations of the molecules and of various exchange-correlation functionals on the adsorption process are shown. Subsequently, water molecules were placed on top of the Fe surface to find an energetically favourable structure for a water mono-layer adsorbed on Fe(100). Finally, the two organic molecules

were brought into contact with the water-covered Fe surface to examine the effect of the water layer.

5.3.1 Organic Molecules on a bare Fe(100) surface

Isooctane on a bare Fe(100) surface

Geometrical effects on the adsorption process were investigated by placing the isooctane molecule in various orientations above the Fe slab (see figure 5.3) and calculating the according potential-energy curves (PEC). For each orientation the isooctane was adsorbed on the top, bridge and hollow sites of the Fe(100) surface. It turns out that it is energetically favourable if the longest continuous chain of carbon atoms is oriented “parallel” to the Fe surface (see figure 5.3a). However, only small differences in the adsorption energies of less than 70 meV occur between the “parallel” orientations 1–3 for all sites (see figure 5.4). Thus, any of these configurations may be reached at room temperature (≈ 25 meV) and no particular one is preferred. Furthermore, the molecule should be able to move on the Fe surface at finite temperatures due to the shallow energy landscape. Only the configuration 4, where the longest carbon chain is “perpendicular” to the Fe surface, exhibits adsorption energies at least 162 meV lower than the other orientations (see figure 5.4). As before, no preference for one of the adsorptions sites is found. In order to understand these results the binding mechanism has to be investigated in more detail. Configuration 1 shows the highest adsorption energy at a distance d of 2.25 Å. However, for the remaining part of this study configuration 2 adsorbed on the top site was used, because this structure is among those likely to be found at room temperature. Furthermore, it has already been employed in a previous study [277] and thus, can be compared.

To gain more insight into the adsorption process various exchange-correlation functionals were used. First, an equilibrium structure was obtained for configuration 2 via relaxations using the PBE parametrization. A second relaxation employing the optB86b functional did not significantly alter the geometry. The largest variations in bond lengths and angles were in the order of 10^{-3} Å and 10^{-3} degree, respectively. Also the energy

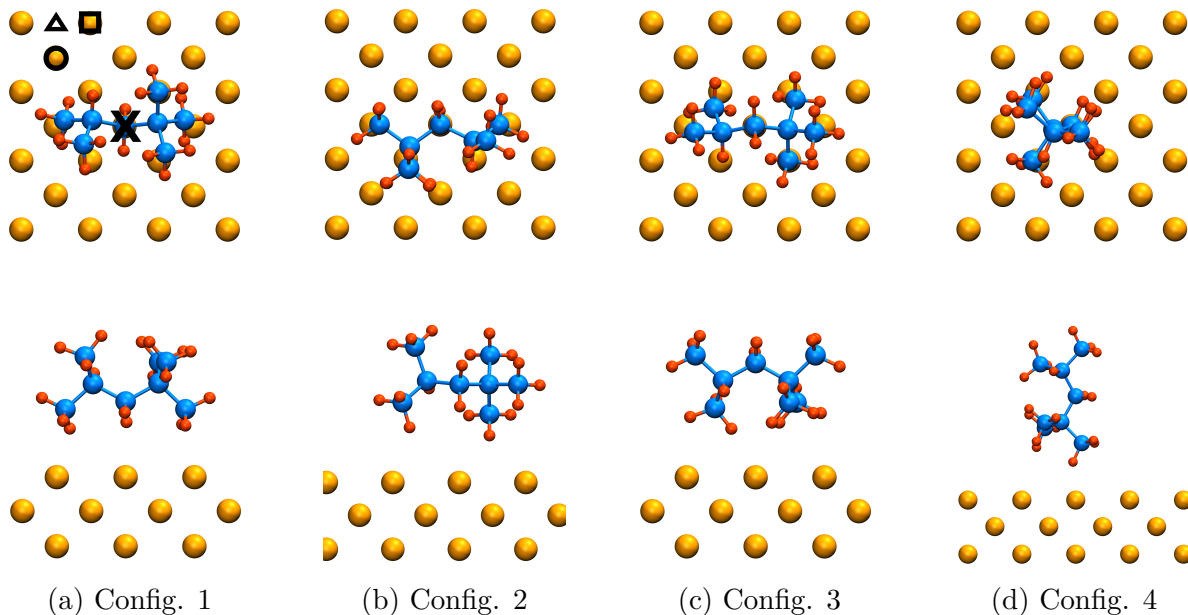


Figure 5.3: Configurations considered for the adsorption of an isooctane molecule on a Fe(100) surface, here displayed with the molecule on the top adsorption site at a distance $d = 2.00$ Å. The top row displays the top view of the system while the bottom row the side view. The atom marked with a cross (X) on the top view of configuration 1 is used as a reference to orient the molecule on the top, bridge and hollow sites, indicated in the same figure with a circle, triangle and square, respectively.

hierarchy between the adsorption sites was not affected. Thus, neither the orientation nor the adsorption site of isooctane are influenced by non-local correlation. However, non-local interactions seem to strongly increase the adsorption energy of isooctane on a Fe(100) surface and to lower the equilibrium distance between the molecule and the slab (see table 5.1). The absolute value of the adsorption energy is enhanced by more than a factor 12 when using optB86b instead of PBE, while the equilibrium distance is decreased by 1.00 Å (see figure 5.5). The two functionals differ not only in the inclusion of a non-local term (see section 5.2), so that the changes can not be attributed unambiguously to non-local effects. Thus, the adsorption energies are recalculated with Dion’s vdW-DF and the revPBE+LDA functional because for these potentials the non-local correlation term presents the sole difference. The resulting energy difference of 418 meV accounts for 95.8% of the adsorption energy obtained with the vdW-DF (see table 5.1 and figure 5.5). Hence, the adsorption is mainly governed by dispersion forces. By the same reasoning, the reduction of the equilibrium distance can be attributed to non-local interactions. The

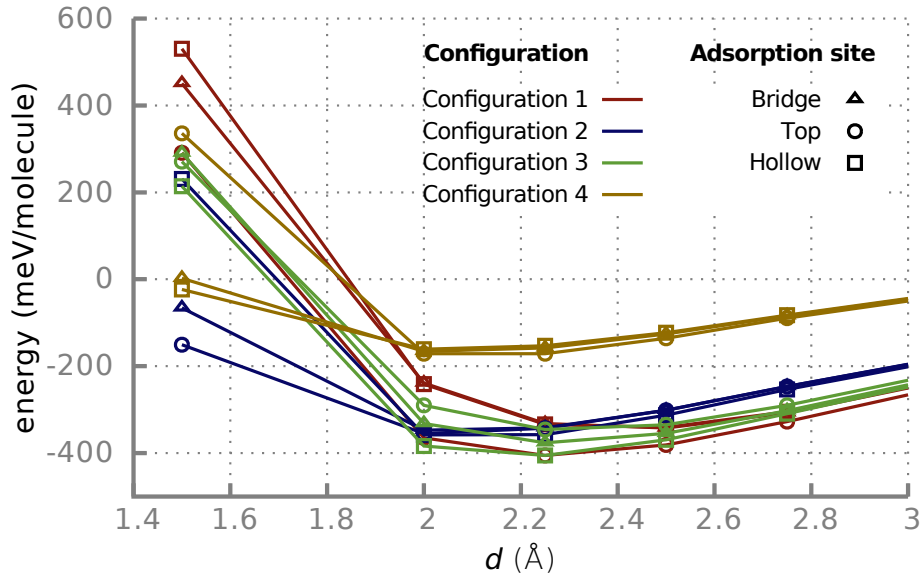


Figure 5.4: Calculated adsorption energies of four different configurations of an isooctane molecule adsorbed on an Fe(100) surface as a function of the vertical distance. The configurations (line colour) and adsorption sites (symbol) are described in figure 5.3. Atomic relaxations were not considered in these calculations.

dominance of vdW interactions also explains the favoured “parallel” isooctane orientation, because it maximises the number of atoms in proximity to the surface; therefore, it strengthens the dispersion forces.

As presented above, the non-local correlation between the electrons caused by dispersion interactions yields changes in the adsorption energies and distances. A balance between the long-range attractive vdW forces and the short-range Pauli repulsion mainly determines the equilibrium distance. Upon the approach of the isooctane molecule toward the Fe slab, the Pauli repulsion induces a redistribution of charge density, particularly among the iron d-orbitals. Nevertheless, no charge is transferred between the molecule and the slab. Due to the overlap of the wave functions between the isooctane molecule and the Fe surface, resulting in electron-electron repulsion, the electrons are shifted towards higher energy states and hence, increase the total energy of the system. This effect is weakened by employing a more accurate description of non-local interactions because non-local correlations decrease the electron-electron repulsion (see figure 5.6). Thus, the equilibrium distance is reduced while the attractive forces become stronger, and con-

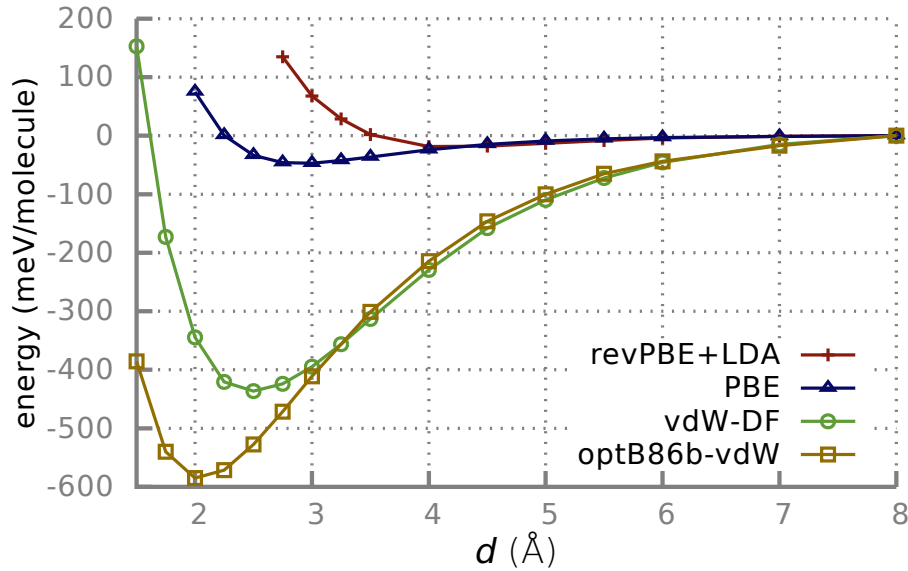


Figure 5.5: Calculated adsorption energies of an isooctane molecule on the bcc Fe(100) surface as a function of the vertical distance for the PBE, revPBE+LDA, vdW-DF and optB86b exchange-correlation potentials.

sequently, the binding energy is increased. From the point of view of the charge density (see figure 5.6) the non-local interactions result in a non-isotropic accumulation of charge between the molecule and the Fe slab. This charge redistribution gives rise to electrostatic forces which are responsible for the adsorption of the isooctane molecule. Since the exchange term differs for the employed vdW functionals, the equilibrium distance is also affected. For example, the calculated binding distance varies between the optB86b and Dion’s vdW functional by 0.5 Å.

Functional	Ads. energy [meV]		Eq. distance [Å]	
	Isooctane	Ethanol	Isooctane	Ethanol
PBE	47	384	3.00	2.00
revPBE+LDA	18	26	4.00	4.00
revPBE	-	144	-	2.25
optB86b	585	795	2.00	2.00
vdW-DF	436	517	2.50	2.25

Table 5.1: Adsorption energies and equilibrium distances calculated with various exchange-correlation functionals.

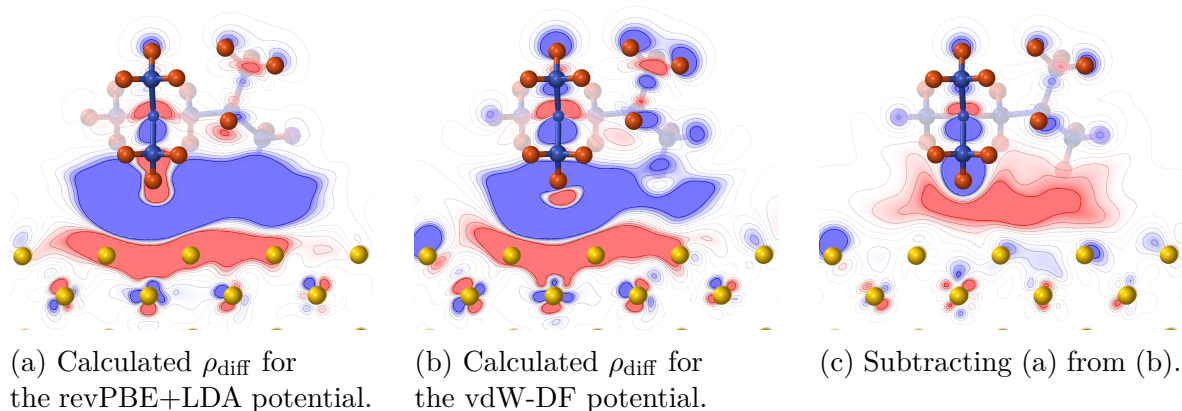


Figure 5.6: Charge density differences (ρ_{diff}) of isooctane adsorbed on the bcc Fe(100) surface at $d = 2.00$ Å. The charge density difference is defined as $\rho_{\text{diff}} = \rho - (\rho_{\text{isooctane}} + \rho_{\text{Fe(100)}})$ where ρ denotes the charge density of isooctane adsorbed on Fe(100), while $\rho_{\text{isooctane}}$ and $\rho_{\text{Fe(100)}}$ represent the charge densities of the isolated molecule and the clean Fe(100) surface, respectively. The charge density difference is plotted in a plane perpendicular to the surface for values between -5×10^{-4} (solid blue, deficit) and 5×10^{-4} (solid red, accumulation) electrons/Å³.

Ethanol on a bare Fe(100) surface

Just as for the isooctane molecule, in the case of ethanol four orientations and three adsorption sites were investigated (see figure 5.7). Compared to isooctane, for the ethanol molecule the adsorption energies are distributed over a more extended range (see figure 5.8). Excluding configuration 4, the various geometries exhibit notable energy differences between the adsorption sites. Consequently, the ethanol molecule is not as mobile as an isooctane one on an Fe(100) surface and more likely to be pinned at one site. Namely, on the top site, the hydroxyl group of the ethanol molecule pointing towards the Fe surface and a parallel orientation of the hydroxyl group with respect to the surface are energetically preferred. These criteria are fulfilled in configurations 1 and 3, which only show small energy differences. Since rotations of the ethanol molecule around its oxygen atom affect the adsorption energy only marginally, they should be observed at room temperature. Relaxing the configurations did not produce changes in the energy hierarchies, but the structures were affected. For the top site, the oxygen atom moved slightly towards the bridge site and the whole ethanol molecule became tilted. P. Tereshchuk

5.3. RESULTS AND DISCUSSION

and J.L.F. Da Silva [364] reported an equilibrium structure of an ethanol molecule on a Fe(110) surface with the carbon chain being almost perpendicular to the Fe surface. Comparing this structure with the equilibrium configuration found here, only gave an energy difference of 3 meV. Hence, both orientations should co-exist at room temperature, and the surface termination does not seem to influence the adsorption orientation in a pronounced way.

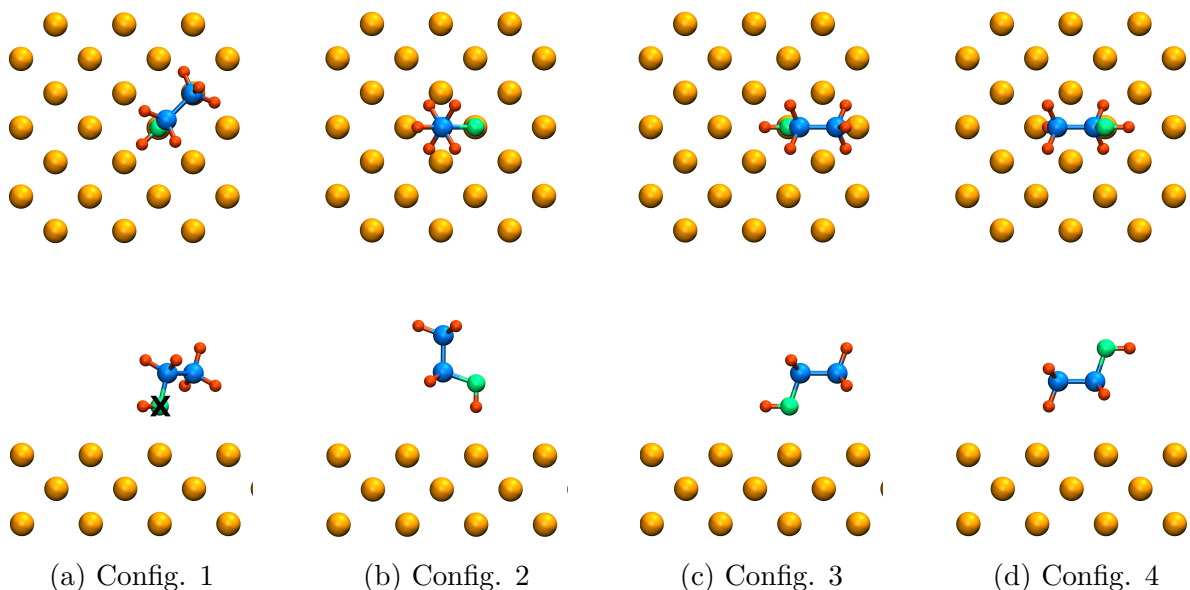


Figure 5.7: Configurations considered for the adsorption of an ethanol molecule on a Fe(100) surface, here presented in an analogous way to figure 5.3. The atom marked with a cross (X) on the side view of configuration 1 (the oxygen atom of the hydroxyl group, coloured in green) is used as a reference to orient the molecule in the adsorption sites.

As in the case of isooctane, the preferred adsorption orientations and sites for an ethanol molecule on an Fe(100) surface were not affected by the inclusion of non-local forces via the vdW functionals. The binding energies were again increased but less pronounced (see table 5.1). In contrast to isooctane, for ethanol already the employment of the PBE functional results in notable adsorption energies, and the optB86b functional enhances the adsorption strength only by a factor two (see figure 5.9). Additionally, the calculated equilibrium distance is the same for both functionals for the chosen accuracy of the calculations. This different behaviour compared to the isooctane case could stem from the involvement of other forces in the adsorption process or be a computational artefact. To

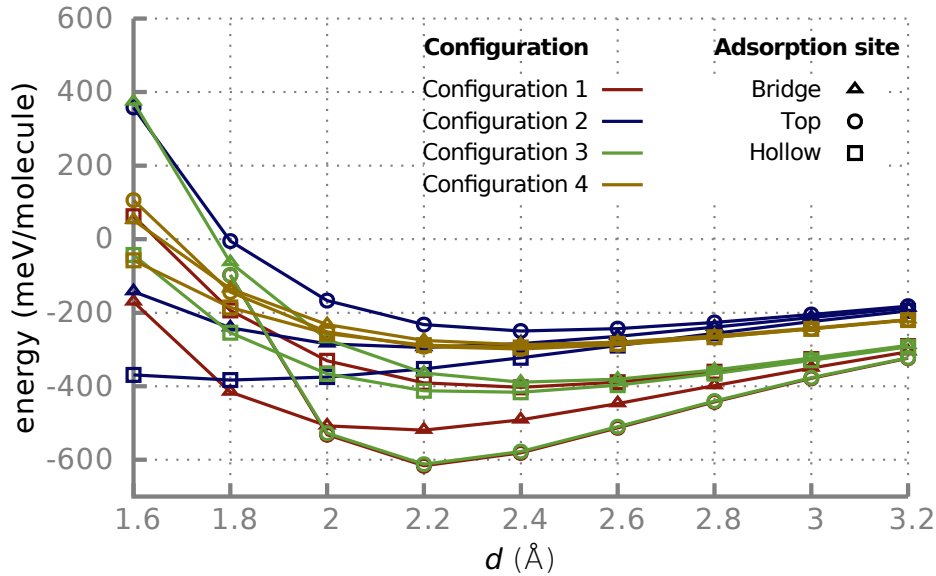


Figure 5.8: Calculated adsorption energies of four different configurations of an ethanol molecule adsorbed on an Fe(100) surface as a function of the vertical distance. The configurations (line colour) and adsorption sites (symbol) are described in figure 5.7. Atomic relaxations were not considered in these calculations.

gain further insight the adsorption energies are recalculated employing Dion’s vdW-DF and the revPBE+LDA functional. According to this comparison 95% of the adsorption energy can be attributed to dispersion interactions (see figure 5.9). Nevertheless, the significant difference of adsorption energies between the two vdW functionals and the two GGA ones, respectively, has to be further examined before additional contributions can be excluded.

In the following the charge density is used to analyze the system. In the introduction (see section 1) a link is provided in Fig. 1.1b which leads to a movie showing changes in the charge density while an ethanol molecule is approaching an iron surface. According to the charge density differences (see figures 5.10 and 5.11) the charge accumulation due to non-local interactions is larger and more extended for ethanol than for isooctane. The charge density differences calculated with the vdW-DF and revPBE+LDA potentials are rather similar in the case of isooctane, whereas they differ distinctively for ethanol. As a consequence of using the revPBE+LDA functional, charge is shifted from the region between the surface and the molecule above the molecule due to Pauli repulsion. Combining

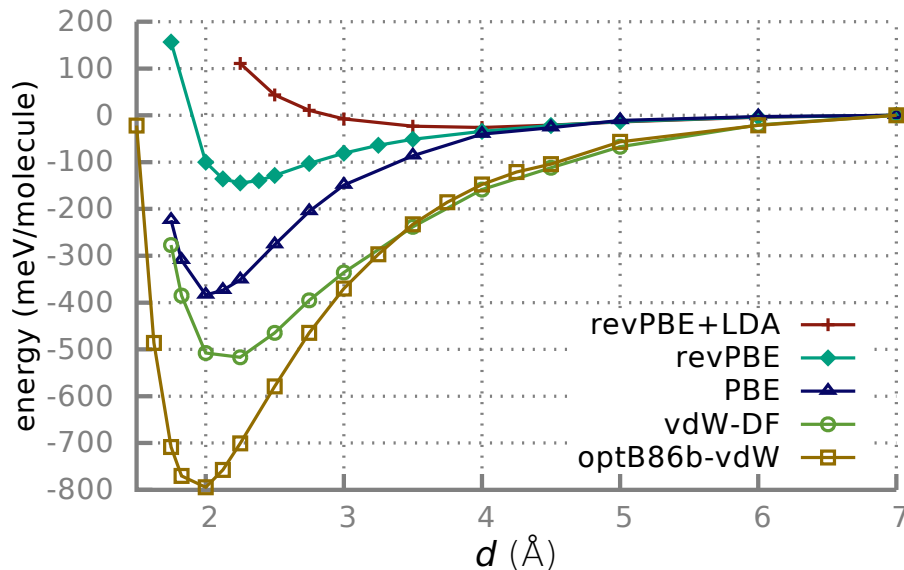


Figure 5.9: Calculated adsorption energies of an ethanol molecule on the bcc Fe(100) surface as a function of the vertical distance for the PBE, revPBE, revPBE+LDA, vdW-DF and optB86b exchange-correlation potentials.

this pronounced charge redistribution (see figure 5.10a) with the small adsorption energy (see table 5.1) suggests that this functional is overly repulsive in this system. A similar behaviour has been found before for molecules at short separations [371]. Employing the pure revPBE functional gives a larger adsorption energy (see figure 5.9), however, the binding is still weaker than for PBE by about a factor two. Since the PBE and the revPBE functionals only differ in the exchange term, the ethanol adsorption seems to be very sensitive to the description of the exchange energy. Comparing the charge redistributions obtained via PBE (see figure 5.11a) and the two vdW functionals (see figures 5.10b and 5.11b) reveals a strong similarity. In summary, PBE, while lacking non-local corrections, is able to produce similar charge redistributions as vdW functionals and also gives half of the adsorption energy. Thus, an important part of the binding between the ethanol molecule and the Fe surface cannot stem from dispersion interactions alone. Previously the involvement of a weak chemisorption was proposed [364], however, the data presented here do not exhibit a charge transfer large enough to indicate the formation of an ionic bond. Furthermore, the electron localisation function (ELF) [372, 373] does not show the existence of localized electrons constituting a bond between the ethanol

5.3. RESULTS AND DISCUSSION

molecule and the Fe surface (see figure 5.12). Additionally, the oxygen states turn out to be almost unperturbed [364], because they do not hybridize strongly with the d states of the binding Fe atom. Figure 5.11c shows that the use of the optB86b functional results in a lesser amount of charge between the molecule and the surface compared to PBE, particularly between the hydroxyl group and the closest Fe atom. Since this effect is accompanied by an enhancement of the adsorption energy, a weak electrostatic interaction joining the dispersion forces may pose the main contributions to the adsorption. Using this comparison, however, it is not possible to separate these contributions due to the different exchange term of the functionals.

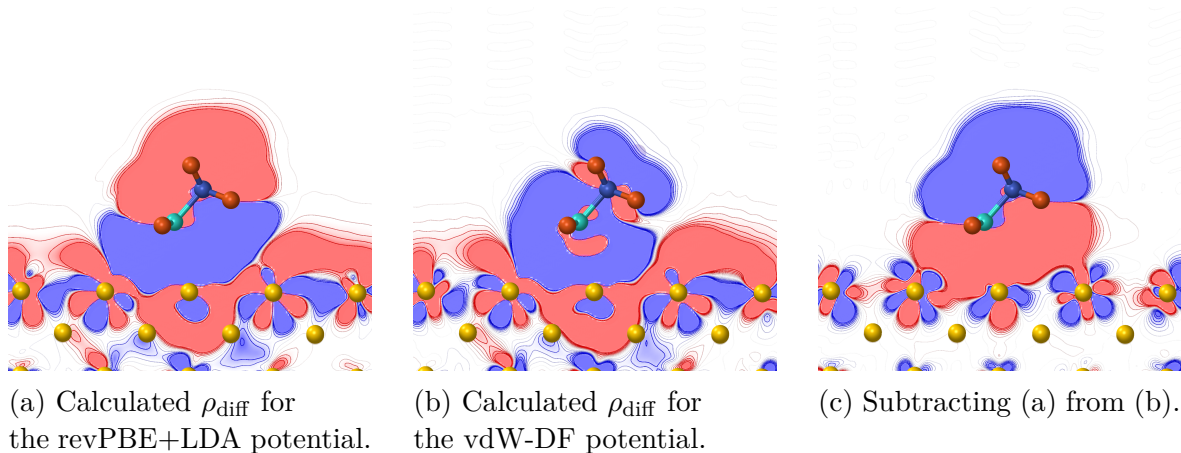


Figure 5.10: Charge density differences (ρ_{diff}) of ethanol adsorbed on the bcc Fe(100) surface at $d = 2.00$ Å. The charge density difference is defined and plotted in an analogous way to figure 5.6. Taken from Bedolla et al. [277].

The differences between the adsorption mechanisms for isooctane and ethanol can be analyzed via the polarisability of the molecules and the charge density distribution within the compounds. An isooctane molecule is supposed to exhibit a stronger polarisability due to its larger molecular size compared to an ethanol molecule. Moreover, alkanes are well-known for being among the most polarizable molecules [374]. Since the formation of instant multipoles causes dispersion forces, their binding strength is directly related to the polarizability. Thus, from this point of view a stronger adsorption of isooctane would be expected. The presence of a hydroxyl group in ethanol, however, opens further possible binding mechanisms. Ethanol exhibits a permanent dipole¹ due to the differences

¹The presence of a functional group is not necessary for the formation of a permanent dipole.

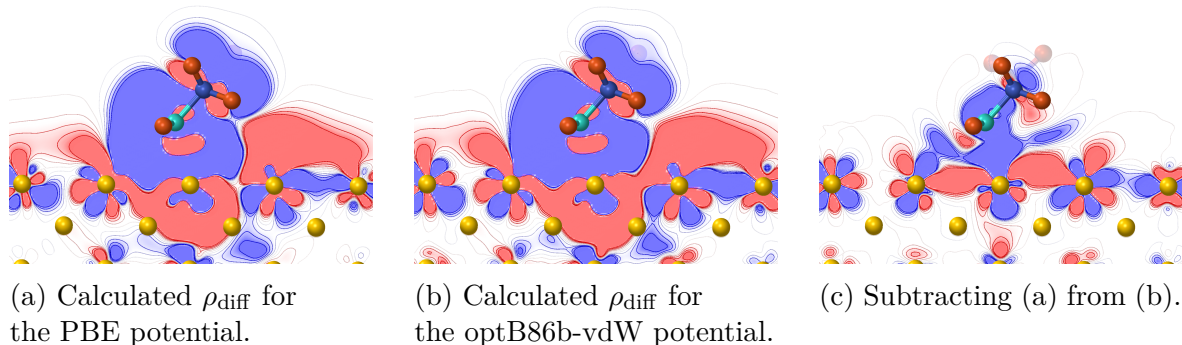


Figure 5.11: Charge density differences (ρ_{diff}) of ethanol adsorbed on the bcc Fe(100) surface at $d = 2.00$ Å. The charge density difference is defined and plotted in an analogous way to figure 5.6.

in electronegativity between the hydrogen and the oxygen atoms in the hydroxyl group as well as non-bonding electrons in the oxygen. Thus, an ethanol molecule can adsorb on the Fe slab not only via dispersion forces but also via a weak electrostatic interaction between the hydroxyl group and the iron surface, where multipoles are formed in the top layer due to the charge redistribution (see figure 5.10 and 5.11). This combination finally allows to bind an ethanol molecule more strongly to the iron surface, although the dispersion interactions are expected to be weaker than for an isooctane molecule.

5.3.2 Water mono-layer on Fe(100)

As a first step to investigate the influence of a water mono-layer placed onto an Fe(100) surface on the adsorption of isooctane and ethanol molecules, the interaction of water molecules and an iron slab was studied. This interaction between water and iron is a complex chemical process. Earlier experimental and theoretical studies [365–368, 375] showed that water molecules can adsorb dissociatively on Fe surfaces, however, the dissociation is influenced by the water coverage. The energy barrier for dissociation increases with the water coverage and for a high coverage, such as a mono-layer, water molecules are likely to adsorb molecularly on an Fe(100) surface. In a similar approach to isooctane and ethanol, water molecules were placed on different sites above the Fe slab and various ori-

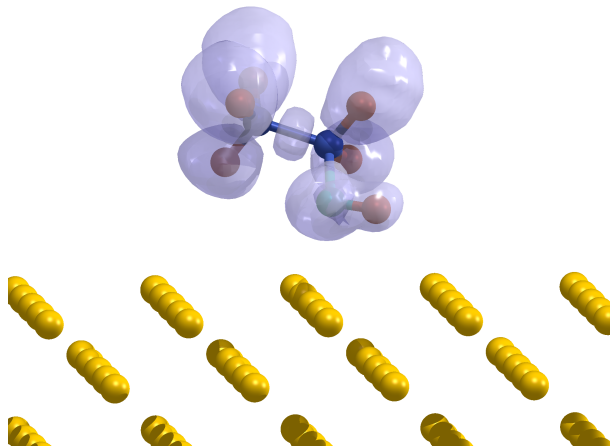


Figure 5.12: Isosurface at $\text{ELF} = 0.50$ of an ethanol molecule adsorbed on an Fe(100) surface at $d = 2.00$ Å calculated with the optB86b functional. Electrons “outside” this isosurface are expected to be delocalized.

entations were investigated. In figure 5.13 four examples for such different configurations are displayed. For a mono-layer, where one water molecule is placed for each iron atom in the top surface layer, the water molecules prefer to be located close to the top sites of the Fe surface, only being slightly shifted toward a bridge position. Since this favoured positioning is in agreement with calculations using lower water coverage as well as with previous studies on the adsorption of single water molecules [365, 367, 369, 370], the site preference is suggested to be independent of the coverage, at least up to one mono-layer. This independence may occur due to the good match between the average distance of oxygen atoms in water of 2.81 Å [376] and the calculated lattice constant of bcc Fe of 2.83 Å. Starting from a mono-layer of flat water molecules, meaning that all O-H bonds lie in a plane parallel to the Fe surface, the water molecules prefer to tilt in the vicinity of the iron slab (see figure 5.13b). This behaviour happens due to the water-slab interactions, because it does not occur if the water layer is placed at a distance to the iron slab where these interactions are negligible. Several configurations were relaxed with diverse algorithms to determine the energetically most favourable structure. To circumvent artificially symmetry effects several lateral surface cell sizes were examined. The energetically

5.3. RESULTS AND DISCUSSION

most favourable structure was found in a 2×1 surface cell with alternating orientations of the water molecules (see figure 5.13a). This pattern will be referred to as “zigzag” in the following. The zigzag was initially obtained starting from a 2×2 surface cell. A similar zigzag pattern, however at a larger distance to the slab and thus exhibiting a lower adsorption energy, was obtained after performing a simulated annealing² [377, 378]. In the zigzag configuration there are two non-equivalent water molecules, one with both O-H bonds almost parallel to the Fe surface (referred to as “parallel” molecule in the following) and the other with one O-H bond oriented towards the slab (named “downward” molecule from here on). Further differences between the two water molecules are the distance between the oxygen and the closest iron atom and the bond angles. These distances are 2.28 Å and 3.35 Å for parallel and downward molecules, respectively, and the angles are 105.36° and 104.20°. For the suggested equilibrium water layer (see figure 5.13a) the average adsorption energy per water molecule is 0.51 eV. This adsorption energy was obtained using the following equation,

$$E_{\text{ads}} = \frac{1}{2} \left(E_{\text{tot}}^{\text{H}_2\text{O}+\text{Fe}(100)} - 2E_{\text{tot}}^{\text{H}_2\text{O}} - E_{\text{tot}}^{\text{Fe}(100)} \right) \quad (5.6)$$

where $E_{\text{tot}}^{\text{H}_2\text{O}+\text{Fe}(100)}$ is the total energy of the water molecules adsorbed on the Fe(100) slab, $E_{\text{tot}}^{\text{Fe}(100)}$ is the total energy of the clean Fe(100) surface and $E_{\text{tot}}^{\text{H}_2\text{O}}$ is the total energy of the isolated water molecule. Since the inclusion of dispersion interactions also does not affect the adsorption geometry of water, all the values reported above for the water layer were calculated using the optB86b functional.

5.3.3 Organic Molecules on a water-covered Fe(100) surface

In the final step the organic molecules (isooctane and ethanol) and the water covered Fe(100) slab (see figure 5.13a) described above were brought together to examine the effect of the water layer on the adsorption. All the calculations described in the following were performed employing the optB86b functional, since dispersion forces are essential

²For this calculation the initial temperature of the simulated annealing of 300 K was gradually reduced to 0 K in 10 ps (10,000 time steps).

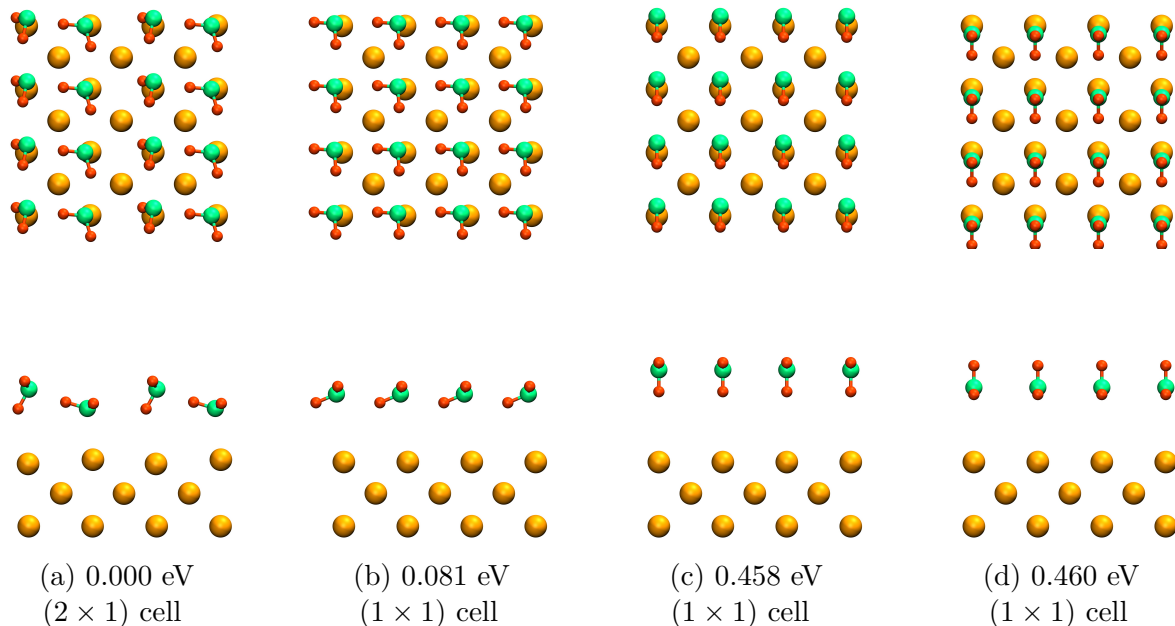


Figure 5.13: Some of the various configurations considered for the water layer and their difference in energy with respect to the lowest energy configuration. The various supercells employed for the simulations are here replicated along the axes parallel to the surface to facilitate their comparison.

for the adsorption of the considered molecules, as demonstrated above.

In the case of the isooctane molecule the adsorption geometry does not significantly change due to the presence of the water layer. This result was obtained by placing the equilibrium structure of isooctane, depicted in figure 5.3b, onto the water-covered Fe surface. The existence of two distinguishable water molecules within the layer doubles the number of possible adsorption sites. Placing the isooctane molecule above the two possible top sites only resulted in an energy difference of about 75 meV. Although this difference is too small to consider one of the adsorption site significantly favourable, the lowest energy structure was used for further calculations. The energy of the system is minimized by placing the longest continuous carbon chain above a row of parallel water molecules. Further relaxations showed only small geometrical changes in the isooctane molecule and yield the equilibrium adsorption geometry (see figure 5.14). The largest variations in bond lengths and bond angles are in the order of 10^{-3} Å and 0.1° , respectively. The water covered Fe slab is, however, subject to a more pronounced modification. Namely, the water layer as well as the top layer of the Fe slab move away from the molecule,

5.3. RESULTS AND DISCUSSION

Molecule	Ads. energy [eV]		Eq. distance [Å]	
	No H ₂ O	With H ₂ O	No H ₂ O	With H ₂ O
Isooctane	0.59	0.40	2.00	1.50
Ethanol	0.80	0.29	2.00	2.10

Table 5.2: Adsorption energies and equilibrium distances of various molecules adsorbed on a bare and on a water-covered Fe(100) surface.

forming a more compact water-covered slab. The displacements are about 0.15 Å and 0.10 Å for the water layer and the top Fe layer, respectively.

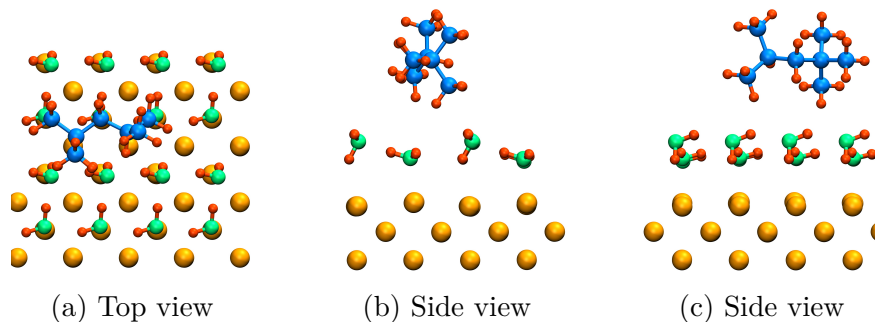


Figure 5.14: Equilibrium structure of isooctane adsorbed on a water-covered Fe(100) surface.

Potential-energy curves (see figure 5.15) clearly demonstrate a reduction of the adsorption energy of an isooctane molecule on an Fe(100) surface due to the presence of an intermediate water layer by 0.19 eV (see table 5.2). This behaviour can be explained via the charge density redistribution due to the introduction of a water layer (see figure 5.16). As already presented above, without a water layer the interaction between the isooctane molecule and the Fe surface induces a non-isotropic accumulation of charge between the molecule and the slab as well as a deficit of charge around the molecule (see figure 5.16a). The binding is accomplished via the forces arising from the charge redistribution. The introduction of a water layer, however, strongly reduces the redistribution (see figure 5.16b) by “screening” the interaction, and thus, yielding a weaker adsorption. The diminished charge redistribution allows the isooctane molecule to form a shorter bond to the water layer than to the bare Fe surface (see figure 5.15).

In the case of ethanol the effect of a water layer is expected to be more important, since

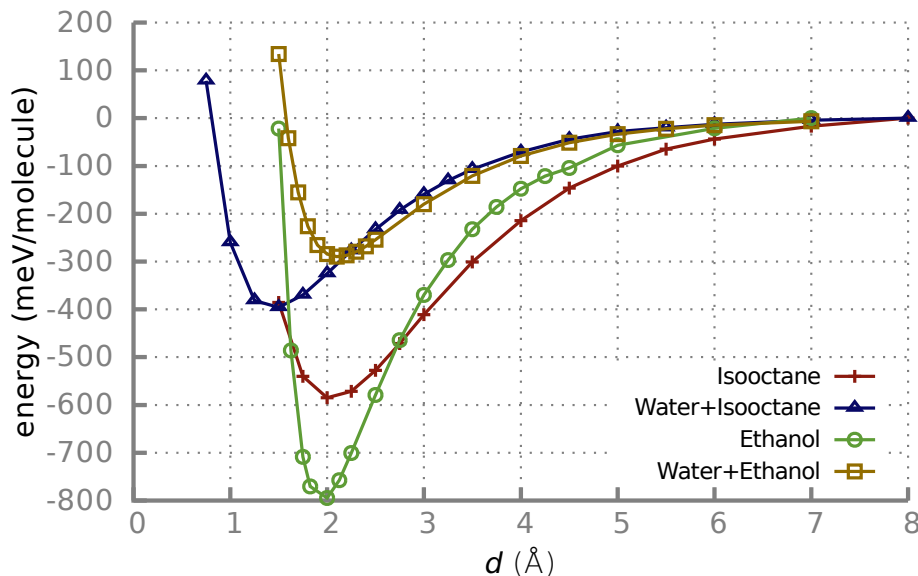


Figure 5.15: Calculated adsorption energies of the isooctane and ethanol molecules adsorbed on an Fe(100) surface (with and without a water layer) as a function of the vertical distance.

a relatively strong interaction between the hydroxyl group of the ethanol and the water molecules is anticipated. Thus, a more complex adsorption study, compared to isooctane, was conducted by including ethanol configurations 1–3 (see figures 5.7a – 5.7c). These configurations were placed on an Fe(100) surface covered with the zigzag water layer (see figure 5.17) and subsequently relaxed. All configurations energetically prefer to be adsorbed above an iron top site covered by a parallel water molecule. In the presence of a water layer configuration 2 exhibits the largest adsorption energy (see figure 5.18) and thus, yields the energetically most favourable structure (see figure 5.19). Nevertheless, the adsorption energy of this equilibrium geometry is only about 5 meV larger than the adsorption energy of configuration 3, which is an equilibrium structure without the water layer. Therefore, both configurations may exist at room temperature. The equilibrium geometries suggest that the stabilization of configuration 2 is probably a result of a hydrogen bond between the hydroxyl group of the ethanol and the oxygen of closest water molecule.

The comparison of the calculated PECs (see figure 5.15) shows that the adsorption

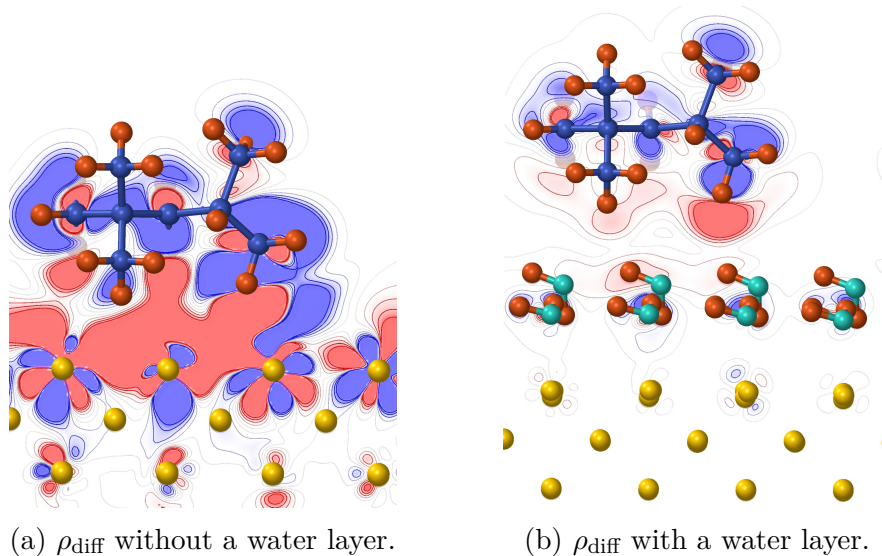


Figure 5.16: Comparison of the charge density differences (ρ_{diff}) of isooctane adsorbed on the bcc Fe(100) surface at the equilibrium distance with and without a water layer. In the absence of a water layer, the charge density difference is defined as $\rho_{\text{diff}} = \rho - (\rho_{\text{isooctane}} + \rho_{\text{Fe(100)}})$ where ρ denotes the charge density of the isooctane adsorbed on Fe(100), while $\rho_{\text{isooctane}}$ and $\rho_{\text{Fe(100)}}$ represent the charge densities of the isolated molecule and clean Fe(100) slab, respectively. In the presence of a water layer, the definition changes to $\rho_{\text{diff}} = \rho - (\rho_{\text{isooctane}} + \rho_{\text{Fe(100)+WL}})$ where $\rho_{\text{Fe(100)+WL}}$ is the charge density of the water-covered Fe(100) slab. The charge difference is plotted in a plane perpendicular to the surface for values between -5×10^{-4} (solid blue, deficit) and 5×10^{-4} (solid red, accumulation) electrons/ \AA^3 .

energy of an ethanol molecule on the Fe(100) is reduced by 0.51 eV due to the presence of an intermediate water layer (see table 5.2). This drop in adsorption energy is notably higher than for the isooctane described above. As explained earlier, an ethanol molecule binds to an Fe(100) surface via dispersion forces as well as a weak electrostatic interaction between the oxygen of the hydroxyl group and the Fe surface. Combining these interactions with the Pauli repulsion causes a charge redistribution in a rather large region mainly around the hydroxyl group (see figure 5.20a). In the presence of a water layer the size of this region is reduced substantially (see figure 5.20b). Moreover, the water layer efficiently screens the effect of the hydroxyl group, which is mainly causing the charge redistribution in the top layer of the Fe slab. Consequently, only the Fe atom directly below the hydroxyl group and in a minor way the nearest neighbours in the top surface layer contribute significantly in the adsorption process. The combination of the described

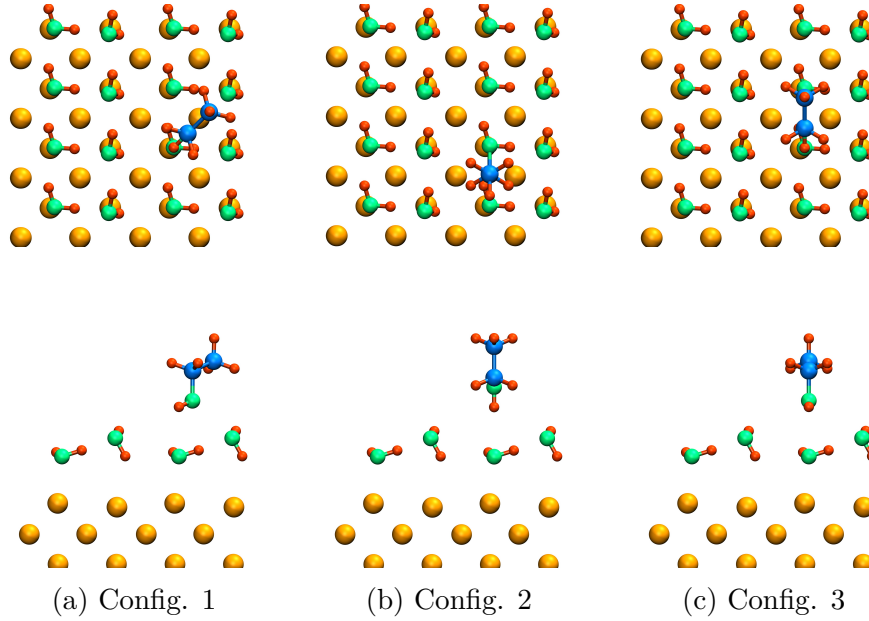


Figure 5.17: Configurations considered for the adsorption of an ethanol molecule on a water-covered Fe(100) surface, here displayed with the molecule on the top adsorption site at a distance $d = 2.00$ Å. The top row displays the top view of the system while the bottom row the side view.

effects yield a weaker bond.

5.4 Conclusion

At first, the adsorption of single isooctane and ethanol molecules was studied on a clean bcc Fe(100) surface. The effect of including van der Waals interactions was investigated by employing various density functionals. The inclusion of vdW forces was shown to be very important for describing the binding process. The long-range vdW interactions lead to non-local correlation which enhances the adsorption energy and decreases the equilibrium distance between the molecule and the surface. In particular, for molecules which can hardly interact by other means, such as isooctane, vdW forces are crucial. For example, the adsorption energy is increased by about one order of magnitude for the isooctane, however, only by a factor two in the case of ethanol. The consideration of vdW forces yields a more attractive potential in the space between the molecule and the surface; therefore, less charge is expelled from this region. Contrary to the energetics

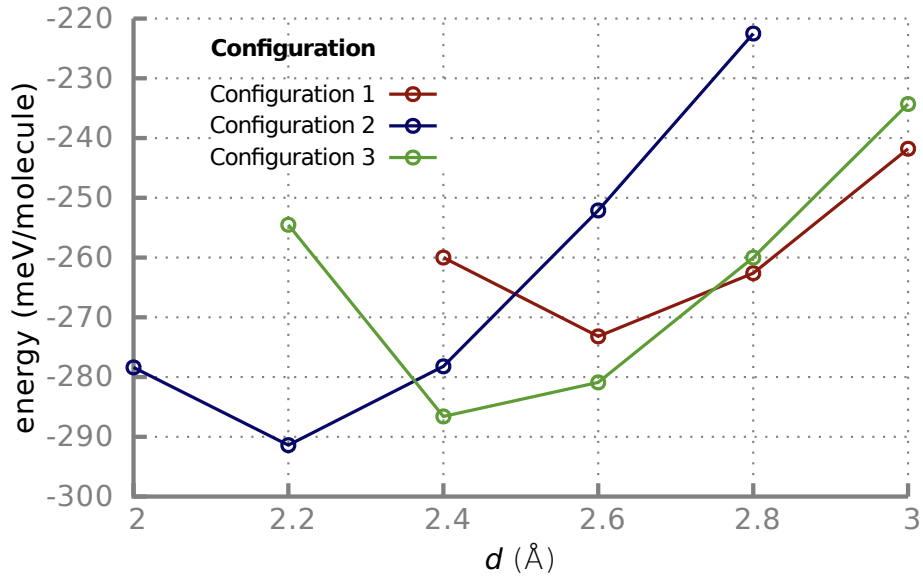


Figure 5.18: Calculated adsorption energies of three different configurations of an ethanol molecule adsorbed on a water-covered Fe(100) surface as a function of the vertical distance. The configurations (line colour) are described in figure 5.17.

and the equilibrium distance, the spatial configuration of the adsorbed molecules is only slightly affected by vdW forces. Moreover, the effect of adsorption site and geometry was examined and energetically favoured configurations were calculated. An isooctane molecule prefers to maximize the area it covers on the Fe(100) surface, whereas an ethanol molecule always favours to orientate its hydroxyl group towards the surface. From the energy landscapes, it was concluded that an isooctane is rather free to move on the Fe(100)

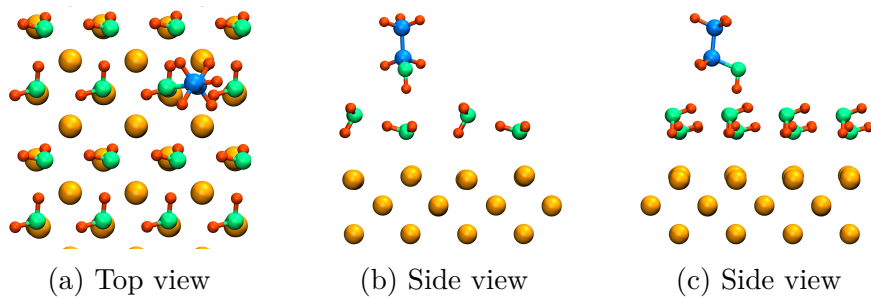


Figure 5.19: Equilibrium structure of ethanol adsorbed on a water-covered Fe(100) surface.

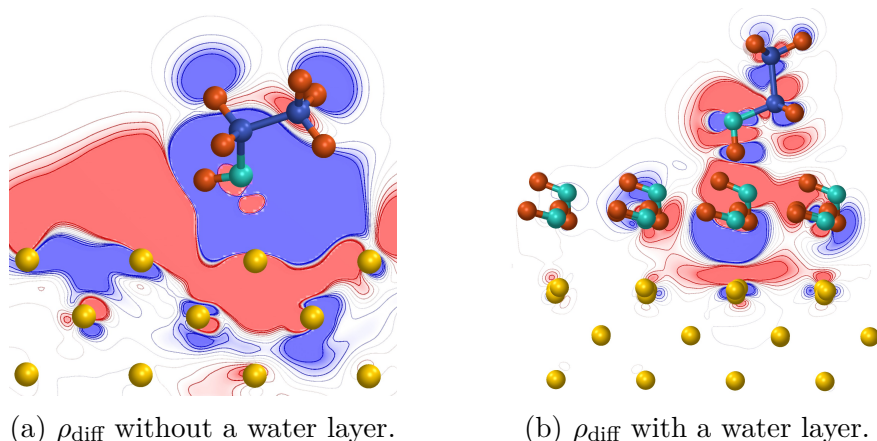


Figure 5.20: Comparison of the charge density differences (ρ_{diff}) of ethanol adsorbed on the bcc Fe(100) surface at the equilibrium distance with and without a water layer. The charge density difference is defined and plotted in an analogous way to figure 5.16.

surface at finite temperature, while ethanol is more likely to be pinned at one adsorption site. A further analysis of the potential-energy curves and charge density distributions leads to the conclusion that isooctane binds to the Fe(100) surface via vdW forces, while for ethanol an additional weak electrostatic interaction between the hydroxyl group of the ethanol and the surface contributes in the adsorption process.

In the second step, a water mono-layer covering the Fe(100) surface was introduced. After an extensive study the water was found to prefer a 2×1 zigzag structure on an iron surface. This structure was used in the following to examine the effect of a water layer on the adsorption of single isooctane and ethanol molecules. For both molecules the adsorption energies are reduced due to the screening effect of the water layer. In the case of ethanol the functional group further enhances this behaviour, resulting in a more pronounced decrease of the adsorption energy. Moreover, the presence of a functional group can influence the adsorption geometry. While for isooctane the preferred configurations are not affected by the introduction a water layer, in the case of ethanol a different geometry is stabilized due to the formation of hydrogen bonds.

The presented study is seen as one step towards a more rigorous treatment of vdW forces in complex systems. The results will contribute to the improvement of vdW density functionals which are independent of external input parameters. In the near future calculations including many-body effects may be feasible for systems as large as the presented

5.4. CONCLUSION

ones. Results of such work combined with the current study will further clarify the binding mechanisms. Furthermore, the obtained results will aid the fitting of accurate surface-molecule interaction potentials, which for example, are important for the study of lubricants. The modelling of such potentials is important for other methods which allow simulations on larger scales such as classical molecular dynamics simulations. In MD simulations the interaction potentials usually pose a considerable uncertainty. This combination of methods should allow to improve the description and understanding of complex systems of fundamental as well as industrial interest, which for example, can be found in the emerging bio-fuels or advanced lubricants.

The main results presented in this chapter were published in two articles in Journal of Physical Chemistry C [277, 278].

List of Abbreviations

ACFDT	Adiabatic-Connection Fluctuation-Dissipation Theorem
AFM	Atomic Force Microscope
bbc	body-centred cubic
CoF	Coefficient of Friction
DF	Density Functional
DFT	Density Functional Theory
DMT	Derjaguin, Muller and Toporov
DOS	Density of State
ELF	Electron Localisation Function
fcc	face-centred cubic
FFM	Friction Force Microscope
GGA	Generalized Gradient Approximation
HF	Hartree-Fock
JKR	Johnson, Kendall and Roberts
LDA	Local Density Approximation
MD	Molecular Dynamics
MEMS	Microelectromechanical Systems
MP2	second order Møller-Plesset perturbation theory
NEMS	Nanoelectromechanical Systems

optB86b	optimised Becke86
PAW	Projector Augmented Wave
PBE	Perdew-Burke-Ernzerhof
PEC	Potential Energy Curve
revPBE	revised Perdew-Burke-Ernzerhof
RPA	Random Phase Approximation
vdW	van der Waals
vdW-DF	van der Waals Density Functional
XC	Exchange-Correlation

Bibliography

- [1] D. Dowson, *History of Tribology*. London: Professional Engineering Pub., 2nd ed., 1998.
- [2] B. Bhushan, *Introduction to Tribology*. Tribology Series, New York: John Wiley & Sons, Inc., 2nd ed., Mar. 2013.
- [3] H. P. Jost, “Lubrication (tribology) - A report of the present position and industry’s needs,” tech. rep., H.M. Stationery Office, London, U.K., 1966.
- [4] K. Holmberg, P. Andersson, and A. Erdemir, “Global energy consumption due to friction in passenger cars,” *Tribology International*, vol. 47, pp. 221–234, Mar. 2012.
- [5] A. Fall, B. Weber, M. Pakpour, N. Lenoir, N. Shahidzadeh, J. Fiscina, C. Wagner, and D. Bonn, “Sliding friction on wet and dry sand,” *Physical Review Letters*, vol. 112, p. 175502, Apr. 2014.
- [6] S. J. Shaffer, “Tribology 101 - Introduction to the basics of tribology,” Jan. 2013. Bruker-TMT.
- [7] G. Amontons, “De la resistance causée dans les machines,” *Mem. Acad. R. A*, pp. 275–282, 1699.
- [8] C.-A. Coulomb, “Essai sur une application des règles de maximis et minimis à quelques problèmes de statique, relatifs à l’architecture, avec 2 planches,” *Mem Acad. Sci. Savants Etrangers*, vol. 7, pp. 343–382, 1773.

BIBLIOGRAPHY

- [9] R. Stribeck, “Kugellager für beliebige Belastungen,” *Zeitschrift des Vereins Deutscher Ingenieure*, vol. 45, no. 3, pp. 73–79, 1901.
- [10] R. Stribeck, “Die wesentlichen Eigenschaften der Gleit- und Rollenlager,” *Zeitschrift des Vereins Deutscher Ingenieure*, vol. 46, pp. 1342–1348, 1902.
- [11] R. H. Thurston, *Friction and lubrication - Determination of the laws and coefficients of friction by new methods and with new apparatus*. Ludgate Hill, London: Trübner and Co., 1879.
- [12] R. H. Thurston, *A treatise on friction and lost work in machinery and millwork*. New York: John Wiley & Sons, Inc., 5th ed., 1894.
- [13] B. V. Derjaguin, “Molekulartheorie der äußeren Reibung,” *Zeitschrift für Physik*, vol. 88, no. 9-10, pp. 661–675, 1934.
- [14] F. P. Bowden and D. Tabor, “The area of contact between stationary and between moving surfaces,” *Proceedings of the Royal Society A: Mathematical, Physical and Engineering Sciences*, vol. 169, pp. 391–413, Feb. 1939.
- [15] J. A. Greenwood and J. B. P. Williamson, “Contact of nominally flat surfaces,” *Proceedings of the Royal Society of London. Series A. Mathematical and Physical Sciences*, vol. 295, no. 1442, pp. 300–319, 1966.
- [16] D. J. Whitehouse and J. F. Archard, “The properties of random surfaces of significance in their contact,” *Proceedings of the Royal Society of London. A. Mathematical and Physical Sciences*, vol. 316, no. 1524, pp. 97–121, 1970.
- [17] F. P. Bowden and D. Tabor, *The Friction and Lubrication of Solids*. London: Oxford University Press, 1950.
- [18] J. C. Chaston, “Wear resistance of gold alloys for coinage: An early example of contract research,” *Gold Bulletin*, vol. 7, pp. 108–112, Dec. 1974.
- [19] T. Reye, “Zur Theorie der Zapfenreibung,” *Der Civilingenieur*, vol. 4, pp. 235–255, 1860.

BIBLIOGRAPHY

- [20] F. Preston, "Theory and design of plate glass polishing machines," *J. Soc. Glass Tech.*, vol. 9, pp. 214–256, 1927.
- [21] R. Holm, *Electrical Contacts*. Stockholm: H. Gerbers, 1946.
- [22] E. Rabinowicz and D. Tabor, "Metallic transfer between sliding metals: An autoradiographic study," *Proceedings of the Royal Society of London. Series A. Mathematical and Physical Sciences*, vol. 208, no. 1095, pp. 455–475, 1951.
- [23] J. F. Archard, "Contact and rubbing of flat surfaces," *Journal of Applied Physics*, vol. 24, no. 8, pp. 981–988, 1953.
- [24] M. C. Shaw, "Dimensional analysis for wear systems," *Wear*, vol. 43, pp. 263–266, 1977.
- [25] I. M. Hutchings, *Tribology : friction and wear of engineering materials*. Oxford: Butterworth-Heinemann, 2003.
- [26] L. Johansson, "Model and numerical algorithm for sliding contact between two elastic half-planes with frictional heat generation and wear," *Wear*, vol. 160, pp. 77–93, 1993.
- [27] C. N. Rowe, "Some aspects of the heat absorption in the function of a boundary lubricant," *Transactions ASLE*, vol. 9, pp. 100–110, 1966.
- [28] E. Rabinowicz, *Friction and wear of materials*. New York: Wiley, 1995.
- [29] J. F. Archard, "Elastic deformation and the laws of friction," *Proceedings of the Royal Society of London. Series A. Mathematical and Physical Sciences*, vol. 243, no. 1233, pp. 190–205, 1957.
- [30] J. F. Archard, "Single contacts and multiple encounters," *Journal of Applied Physics*, vol. 32, no. 8, pp. 1420–1425, 1961.
- [31] H. C. Meng and K. C. Ludema, "Wear models and predictive equations: Their form and content," *Wear*, vol. 181, pp. 443–457, 1995.

BIBLIOGRAPHY

- [32] F. T. Barwell, “Wear of metals,” *Wear*, vol. 1, pp. 317–332, 1957.
- [33] S. K. Rhee, “Wear equation for polymers sliding against metal surfaces,” *Wear*, vol. 16, pp. 431–445, 1970.
- [34] N. P. Suh, “The delamination theory of wear,” *Wear*, vol. 25, pp. 111–124, 1973.
- [35] T. F. Quinn, “Oxidational wear,” *Wear*, vol. 18, pp. 413–419, 1971.
- [36] H. Czichos, *Tribology : A systems approach to the science and technology of friction, lubrication and wear*. Amsterdam: Elsevier, 1986.
- [37] M. Godet, “The third-body approach: A mechanical view of wear,” *Wear*, vol. 100, pp. 437–452, 1984.
- [38] N. Fillot, I. Iordanoff, and Y. Berthier, “A granular dynamic model for the degradation of material,” *Journal of Tribology*, vol. 126, pp. 606–614, 2004.
- [39] Y. Berthier, “Maurice godet’s third body,” vol. 31 of *Elsevier Tribology Series*, pp. 21–30, 1995.
- [40] I. Iordanoff, B. Seve, and Y. Berthier, “Solid third body analysis using a discrete approach: Influence of adhesion and particle size on macroscopic properties,” *Journal of Tribology*, vol. 124, pp. 530–538, 2002.
- [41] H.-P. Cao, M. Renouf, F. Dubois, and Y. Berthier, “Coupling continuous and discontinuous descriptions to model first body deformation in third body flows,” *Journal of Tribology*, vol. 133, no. 4, p. 041601, 2011.
- [42] N. Fillot, I. Iordanoff, and Y. Berthier, “Simulation of wear through mass balance in a dry contact,” *Journal of Tribology*, vol. 127, pp. 230–237, 2005.
- [43] N. Fillot, I. Iordanoff, and Y. Berthier, “Wear modeling and the third body concept,” *Wear*, vol. 262, no. 7-8, pp. 949–957, 2007.
- [44] M. Z. Huq and J.-P. Celis, “Expressing wear rate in sliding contacts based on dissipated energy,” *Wear*, vol. 252, pp. 375–383, 2002.

BIBLIOGRAPHY

- [45] A. Ramalho and J. C. Miranda, “The relationship between wear and dissipated energy in sliding systems,” *Wear*, vol. 260, no. 4-5, pp. 361–367, 2006.
- [46] S. Fouvry, T. Liskiewicz, P. Kapsa, S. Hannel, and E. Sauger, “An energy description of wear mechanisms and its applications to oscillating sliding contacts,” *Wear*, vol. 255, no. 1-6, pp. 287–298, 2003.
- [47] T. Liskiewicz and S. Fouvry, “Development of a friction energy capacity approach to predict the surface coating endurance under complex oscillating sliding conditions,” *Tribology International*, vol. 38, no. 1, pp. 69–79, 2005.
- [48] R. M. Matveesky, “The critical temperature of oil with point and line contact machines,” *Transactions of the ASME*, vol. 87, p. 754, 1965.
- [49] H. Mohrbacher, J.-P. Celis, and J. R. Roos, “Laboratory testing of displacement and load induced fretting,” *Tribology International*, vol. 28, no. 5, pp. 269–278, 1995.
- [50] M. Z. Huq and J.-P. Celis, “Reproducibility of friction and wear results in ball-on-disc unidirectional sliding tests of TiN-alumina pairings,” *Wear*, vol. 212, no. 2, pp. 151–159, 1997.
- [51] B. E. Klamecki, “Wear - An entropy production model,” *Wear*, vol. 58, pp. 325–330, 1980.
- [52] B. E. Klamecki, “A thermodynamic model of friction,” *Wear*, vol. 63, pp. 113–120, 1980.
- [53] B. E. Klamecki, “Energy dissipation in sliding,” *Wear*, vol. 77, pp. 112–128, 1982.
- [54] B. E. Klamecki, “An entropy-based model of plastic deformation energy dissipation in sliding,” *Wear*, vol. 96, pp. 319–329, 1984.
- [55] H. A. Abdel-Aal, “Wear and irreversible entropy generation in the dry sliding,” *Annals Dunarea de Jos of Galati (Tribology)*, pp. 34–44, 2006.

BIBLIOGRAPHY

- [56] A. Zmitrowicz, “A thermodynamical model of contact, friction and wear: I. Governing equations,” *Wear*, vol. 114, pp. 135–168, 1987.
- [57] A. Zmitrowicz, “A thermodynamical model of contact, friction and wear: II. Constitutive equations for metals and linearized theories,” *Wear*, vol. 114, pp. 169–197, 1987.
- [58] A. Zmitrowicz, “A thermodynamical model of contact, friction and wear: III. Constitutive equations for friction, wear and frictional heat,” *Wear*, vol. 114, pp. 199–221, 1987.
- [59] G. Lebon, D. Jou, and J. Casas-Vázquez, *Understanding Non-equilibrium Thermodynamics : Foundations, Applications, Frontiers*. Berlin: Springer, 2008.
- [60] M. Dragon-Louiset, “On a predictive macroscopic contact-sliding wear model based on micromechanical considerations,” *International journal of solids and structures*, vol. 38, no. 9, pp. 1625–1639, 2001.
- [61] C. Stolz, “A thermodynamical approach to contact wear as application of moving discontinuities,” *Archive of Applied Mechanics*, vol. 77, no. 2-3, pp. 165–175, 2006.
- [62] M. D. Bryant, “Entropy and dissipative processes of friction and wear,” *FME Transactions*, vol. 37, no. 2, pp. 55–60, 2009.
- [63] M. D. Bryant, F. F. Ling, and M. A. Wortman, “Theoretical and empirical investigation of stochastic degradation in machinery components,” in *NSF Design & Manufacturing Grantees Conference*, (Long Beach, USA), p. 102, 1999.
- [64] K. L. Doelling, F. F. Ling, M. D. Bryant, and B. P. Heilman, “An experimental study of the correlation between wear and entropy flow in machinery components,” *Journal of Applied Physics*, vol. 88, no. 5, pp. 2999–3003, 2000.
- [65] F. F. Ling, M. D. Bryant, and K. L. Doelling, “On irreversible thermodynamics for wear prediction,” *Wear*, vol. 253, no. 11-12, pp. 1165–1172, 2002.

- [66] A. B. Aghdam and M. M. Khonsari, “On the correlation between wear and entropy in dry sliding contact,” *Wear*, vol. 270, no. 11-12, pp. 781–790, 2011.
- [67] M. D. Bryant, M. M. Khonsari, and F. F. Ling, “On the thermodynamics of degradation,” *Proceedings of the Royal Society A: Mathematical, Physical and Engineering Sciences*, vol. 464, no. 2096, pp. 2001–2014, 2008.
- [68] A. A. Feinberg and A. Widom, “On thermodynamic reliability engineering,” *IEEE Transactions on Reliability*, vol. 49, no. 2, pp. 136–146, 2000.
- [69] I. S. Gershman and N. A. Bushe, “Elements of thermodynamics and self-organization during friction,” in *Self-organization during friction: Advanced surface-engineered materials and systems design*, Boca Raton, FL: CRC Taylor & Francis, 2006.
- [70] T. D. B. Jacobs and R. W. Carpick, “Nanoscale wear as a stress-assisted chemical reaction,” *Nature Nanotechnology*, vol. 8, no. 2, pp. 108–112, 2013.
- [71] H. Kloss and R. Wasche, “Analytical approach for wear prediction of metallic and ceramic materials in tribological applications,” *Wear*, vol. 266, pp. 476–481, 2009.
- [72] A. Schirmeisen, “Wear: One atom after the other,” *Nature Nanotechnology*, vol. 8, no. 2, pp. 81–82, 2013.
- [73] J. P. Davim, *Biotribology*. London; Hoboken, NJ: ISTE ; John Wiley & Sons, 2010.
- [74] M. Nosonovsky and B. Bhushan, “Green tribology: principles, research areas and challenges,” *Philosophical Transactions of the Royal Society A: Mathematical, Physical and Engineering Sciences*, vol. 368, pp. 4677–4694, Sept. 2010.
- [75] B. Bhushan, J. Israelachvili, and U. Landman, “Nanotribology - friction, wear and lubrication on the atomic scale,” *Nature*, vol. 374, pp. 607–616, Apr. 1995.
- [76] I. Szlufarska, M. Chandross, and R. W. Carpick, “Recent advances in single-asperity nanotribology,” *Journal of Physics D: Applied Physics*, vol. 41, p. 123001, June 2008.

BIBLIOGRAPHY

- [77] B. Bhushan, “Nanotribology, nanomechanics and nanomaterials characterization,” *Philosophical Transactions of the Royal Society A: Mathematical, Physical and Engineering Sciences*, vol. 366, pp. 1351–1381, Apr. 2008.
- [78] B. Bhushan, *Nanotribology and Nanomechanics : Biomimetics and Industrial Applications*. Berlin: Springer, 2011.
- [79] eOrthopod, *A Patient’s Guide to Artificial Joint Replacement of the Hip*. Missoula, Montana, USA: Medical Multimedia Group, LLC, 2002.
- [80] H.-C. Chiu, B. Ritz, S. Kim, E. Tosatti, C. Klinke, and E. Riedo, “Sliding on a nanotube: Interplay of friction, deformations and structure,” *Advanced Materials*, vol. 24, pp. 2879–2884, June 2012.
- [81] GWEC, *Global Wind Report 2013*. Brussels, Belgium: Global Wind Energy Council, 2013.
- [82] M. N. Kotzalas and G. L. Doll, “Tribological advancements for reliable wind turbine performance,” *Philosophical Transactions of the Royal Society A: Mathematical, Physical and Engineering Sciences*, vol. 368, pp. 4829–4850, Oct. 2010.
- [83] W. M. J. Batten, A. S. Bahaj, A. F. Molland, and J. R. Chaplin, “The prediction of the hydrodynamic performance of marine current turbines,” *Renewable Energy*, vol. 33, pp. 1085–1096, May 2008.
- [84] L. Rybach, “Geothermal sustainability,” *Geo-Heat Cent. Q. Bull.*, vol. 28, pp. 2–7, Sept. 2007.
- [85] R. Bertani, “Geothermal power generation in the world 2005–2010 update report,” *Geothermics*, vol. 41, pp. 1–29, Jan. 2012.
- [86] C. I. Betton, “Lubricants and their environmental impact,” in *Chemistry and Technology of Lubricants* (R. M. Mortier, M. F. Fox, and S. T. Orszulik, eds.), pp. 435–457, Dordrecht: Springer Netherlands, 2009.

BIBLIOGRAPHY

- [87] J. K. Mannekote and S. V. Kailas, “Performance evaluation of vegetable oils as lubricant in a four stroke engine,” in *Proc. 4th World Tribology Congress*, (Kyoto, Japan), p. 331, Sept. 2009.
- [88] M. A. Kabir, C. F. Higgs, and M. R. Lovell, “A pin-on-disk experimental study on a green particulate-fluid lubricant,” *Journal of Tribology*, vol. 130, p. 041801, Aug. 2008.
- [89] P. Fratzl and R. Weinkamer, “Nature’s hierarchical materials,” *Progress in Materials Science*, vol. 52, pp. 1263–1334, Nov. 2007.
- [90] U. G. K. Wegst, H. Bai, E. Saiz, A. P. Tomsia, and R. O. Ritchie, “Bioinspired structural materials,” *Nature Materials*, vol. 14, pp. 23–36, Oct. 2014.
- [91] M. Nosonovsky and S. K. Esche, “A paradox of decreasing entropy in multiscale monte carlo grain growth simulations,” *Entropy*, vol. 10, pp. 49–54, June 2008.
- [92] M. Nosonovsky and B. Bhushan, “Thermodynamics of surface degradation, self-organization and self-healing for biomimetic surfaces,” *Philosophical Transactions of the Royal Society A: Mathematical, Physical and Engineering Sciences*, vol. 367, pp. 1607–1627, Mar. 2009.
- [93] M. Nosonovsky, R. Amano, J. M. Lucci, and P. K. Rohatgi, “Physical chemistry of self-organization and self-healing in metals,” *Physical Chemistry Chemical Physics*, vol. 11, pp. 9530–9536, Aug. 2009.
- [94] M. Nosonovsky and B. Bhushan, “Surface self-organization: From wear to self-healing in biological and technical surfaces,” *Applied Surface Science*, vol. 256, pp. 3982–3987, Jan. 2010.
- [95] B. Bhushan, Y. C. Jung, and K. Koch, “Micro-, nano- and hierarchical structures for superhydrophobicity, self-cleaning and low adhesion,” *Philosophical Transactions of the Royal Society A: Mathematical, Physical and Engineering Sciences*, vol. 367, pp. 1631–1672, May 2009.

BIBLIOGRAPHY

- [96] B. Dean and B. Bhushan, “Shark-skin surfaces for fluid-drag reduction in turbulent flow: a review,” *Philosophical Transactions of the Royal Society A: Mathematical, Physical and Engineering Sciences*, vol. 368, pp. 4775–4806, Oct. 2010.
- [97] L. D. Chambers, K. R. Stokes, F. C. Walsh, and R. J. K. Wood, “Modern approaches to marine antifouling coatings,” *Surface and Coatings Technology*, vol. 201, pp. 3642–3652, Dec. 2006.
- [98] L. Raibeck, J. Reap, and B. Bras, “Investigating environmental burdens and benefits of biologically inspired self-cleaning surfaces,” *CIRP Journal of Manufacturing Science and Technology*, vol. 1, pp. 230–236, Jan. 2009.
- [99] W.-E. Reif, *Squamation and Ecology of Sharks*. Stuttgart, Germany: Schweizerbart Science Publishers, Dec. 1985.
- [100] K. Komvopoulos, “Surface engineering and microtribology for microelectromechanical systems,” *Wear*, vol. 200, pp. 305–327, Dec. 1996.
- [101] S. M. Spearing, “Materials issues in microelectromechanical systems (MEMS),” *Acta Materialia*, vol. 48, pp. 179–196, Jan. 2000.
- [102] R. Maboudian and C. Carraro, “Surface chemistry and tribology of MEMS,” *Annual Review of Physical Chemistry*, vol. 55, pp. 35–54, June 2004.
- [103] S. H. Kim, D. B. Asay, and M. T. Dugger, “Nanotribology and MEMS,” *Nano Today*, vol. 2, pp. 22–29, Oct. 2007.
- [104] B. Bhushan, “Nanotribology and nanomechanics in nano/biotechnology,” *Philos. Trans. R. S. A*, vol. 366, pp. 1499–1537, May 2008.
- [105] D. Tabor and R. H. S. Winterton, “The direct measurement of normal and retarded van der Waals forces,” *Proceedings of the Royal Society A: Mathematical, Physical and Engineering Sciences*, vol. 312, pp. 435–450, Sept. 1969.

BIBLIOGRAPHY

- [106] J. N. Israelachvili and G. E. Adams, “Measurement of forces between two mica surfaces in aqueous electrolyte solutions in the range 0–100 nm,” *Journal of the Chemical Society, Faraday Transactions 1: Physical Chemistry in Condensed Phases*, vol. 74, no. 0, p. 975, 1978.
- [107] G. Binnig, H. Rohrer, C. Gerber, and E. Weibel, “Surface studies by scanning tunneling microscopy,” *Physical Review Letters*, vol. 49, pp. 57–61, July 1982.
- [108] G. Binnig, C. F. Quate, and C. Gerber, “Atomic force microscope,” *Physical Review Letters*, vol. 56, pp. 930–933, Mar. 1986.
- [109] R. Bennewitz, “Friction force microscopy,” *Materials Today*, vol. 8, pp. 42–48, May 2005.
- [110] E. Meyer, H. J. Hug, and R. Bennewitz, *Scanning Probe Microscopy: The Lab on a Tip*. Berlin: Springer, 2004.
- [111] P. A. Thompson and M. O. Robbins, “Simulations of contact-line motion: Slip and the dynamic contact angle,” *Physical Review Letters*, vol. 63, pp. 766–769, Aug. 1989.
- [112] U. Landman, W. D. Luedtke, and N. W. Ribarsky, “Structural and dynamical consequences of interactions in interfacial systems,” *Journal of Vacuum Science & Technology A: Vacuum, Surfaces, and Films*, vol. 7, pp. 2829–2839, July 1989.
- [113] M. O. Robbins and M. Müser, “Computer simulations of friction, lubrication, and wear,” in *Modern Tribology Handbook*, vol. 5, pp. 717–765, Boca Raton, FL: CRC Press, Dec. 2000.
- [114] D. Mulliah, S. D. Kenny, R. Smith, and C. F. Sanz-Navarro, “Molecular dynamic simulations of nanoscratching of silver (100),” *Nanotechnology*, vol. 15, pp. 243–249, Mar. 2004.
- [115] S. D. Kenny, D. Mulliah, C. F. Sanz-Navarro, and R. Smith, “Molecular dynamics simulations of nanoindentation and nanotribology,” *Philosophical Transactions of*

BIBLIOGRAPHY

- the Royal Society A: Mathematical, Physical and Engineering Sciences*, vol. 363, pp. 1949–1959, Aug. 2005.
- [116] J. D. Schall, P. T. Mikulski, G. M. Chateauneuf, G. Gao, and J. A. Harrison, “Molecular dynamics simulations of tribology,” in *Superlubricity*, pp. 79–102, Elsevier, 2007.
- [117] L. Pastewka, S. Moser, P. Gumbsch, and M. Moseler, “Anisotropic mechanical amorphization drives wear in diamond,” *Nature Materials*, vol. 10, no. 1, pp. 34–38, 2010.
- [118] A. Vernes, S. Eder, G. Vorlaufer, and G. Betz, “On the three-term kinetic friction law in nanotribological systems,” *Faraday Discussions*, vol. 156, p. 173, 2012.
- [119] S. J. Eder, A. Vernes, and G. Betz, “On the derjaguin offset in boundary-lubricated nanotribological systems,” *Langmuir*, vol. 29, pp. 13760–13772, Nov. 2013.
- [120] S. Eder, A. Vernes, and G. Betz, “Methods and numerical aspects of nanoscopic contact area estimation in atomistic tribological simulations,” *Computer Physics Communications*, vol. 185, pp. 217–228, Jan. 2014.
- [121] S. J. Eder, D. Bianchi, U. Cihak-Bayr, A. Vernes, and G. Betz, “An analysis method for atomistic abrasion simulations featuring rough surfaces and multiple abrasive particles,” *Computer Physics Communications*, vol. 185, pp. 2456–2466, Oct. 2014.
- [122] W. Zhong and D. Tománek, “First-principles theory of atomic-scale friction,” *Physical Review Letters*, vol. 64, no. 25, pp. 3054–3057, 1990.
- [123] R. Neitola and T. A. Pakkanen, “Ab initio studies on the atomic-scale origin of friction between diamond (111) surfaces,” *The Journal of Physical Chemistry B*, vol. 105, pp. 1338–1343, Feb. 2001.
- [124] S. Dag and S. Ciraci, “Atomic scale study of superlow friction between hydrogenated diamond surfaces,” *Physical Review B*, vol. 70, no. 24, p. 241401, 2004.

BIBLIOGRAPHY

- [125] R. Neitola, H. Ruuska, and T. A. Pakkanen, “Ab initio studies on nanoscale friction between graphite layers: Effect of model size and level of theory,” *The Journal of Physical Chemistry B*, vol. 109, pp. 10348–10354, May 2005.
- [126] S. Ciraci, T. Yildirim, S. Dag, and O. Gulseren, “Ab-initio atomic scale study of nearly frictionless surfaces,” in *Superlubricity*, pp. 57–77, Elsevier, 2007.
- [127] G. Zilibotti, M. Righi, and M. Ferrario, “Ab initio study on the surface chemistry and nanotribological properties of passivated diamond surfaces,” *Physical Review B*, vol. 79, no. 7, p. 075420, 2009.
- [128] M. Garvey, O. J. Furlong, M. Weinert, and W. T. Tysoe, “Shear properties of potassium chloride films on iron obtained using density functional theory,” *Journal of Physics: Condensed Matter*, vol. 23, no. 26, p. 265003, 2011.
- [129] G. Zilibotti and M. C. Righi, “Ab initio calculation of the adhesion and ideal shear strength of planar diamond interfaces with different atomic structure and hydrogen coverage,” *Langmuir*, vol. 27, no. 11, pp. 6862–6867, 2011.
- [130] S. Cahangirov, C. Ataca, M. Topsakal, H. Sahin, and S. Ciraci, “Frictional figures of merit for single layered nanostructures,” *Physical Review Letters*, vol. 108, no. 12, p. 126103, 2012.
- [131] S. Kwon, J.-H. Ko, K.-J. Jeon, Y.-H. Kim, and J. Y. Park, “Enhanced nanoscale friction on fluorinated graphene,” *Nano Letters*, vol. 12, pp. 6043–6048, Dec. 2012.
- [132] J. Wang, F. Wang, J. Li, S. Wang, Y. Song, Q. Sun, and Y. Jia, “Theoretical study of superlow friction between two single-side hydrogenated graphene sheets,” *Tribology Letters*, vol. 48, no. 2, pp. 255–261, 2012.
- [133] L.-F. Wang, T.-B. Ma, Y.-Z. Hu, and H. Wang, “Atomic-scale friction in graphene oxide: An interfacial interaction perspective from first-principles calculations,” *Physical Review B*, vol. 86, p. 125436, Sept. 2012.

BIBLIOGRAPHY

- [134] M. Garvey, M. Weinert, and W. T. Tysoe, “Pressure dependence of the shear strengths of the tungsten carbide-potassium chloride interface,” *Tribology Letters*, vol. 50, no. 1, pp. 105–113, 2013.
- [135] M. Wolloch, G. Feldbauer, P. Mohn, J. Redinger, and A. Vernes, “Ab initio friction forces on the nanoscale: A density functional theory study of fcc Cu(111),” *Physical Review B*, vol. 90, p. 195418, Nov. 2014.
- [136] Y. Mo, K. T. Turner, and I. Szlufarska, “Friction laws at the nanoscale,” *Nature*, vol. 457, no. 7233, pp. 1116–1119, 2009.
- [137] S. J. Eder, G. Feldbauer, D. Bianchi, U. Cihak-Bayr, G. Betz, and A. Vernes, “Applicability of macroscopic wear and friction laws on the atomic length scale,” *Physical Review Letters*, 2015. under review.
- [138] B. Luan and M. O. Robbins, “The breakdown of continuum models for mechanical contacts,” *Nature*, vol. 435, no. 7044, pp. 929–932, 2005.
- [139] H.-J. Kim, S.-S. Yoo, and D.-E. Kim, “Nano-scale wear: A review,” *International Journal of Precision Engineering and Manufacturing*, vol. 13, pp. 1709–1718, Sept. 2012.
- [140] W. Maw, F. Stevens, S. C. Langford, and J. T. Dickinson, “Single asperity tribochemical wear of silicon nitride studied by atomic force microscopy,” *Journal of Applied Physics*, vol. 92, no. 9, p. 5103, 2002.
- [141] B. Gotsmann and M. Lantz, “Atomistic wear in a single asperity sliding contact,” *Physical Review Letters*, vol. 101, p. 125501, 2008.
- [142] R. Cola  go, “An AFM study of single-contact abrasive wear: The rabinowicz wear equation revisited,” *Wear*, vol. 267, no. 11, pp. 1772–1776, 2009.
- [143] M. Vargonen, Y. Yang, L. Huang, and Y. Shi, “Molecular simulation of tip wear in a single asperity sliding contact,” *Wear*, vol. 307, no. 1-2, pp. 150–154, 2013.

BIBLIOGRAPHY

- [144] Z.-D. Sha, V. Sorkin, P. S. Branicio, Q.-X. Pei, Y.-W. Zhang, and D. J. Srolovitz, “Large-scale molecular dynamics simulations of wear in diamond-like carbon at the nanoscale,” *Applied Physics Letters*, vol. 103, no. 7, p. 073118, 2013.
- [145] B. Bhushan and K. Kwak, “Velocity dependence of nanoscale wear in atomic force microscopy,” *Applied Physics Letters*, vol. 91, no. 16, p. 163113, 2007.
- [146] M. Hirano and K. Shinjo, “Atomistic locking and friction,” *Physical Review B*, vol. 41, pp. 11837–11851, June 1990.
- [147] M. Hirano, K. Shinjo, R. Kaneko, and Y. Murata, “Observation of superlubricity by scanning tunneling microscopy,” *Physical Review Letters*, vol. 78, pp. 1448–1451, Feb. 1997.
- [148] M. Dienwiebel, G. Verhoeven, N. Pradeep, J. Frenken, J. Heimberg, and H. Zandbergen, “Superlubricity of graphite,” *Physical Review Letters*, vol. 92, p. 126101, Mar. 2004.
- [149] D. Dietzel, M. Feldmann, U. Schwarz, H. Fuchs, and A. Schirmeisen, “Scaling laws of structural lubricity,” *Physical Review Letters*, vol. 111, p. 235502, Dec. 2013.
- [150] R. Zhang, Z. Ning, Y. Zhang, Q. Zheng, Q. Chen, H. Xie, Q. Zhang, W. Qian, and F. Wei, “Superlubricity in centimetres-long double-walled carbon nanotubes under ambient conditions,” *Nature Nanotechnology*, vol. 8, pp. 912–916, Nov. 2013.
- [151] A. Filippov, M. Dienwiebel, J. Frenken, J. Klafter, and M. Urbakh, “Torque and twist against superlubricity,” *Physical Review Letters*, vol. 100, p. 046102, Jan. 2008.
- [152] X. Feng, S. Kwon, J. Y. Park, and M. Salmeron, “Superlubric sliding of graphene nanoflakes on graphene,” *ACS Nano*, vol. 7, pp. 1718–1724, Feb. 2013.
- [153] S. Krylov, K. Jinesh, H. Valk, M. Dienwiebel, and J. Frenken, “Thermally induced suppression of friction at the atomic scale,” *Physical Review E*, vol. 71, p. 065101(R), June 2005.

BIBLIOGRAPHY

- [154] S. Maier, Y. Sang, T. Filleter, M. Grant, R. Bennewitz, E. Gnecco, and E. Meyer, “Fluctuations and jump dynamics in atomic friction experiments,” *Physical Review B*, vol. 72, p. 245418, Dec. 2005.
- [155] G. He, M. H. Müser, and M. O. Robbins, “Adsorbed layers and the origin of static friction,” *Science*, vol. 284, pp. 1650–1652, June 1999.
- [156] M. H. Müser, L. Wenning, and M. Robbins, “Simple microscopic theory of amon-ton’s laws for static friction,” *Physical Review Letters*, vol. 86, pp. 1295–1298, Feb. 2001.
- [157] N. N. Gosvami, T. Filleter, P. Egberts, and R. Bennewitz, “Microscopic friction studies on metal surfaces,” *Tribology Letters*, vol. 39, pp. 19–24, July 2010.
- [158] L. Wenning and M. H. Müser, “Friction laws for elastic nanoscale contacts,” *Euro-physics Letters (EPL)*, vol. 54, pp. 693–699, June 2001.
- [159] S. Eder, A. Vernes, G. Vorlaufer, and G. Betz, “Molecular dynamics simulations of mixed lubrication with smooth particle post-processing,” *Journal of Physics: Condensed Matter*, vol. 23, p. 175004, May 2011.
- [160] R. Overney, H. Takano, M. Fujihira, W. Paulus, and H. Ringsdorf, “Anisotropy in friction and molecular stick-slip motion,” *Physical Review Letters*, vol. 72, pp. 3546–3549, May 1994.
- [161] J. Y. Park, D. F. Ogletree, M. Salmeron, R. A. Ribeiro, P. C. Canfield, C. J. Jenks, and P. A. Thiel, “High frictional anisotropy of periodic and aperiodic directions on a quasicrystal surface,” *Science*, vol. 309, pp. 1354–1356, Aug. 2005.
- [162] A. J. Weymouth, D. Meuer, P. Mutombo, T. Wutscher, M. Ondracek, P. Jelinek, and F. J. Giessibl, “Atomic structure affects the directional dependence of friction,” *Physical Review Letters*, vol. 111, p. 126103, Sept. 2013.

BIBLIOGRAPHY

- [163] A. Vanossi, N. Manini, M. Urbakh, S. Zapperi, and E. Tosatti, “Colloquium: Modeling friction: From nanoscale to mesoscale,” *Reviews of Modern Physics*, vol. 85, no. 2, pp. 529–552, 2013.
- [164] Y. Dong, Q. Li, and A. Martini, “Molecular dynamics simulation of atomic friction: A review and guide,” *Journal of Vacuum Science & Technology A: Vacuum, Surfaces, and Films*, vol. 31, p. 030801, Mar. 2013.
- [165] L. Prandtl, “Ein Gedankenmodell zur kinetischen Theorie der festen Körper,” *ZAMM - Zeitschrift für Angewandte Mathematik und Mechanik*, vol. 8, pp. 85–106, Apr. 1928.
- [166] G. Tomlinson, “A molecular theory of friction,” *Philosophical Magazine and Journal of Science*, vol. 7, pp. 905–939, June 1929.
- [167] W. Zhong and D. Tománek, “First-principles theory of atomic-scale friction,” *Physical Review Letters*, vol. 64, pp. 3054–3057, June 1990.
- [168] D. Tománek, W. Zhong, and H. Thomas, “Calculation of an atomically modulated friction force in atomic-force microscopy,” *Europhysics Letters (EPL)*, vol. 15, pp. 887–892, Aug. 1991.
- [169] H. Hertz, “Über die Berührung fester elastischer Körper,” *Journal für reine und angewandte Mathematik*, vol. 92, pp. 156–171, 1882.
- [170] K. L. Johnson, K. Kendall, and A. D. Roberts, “Surface energy and the contact of elastic solids,” *Proceedings of the Royal Society A: Mathematical, Physical and Engineering Sciences*, vol. 324, no. 1558, pp. 301–313, 1971.
- [171] B. V. Derjaguin, V. M. Muller, and Y. P. Toporov, “Effect of contact deformations on the adhesion of particles,” *Journal of Colloid and Interface Science*, vol. 53, no. 2, pp. 314–326, 1975.
- [172] D. Tabor, “Surface forces and surface interactions,” *Journal of Colloid and Interface Science*, vol. 58, pp. 2–13, Jan. 1977.

BIBLIOGRAPHY

- [173] D. Maugis, “Adhesion of spheres: The JKR-DMT transition using a Dugdale model,” *Journal of Colloid and Interface Science*, vol. 150, pp. 243–269, Apr. 1992.
- [174] S. Cheng and M. O. Robbins, “Defining contact at the atomic scale,” *Tribology Letters*, vol. 39, pp. 329–348, Apr. 2010.
- [175] M. Wolloch, G. Feldbauer, P. Mohn, J. Redinger, and A. Vernes, “Ab-initio calculation of the real contact area on the atomic scale,” *Physical Review B*, 2015. under review.
- [176] R. F. W. Bader, *Atoms in molecules: a quantum theory*. Oxford; New York: Clarendon Press, 1990.
- [177] N. W. Ashcroft and N. D. Mermin, *Solid state physics*. New York: Holt, Rinehart and Winston, 1976.
- [178] C. Kittel, *Introduction to solid state physics*. New York: Wiley, 1996.
- [179] D. R. Hartree, “The wave mechanics of an atom with a non-Coulomb central field. part I. Theory and methods,” *Mathematical Proceedings of the Cambridge Philosophical Society*, vol. 24, p. 89, Jan. 1928.
- [180] V. Fock, “Näherungsmethode zur Lösung des quantenmechanischen Mehrkörperproblems,” *Zeitschrift für Physik*, vol. 61, pp. 126–148, Jan. 1930.
- [181] P. A. M. Dirac, “On the theory of quantum mechanics,” *Proceedings of the Royal Society A: Mathematical, Physical and Engineering Sciences*, vol. 112, pp. 661–677, Oct. 1926.
- [182] W. Heisenberg, “Mehrkörperproblem und Resonanz in der Quantenmechanik,” *Zeitschrift für Physik*, vol. 38, pp. 411–426, June 1926.
- [183] C. David Sherrill and H. F. Schaefer III., “The configuration interaction method: Advances in highly correlated approaches,” in *Advances in Quantum Chemistry*, vol. 34, pp. 143–269, Elsevier, 1999.

BIBLIOGRAPHY

- [184] C. J. Cramer, *Essentials of computational chemistry: Theories and models*. New York: J. Wiley, 2002.
- [185] H. G. Kümmel, “A biography of the coupled cluster method,” in *Recent progress in many-body theories*, (Singapore), pp. 334–348, World Scientific Publishing, 2002.
- [186] I. Shavitt and R. J. Bartlett, *Many-body methods in chemistry and physics: MBPT and coupled-cluster theory*. Cambridge: Cambridge University Press, 2009.
- [187] C. Møller and M. S. Plesset, “Note on an approximation treatment for many-electron systems,” *Physical Review*, vol. 46, pp. 618–622, Oct. 1934.
- [188] K. Burke, “Perspective on density functional theory,” *The Journal of Chemical Physics*, vol. 136, p. 150901, Apr. 2012.
- [189] A. D. Becke, “Perspective: Fifty years of density-functional theory in chemical physics,” *The Journal of Chemical Physics*, vol. 140, p. 18A301, May 2014.
- [190] L. H. Thomas, “The calculation of atomic fields,” *Mathematical Proceedings of the Cambridge Philosophical Society*, vol. 23, p. 542, Jan. 1927.
- [191] E. Fermi, “Eine statistische Methode zur Bestimmung einiger Eigenschaften des Atoms und ihre Anwendung auf die Theorie des periodischen Systems der Elemente,” *Zeitschrift für Physik*, vol. 48, pp. 73–79, Jan. 1928.
- [192] W. Kohn, “Nobel lecture: Electronic structure of matter-wave functions and density functionals,” *Reviews of Modern Physics*, vol. 71, pp. 1253–1266, Oct. 1999.
- [193] P. Hohenberg and W. Kohn, “Inhomogeneous electron gas,” *Physical Review*, vol. 136, pp. B864–B871, Nov. 1964.
- [194] W. Kohn and L. J. Sham, “Self-consistent equations including exchange and correlation effects,” *Physical Review*, vol. 140, pp. A1133–A1138, Nov. 1965.
- [195] J. T. Chayes, L. Chayes, and M. B. Ruskai, “Density functional approach to quantum lattice systems,” *Journal of Statistical Physics*, vol. 38, pp. 497–518, Feb. 1985.

BIBLIOGRAPHY

- [196] A. Rajagopal and J. Callaway, “Inhomogeneous electron gas,” *Physical Review B*, vol. 7, pp. 1912–1919, Mar. 1973.
- [197] R. Wesendrup, J. K. Laerdahl, and P. Schwerdtfeger, “Relativistic effects in gold chemistry. VI. Coupled cluster calculations for the isoelectronic series AuPt^- , Au_2 , and AuHg^+ ,” *The Journal of Chemical Physics*, vol. 110, no. 19, pp. 9457–9462, 1999.
- [198] J. P. Perdew and A. Zunger, “Self-interaction correction to density-functional approximations for many-electron systems,” *Physical Review B*, vol. 23, pp. 5048–5079, May 1981.
- [199] M. P. Marder, *Condensed Matter Physics*. Wiley-Interscience, 2nd ed., Nov. 2010.
- [200] D. M. Ceperley and B. J. Alder, “Ground state of the electron gas by a stochastic method,” *Physical Review Letters*, vol. 45, pp. 566–569, Aug. 1980.
- [201] M. C. Payne, M. P. Teter, D. C. Allan, T. A. Arias, and J. D. Joannopoulos, “Iterative minimization techniques for ab initio total-energy calculations: Molecular dynamics and conjugate gradients,” *Reviews of Modern Physics*, vol. 64, pp. 1045–1097, Oct. 1992.
- [202] O. Gunnarsson, M. Jonson, and B. Lundqvist, “Descriptions of exchange and correlation effects in inhomogeneous electron systems,” *Physical Review B*, vol. 20, pp. 3136–3164, Oct. 1979.
- [203] A. van de Walle and G. Ceder, “Correcting overbinding in local-density-approximation calculations,” *Physical Review B*, vol. 59, pp. 14992–15001, June 1999.
- [204] J. P. Perdew, K. Burke, and M. Ernzerhof, “Generalized gradient approximation made simple,” *Physical Review Letters*, vol. 77, pp. 3865–3868, Oct. 1996.
- [205] J. P. Perdew, K. Burke, and M. Ernzerhof, “Generalized gradient approximation

BIBLIOGRAPHY

- made simple [phys. rev. lett. 77, 3865 (1996)],” *Physical Review Letters*, vol. 78, pp. 1396–1396, Feb. 1997.
- [206] J. P. Perdew, J. A. Chevary, S. H. Vosko, K. A. Jackson, M. R. Pederson, D. J. Singh, and C. Fiolhais, “Atoms, molecules, solids, and surfaces: Applications of the generalized gradient approximation for exchange and correlation,” *Physical Review B*, vol. 46, pp. 6671–6687, Sept. 1992.
- [207] V. Ozoliņš and M. Körling, “Full-potential calculations using the generalized gradient approximation: Structural properties of transition metals,” *Physical Review B*, vol. 48, pp. 18304–18307, Dec. 1993.
- [208] C. Filippi, D. Singh, and C. Umrigar, “All-electron local-density and generalized-gradient calculations of the structural properties of semiconductors,” *Physical Review B*, vol. 50, pp. 14947–14951, Nov. 1994.
- [209] C. Stampfl and C. Van de Walle, “Density-functional calculations for III-V nitrides using the local-density approximation and the generalized gradient approximation,” *Physical Review B*, vol. 59, pp. 5521–5535, Feb. 1999.
- [210] J. Perdew, S. Kurth, A. Zupan, and P. Blaha, “Accurate density functional with correct formal properties: A step beyond the generalized gradient approximation,” *Physical Review Letters*, vol. 82, pp. 2544–2547, Mar. 1999.
- [211] J. Heyd, G. E. Scuseria, and M. Ernzerhof, “Hybrid functionals based on a screened coulomb potential,” *The Journal of Chemical Physics*, vol. 118, no. 18, p. 8207, 2003.
- [212] C. Lee, W. Yang, and R. G. Parr, “Development of the Colle-Salvetti correlation-energy formula into a functional of the electron density,” *Physical Review B*, vol. 37, pp. 785–789, Jan. 1988.
- [213] A. D. Becke, “A new mixing of Hartree-Fock and local density-functional theories,” *The Journal of Chemical Physics*, vol. 98, no. 2, p. 1372, 1993.

BIBLIOGRAPHY

- [214] E. Lieb and W. Thirring, “Universal nature of van der Waals forces for Coulomb systems,” *Physical Review A*, vol. 34, pp. 40–46, July 1986.
- [215] R. H. S. Winterton, “Van der Waals forces,” *Contemporary Physics*, vol. 11, pp. 559–574, Nov. 1970.
- [216] H.-J. Butt and M. Kappl, *Surface and Interfacial Forces*. Weinheim, Germany: Wiley-VCH Verlag GmbH & Co. KGaA, Jan. 2010.
- [217] J. D. Van der Waals, *Over de Continuïteit van den Gas en Vloeistofoestand*. PhD thesis, Leiden University, 1873.
- [218] “Van der Waals forces,” in *IUPAC Compendium of Chemical Terminology* (M. Nič, J. Jiráť, B. Košata, A. Jenkins, and A. McNaught, eds.), Research Triangle Park, NC: IUPAC, 2.1.0 ed., June 2009.
- [219] F. London, “Zur Theorie und Systematik der Molekularkräfte,” *Zeitschrift für Physik*, vol. 63, pp. 245–279, Mar. 1930.
- [220] R. Eisenschitz and F. London, “Über das Verhältnis der van der Waalsschen Kräfte zu den homöopolaren Bindungskräften,” *Zeitschrift für Physik*, vol. 60, pp. 491–527, July 1930.
- [221] F. London, “The general theory of molecular forces,” *Transactions of the Faraday Society*, vol. 33, p. 8b, 1937.
- [222] H. C. Hamaker, “The London-van der Waals attraction between spherical particles,” *Physica*, vol. 4, pp. 1058–1072, Oct. 1937.
- [223] J. L. Atwood and J. W. Steed, *Encyclopedia of supramolecular chemistry*. New York: M. Dekker, 2004.
- [224] K. P. Lawley, *Ab initio methods in quantum chemistry. II*. Hoboken: John Wiley & Sons, 2009.
- [225] J. Jortner, *Photosensitive Chemistry*. Hoboken: John Wiley & Sons, 2009.

BIBLIOGRAPHY

- [226] H. Zeng, “Polymer Adhesion, Friction, and Lubrication,” Hoboken, NJ, USA: John Wiley & Sons, Inc., Feb. 2013.
- [227] S. Lebègue, J. Harl, T. Gould, J. G. Ángyán, G. Kresse, and J. F. Dobson, “Cohesive properties and asymptotics of the dispersion interaction in graphite by the random phase approximation,” *Physical Review Letters*, vol. 105, p. 196401, Nov. 2010.
- [228] G.-X. Zhang, A. Tkatchenko, J. Paier, H. Appel, and M. Scheffler, “Van der Waals interactions in ionic and semiconductor solids,” *Physical Review Letters*, vol. 107, p. 245501, Dec. 2011.
- [229] F. Mittendorfer, A. Garhofer, J. Redinger, J. Klimeš, J. Harl, and G. Kresse, “Graphene on Ni(111): Strong interaction and weak adsorption,” *Physical Review B*, vol. 84, p. 201401(R), Nov. 2011.
- [230] G. Graziano, J. Klimeš, F. Fernandez-Alonso, and A. Michaelides, “Improved description of soft layered materials with van der Waals density functional theory,” *Journal of Physics: Condensed Matter*, vol. 24, no. 42, p. 424216, 2012.
- [231] J. Klimeš, D. R. Bowler, and A. Michaelides, “Chemical accuracy for the van der Waals density functional,” *Journal of Physics: Condensed Matter*, vol. 22, p. 022201, Dec. 2009.
- [232] J. Klimeš and A. Michaelides, “Perspective: Advances and challenges in treating van der Waals dispersion forces in density functional theory,” *The Journal of Chemical Physics*, vol. 137, no. 12, p. 120901, 2012.
- [233] X. Wu, M. C. Vargas, S. Nayak, V. Lotrich, and G. Scoles, “Towards extending the applicability of density functional theory to weakly bound systems,” *The Journal of Chemical Physics*, vol. 115, no. 19, pp. 8748–8757, 2001.
- [234] Q. Wu and W. Yang, “Empirical correction to density functional theory for van der Waals interactions,” *The Journal of Chemical Physics*, vol. 116, no. 2, pp. 515–523, 2002.

BIBLIOGRAPHY

- [235] U. Zimmerli, M. Parrinello, and P. Koumoutsakos, "Dispersion corrections to density functionals for water aromatic interactions," *The Journal of Chemical Physics*, vol. 120, no. 6, pp. 2693–2699, 2004.
- [236] S. Grimme, "Semiempirical GGA-type density functional constructed with a long-range dispersion correction," *Journal of Computational Chemistry*, vol. 27, pp. 1787–1799, Nov. 2006.
- [237] J. Antony and S. Grimme, "Density functional theory including dispersion corrections for intermolecular interactions in a large benchmark set of biologically relevant molecules," *Physical Chemistry Chemical Physics*, vol. 8, no. 45, pp. 5287–5293, 2006.
- [238] F. Ortmann, F. Bechstedt, and W. Schmidt, "Semiempirical van der Waals correction to the density functional description of solids and molecular structures," *Physical Review B*, vol. 73, p. 205101, May 2006.
- [239] P. Jurečka, J. Černý, P. Hobza, and D. R. Salahub, "Density functional theory augmented with an empirical dispersion term. Interaction energies and geometries of 80 noncovalent complexes compared with *ab initio* quantum mechanics calculations," *Journal of Computational Chemistry*, vol. 28, pp. 555–569, Jan. 2007.
- [240] A. Tkatchenko and M. Scheffler, "Accurate molecular van der Waals interactions from ground-state electron density and free-atom reference data," *Physical Review Letters*, vol. 102, p. 073005, Feb. 2009.
- [241] S. Grimme, J. Antony, S. Ehrlich, and H. Krieg, "A consistent and accurate *ab initio* parametrization of density functional dispersion correction (DFT-D) for the 94 elements H-Pu," *The Journal of Chemical Physics*, vol. 132, no. 15, p. 154104, 2010.
- [242] S. Grimme, "Density functional theory with London dispersion corrections," *Wiley Interdisciplinary Reviews: Computational Molecular Science*, vol. 1, pp. 211–228, Mar. 2011.

BIBLIOGRAPHY

- [243] J. Klimeš, *Towards an accurate theoretical description of surface processes*. PhD thesis, University College London, 2011.
- [244] M. W. Cole, D. Velegol, H.-Y. Kim, and A. A. Lucas, “Nanoscale van der Waals interactions,” *Macromolecular Symposia*, vol. 35, pp. 849–866, 2009.
- [245] A. Tkatchenko, R. A. DiStasio, R. Car, and M. Scheffler, “Accurate and efficient method for many-body van der Waals interactions,” *Physical Review Letters*, vol. 108, p. 236402, June 2012.
- [246] R. A. DiStasio, O. A. von Lilienfeld, and A. Tkatchenko, “Collective many-body van der Waals interactions in molecular systems,” *Proceedings of the National Academy of Sciences*, vol. 109, pp. 14791–14795, Sept. 2012.
- [247] R. A. DiStasio, V. V. Gobre, and A. Tkatchenko, “Many-body van der Waals interactions in molecules and condensed matter,” *Journal of Physics: Condensed Matter*, vol. 26, p. 213202, May 2014.
- [248] F. Furche, “Molecular tests of the random phase approximation to the exchange-correlation energy functional,” *Physical Review B*, vol. 64, p. 195120, Oct. 2001.
- [249] J. G. Ángyán, R.-F. Liu, J. Toulouse, and G. Jansen, “Correlation energy expressions from the Adiabatic-Connection Fluctuation-Dissipation Theorem approach,” *Journal of Chemical Theory and Computation*, vol. 7, pp. 3116–3130, Oct. 2011.
- [250] A. Heßelmann, “Random-phase-approximation correlation method including exchange interactions,” *Physical Review A*, vol. 85, p. 012517, Jan. 2012.
- [251] J. Harl and G. Kresse, “Accurate bulk properties from approximate many-body techniques,” *Physical Review Letters*, vol. 103, p. 056401, July 2009.
- [252] J. Dobson and B. Dinte, “Constraint satisfaction in local and gradient susceptibility approximations: Application to a van der Waals Density Functional,” *Physical Review Letters*, vol. 76, pp. 1780–1783, Mar. 1996.

BIBLIOGRAPHY

- [253] F. Furche and T. Van Voorhis, “Fluctuation-dissipation theorem density-functional theory,” *The Journal of Chemical Physics*, vol. 122, no. 16, p. 164106, 2005.
- [254] J. Harl, L. Schimka, and G. Kresse, “Assessing the quality of the random phase approximation for lattice constants and atomization energies of solids,” *Physical Review B*, vol. 81, p. 115126, Mar. 2010.
- [255] O. A. Vydrov and T. Van Voorhis, “Nonlocal van der Waals density functional: The simpler the better,” *The Journal of Chemical Physics*, vol. 133, no. 24, p. 244103, 2010.
- [256] T. Sato and H. Nakai, “Density functional method including weak interactions: Dispersion coefficients based on the local response approximation,” *The Journal of Chemical Physics*, vol. 131, no. 22, p. 224104, 2009.
- [257] T. Sato and H. Nakai, “Local response dispersion method. II. Generalized multi-center interactions,” *The Journal of Chemical Physics*, vol. 133, no. 19, p. 194101, 2010.
- [258] M. Dion, H. Rydberg, E. Schröder, D. C. Langreth, and B. I. Lundqvist, “Van der Waals density functional for general geometries,” *Physical Review Letters*, vol. 92, p. 246401, June 2004.
- [259] Y. Zhang and W. Yang, “Comment on “Generalized gradient approximation made simple”,” *Physical Review Letters*, vol. 80, pp. 890–890, Jan. 1998.
- [260] O. Vydrov and T. Van Voorhis, “Nonlocal van der Waals Density Functional made simple,” *Physical Review Letters*, vol. 103, p. 063004, Aug. 2009.
- [261] P. Jurečka, J. Čponer, J. Černý, and P. Hobza, “Benchmark database of accurate (MP2 and CCSD(T) complete basis set limit) interaction energies of small model complexes, DNA base pairs, and amino acid pairs,” *Physical Chemistry Chemical Physics*, vol. 8, no. 17, p. 1985, 2006.

- [262] J. Klimeš, D. R. Bowler, and A. Michaelides, “Chemical accuracy for the van der Waals density functional,” *Journal of Physics: Condensed Matter*, vol. 22, p. 022201, Dec. 2009.
- [263] J. Klimeš, D. R. Bowler, and A. Michaelides, “Van der Waals density functionals applied to solids,” *Physical Review B*, vol. 83, p. 195131, May 2011.
- [264] A. D. Becke, “On the large-gradient behavior of the density functional exchange energy,” *The Journal of Chemical Physics*, vol. 85, p. 7184, Dec. 1986.
- [265] J. Carrasco, “Role of van der Waals forces in thermodynamics and kinetics of layered transition metal oxide electrodes: Alkali and alkaline-earth ion insertion into V_2O_5 ,” *The Journal of Physical Chemistry C*, vol. 118, pp. 19599–19607, Aug. 2014.
- [266] B. Santra, J. Klimeš, D. Alfè, A. Tkatchenko, B. Slater, A. Michaelides, R. Car, and M. Scheffler, “Hydrogen bonds and van der Waals forces in ice at ambient and high pressures,” *Physical Review Letters*, vol. 107, p. 185701, Oct. 2011.
- [267] C. Eames, J. M. Clark, G. Rousse, J.-M. Tarascon, and M. S. Islam, “Lithium migration pathways and van der Waals effects in the $LiFeSO_4OH$ battery material,” *Chemistry of Materials*, vol. 26, pp. 3672–3678, June 2014.
- [268] D. C. Sorescu, E. F. C. Byrd, B. M. Rice, and K. D. Jordan, “Assessing the performances of dispersion-corrected density functional methods for predicting the crystallographic properties of high nitrogen energetic salts,” *Journal of Chemical Theory and Computation*, vol. 10, pp. 4982–4994, Nov. 2014.
- [269] S. Chakarova-Käck, E. Schröder, B. Lundqvist, and D. Langreth, “Application of van der Waals Density Functional to an extended system: Adsorption of benzene and naphthalene on graphite,” *Physical Review Letters*, vol. 96, p. 146107, Apr. 2006.
- [270] S. Chakarova-Käck, Ø. Borck, E. Schröder, and B. Lundqvist, “Adsorption of phenol on graphite(0001) and α - Al_2O_3 (0001): Nature of van der Waals bonds from first-principles calculations,” *Physical Review B*, vol. 74, p. 155402, Oct. 2006.

BIBLIOGRAPHY

- [271] J. Carrasco, B. Santra, J. Klimeš, and A. Michaelides, “To wet or not to wet? Dispersion forces tip the balance for water ice on metals,” *Physical Review Letters*, vol. 106, p. 026101, Jan. 2011.
- [272] W. Lew, M. C. Crowe, C. T. Campbell, J. Carrasco, and A. Michaelides, “The energy of hydroxyl coadsorbed with water on Pt(111),” *The Journal of Physical Chemistry C*, vol. 115, pp. 23008–23012, Nov. 2011.
- [273] T. J. Lawton, J. Carrasco, A. E. Baber, A. Michaelides, and E. C. H. Sykes, “Visualization of hydrogen bonding and associated chirality in methanol hexamers,” *Physical Review Letters*, vol. 107, p. 256101, Dec. 2011.
- [274] W. Liu, J. Carrasco, B. Santra, A. Michaelides, M. Scheffler, and A. Tkatchenko, “Benzene adsorbed on metals: Concerted effect of covalency and van der Waals bonding,” *Physical Review B*, vol. 86, p. 245405, Dec. 2012.
- [275] H. Yildirim, T. Greber, and A. Kara, “Trends in adsorption characteristics of benzene on transition metal surfaces: Role of surface chemistry and van der Waals interactions,” *The Journal of Physical Chemistry C*, vol. 117, pp. 20572–20583, Oct. 2013.
- [276] J. Carrasco, W. Liu, A. Michaelides, and A. Tkatchenko, “Insight into the description of van der Waals forces for benzene adsorption on transition metal (111) surfaces,” *The Journal of Chemical Physics*, vol. 140, p. 084704, Feb. 2014.
- [277] P. O. Bedolla, G. Feldbauer, M. Wolloch, S. J. Eder, N. Dörr, P. Mohn, J. Redinger, and A. Vernes, “Effects of van der Waals interactions in the adsorption of isooctane and ethanol on Fe(100) surfaces,” *The Journal of Physical Chemistry C*, vol. 118, pp. 17608–17615, July 2014.
- [278] P. O. Bedolla, G. Feldbauer, M. Wolloch, C. Gruber, S. J. Eder, N. Dörr, P. Mohn, J. Redinger, and A. Vernes, “Density functional investigation of the adsorption of isooctane, ethanol, and acetic acid on a water-covered Fe(100) surface,” *The Journal of Physical Chemistry C*, vol. 118, pp. 21428–21437, Sept. 2014.

BIBLIOGRAPHY

- [279] M. Vanin, J. J. Mortensen, A. K. Kelkkanen, J. M. Garcia-Lastra, K. S. Thygesen, and K. W. Jacobsen, “Graphene on metals: A van der Waals density functional study,” *Physical Review B*, vol. 81, p. 081408(R), Feb. 2010.
- [280] D.-L. Chen, W. A. Al-Saidi, and J. K. Johnson, “Noble gases on metal surfaces: Insights on adsorption site preference,” *Physical Review B*, vol. 84, p. 241405(R), Dec. 2011.
- [281] M. Antlanger, W. Mayr-Schmölzer, J. Pavelec, F. Mittendorfer, J. Redinger, P. Varga, U. Diebold, and M. Schmid, “Pt₃Zr(0001): A substrate for growing well-ordered ultrathin zirconia films by oxidation,” *Physical Review B*, vol. 86, p. 035451, July 2012.
- [282] A. Garhofer, *Ab Initio studies of graphene-metal interfaces*. PhD thesis, Vienna University of Technology, Vienna, 2013.
- [283] J. I. J. Choi, W. Mayr-Schmölzer, F. Mittendorfer, J. Redinger, U. Diebold, and M. Schmid, “The growth of ultra-thin zirconia films on Pd₃Zr(0001),” *Journal of Physics: Condensed Matter*, vol. 26, p. 225003, June 2014.
- [284] G. Kresse and J. Hafner, “Ab initio molecular dynamics for liquid metals,” *Physical Review B*, vol. 47, pp. 558–561, Jan. 1993.
- [285] G. Kresse and J. Hafner, “Ab initio molecular-dynamics simulation of the liquid-metal–amorphous-semiconductor transition in germanium,” *Physical Review B*, vol. 49, pp. 14251–14269, May 1994.
- [286] G. Kresse and J. Furthmüller, “Efficient iterative schemes for ab initio total-energy calculations using a plane-wave basis set,” *Physical Review B*, vol. 54, pp. 11169–11186, Oct. 1996.
- [287] G. Kresse and J. Furthmüller, “Efficiency of ab-initio total energy calculations for metals and semiconductors using a plane-wave basis set,” *Computational Materials Science*, vol. 6, pp. 15–50, July 1996.

BIBLIOGRAPHY

- [288] J. Paier, R. Hirschl, M. Marsman, and G. Kresse, “The Perdew-Burke-Ernzerhof exchange-correlation functional applied to the G2-1 test set using a plane-wave basis set,” *The Journal of Chemical Physics*, vol. 122, no. 23, p. 234102, 2005.
- [289] J. Paier, M. Marsman, K. Hummer, G. Kresse, I. C. Gerber, and J. G. Ángyán, “Screened hybrid density functionals applied to solids,” *The Journal of Chemical Physics*, vol. 124, no. 15, p. 154709, 2006.
- [290] T. Bučko, J. Hafner, S. Lebègue, and J. G. Ángyán, “Improved description of the structure of molecular and layered crystals: Ab initio DFT calculations with van der Waals corrections,” *The Journal of Physical Chemistry A*, vol. 114, pp. 11814–11824, Nov. 2010.
- [291] T. Bučko, S. Lebègue, J. Hafner, and J. G. Ángyán, “Tkatchenko-Scheffler van der Waals correction method with and without self-consistent screening applied to solids,” *Physical Review B*, vol. 87, p. 064110, Feb. 2013.
- [292] M. Shishkin and G. Kresse, “Self-consistent GW calculations for semiconductors and insulators,” *Physical Review B*, vol. 75, p. 235102, June 2007.
- [293] F. Fuchs, J. Furthmüller, F. Bechstedt, M. Shishkin, and G. Kresse, “Quasiparticle band structure based on a generalized Kohn-Sham scheme,” *Physical Review B*, vol. 76, p. 115109, Sept. 2007.
- [294] M. Shishkin and G. Kresse, “Implementation and performance of the frequency-dependent GW method within the PAW framework,” *Physical Review B*, vol. 74, p. 035101, July 2006.
- [295] M. Shishkin, M. Marsman, and G. Kresse, “Accurate quasiparticle spectra from self-consistent GW calculations with vertex corrections,” *Physical Review Letters*, vol. 99, p. 246403, Dec. 2007.
- [296] J. Harl and G. Kresse, “Cohesive energy curves for noble gas solids calculated by adiabatic connection fluctuation-dissipation theory,” *Physical Review B*, vol. 77, p. 045136, Jan. 2008.

- [297] M. Marsman, A. Grüneis, J. Paier, and G. Kresse, “Second-order Møller-Plesset perturbation theory applied to extended systems. I. Within the projector-augmented-wave formalism using a plane wave basis set,” *The Journal of Chemical Physics*, vol. 130, no. 18, p. 184103, 2009.
- [298] A. Grüneis, M. Marsman, and G. Kresse, “Second-order Møller-Plesset perturbation theory applied to extended systems. II. Structural and energetic properties,” *The Journal of Chemical Physics*, vol. 133, no. 7, p. 074107, 2010.
- [299] D. Vanderbilt, “Soft self-consistent pseudopotentials in a generalized eigenvalue formalism,” *Physical Review B*, vol. 41, pp. 7892–7895, Apr. 1990.
- [300] G. Kresse and J. Hafner, “Norm-conserving and ultrasoft pseudopotentials for first-row and transition elements,” *Journal of Physics: Condensed Matter*, vol. 6, pp. 8245–8257, Oct. 1994.
- [301] P. E. Blöchl, “Projector augmented-wave method,” *Physical Review B*, vol. 50, no. 24, pp. 17953–17979, 1994.
- [302] G. Kresse and D. Joubert, “From ultrasoft pseudopotentials to the projector augmented-wave method,” *Physical Review B*, vol. 59, no. 3, pp. 1758–1775, 1999.
- [303] K. Momma and F. Izumi, “VESTA 3 for three-dimensional visualization of crystal, volumetric and morphology data,” *Journal of Applied Crystallography*, vol. 44, no. 6, pp. 1272–1276, 2011.
- [304] H. Childs, E. Brugger, B. Whitlock, J. Meredith, S. Ahern, D. Pugmire, K. Biagas, M. Miller, C. Harrison, G. H. Weber, H. Krishnan, T. Fogal, A. Sanderson, C. Garth, E. W. Bethel, D. Camp, O. Rübel, M. Durant, J. M. Favre, and P. Navrátil, “VisIt: An end-user tool for visualizing and analyzing very large data,” in *High Performance Visualization—Enabling Extreme-Scale Scientific Insight*, pp. 357–372, Boca Raton, FL: CRC Press, Oct. 2012.
- [305] W. Humphrey, A. Dalke, and K. Schulten, “VMD: Visual molecular dynamics,” *Journal of Molecular Graphics*, vol. 14, pp. 33–38, Feb. 1996.

BIBLIOGRAPHY

- [306] U. Landman, W. D. Luedtke, N. A. Burnham, and R. J. Colton, “Atomistic mechanisms and dynamics of adhesion, nanoindentation, and fracture,” *Science*, vol. 248, pp. 454–461, Apr. 1990.
- [307] W. C. Oliver and G. M. Pharr, “Measurement of hardness and elastic modulus by instrumented indentation: Advances in understanding and refinements to methodology,” *Journal of Materials Research*, vol. 19, pp. 3–20, Jan. 2004.
- [308] A. C. Fischer-Cripps, *Nanoindentation*. New York: Springer, 2004.
- [309] E. Gnecco, R. Bennewitz, and E. Meyer, “Abrasive wear on the atomic scale,” *Physical Review Letters*, vol. 88, p. 215501, 2002.
- [310] B. Bhushan, “Nanotribology and nanomechanics,” *Wear*, vol. 259, no. 7-12, pp. 1507–1531, 2005.
- [311] E. Gnecco, *Fundamentals of Friction and Wear on the Nanoscale*. Nanoscience and Technology, Berlin: Springer, 2007.
- [312] H. Bhaskaran, B. Gotsmann, A. Sebastian, U. Drechsler, M. A. Lantz, M. Despont, P. Jaroenapibal, R. W. Carpick, Y. Chen, and K. Sridharan, “Ultralow nanoscale wear through atom-by-atom attrition in silicon-containing diamond-like carbon,” *Nature Nanotechnology*, vol. 5, no. 3, pp. 181–185, 2010.
- [313] H. Mishina and A. Hase, “Wear equation for adhesive wear established through elementary process of wear,” *Wear*, vol. 308, pp. 186–192, Nov. 2013.
- [314] J. M. Howe, “Bonding, structure, and properties of metal/ceramic interfaces: Part 1 Chemical bonding, chemical reaction, and interfacial structure,” *International Materials Reviews*, vol. 38, pp. 233–256, Jan. 1993.
- [315] L. Johansson, “Electronic and structural properties of transition-metal carbide and nitride surfaces,” *Surface Science Reports*, vol. 21, no. 5-6, pp. 177–250, 1995.
- [316] M. Rühle, A. H. Heuer, A. G. Evans, and M. F. Ashby, “Preface,” *Acta Metallurgica et Materialia*, vol. 40, pp. vii–viii, Jan. 1992.

- [317] M. W. Finnis, “The theory of metal-ceramic interfaces,” *Journal of Physics: Condensed Matter*, vol. 8, pp. 5811–5836, Aug. 1996.
- [318] B. I. Lundqvist, A. Bogicevic, K. Carling, S. V. Dudiy, S. Gao, J. Hartford, P. Hyldgaard, N. Jacobson, D. C. Langreth, N. Lorente, S. Ovesson, B. Razaznejad, C. Ruberto, H. Rydberg, E. Schröder, S. I. Simak, G. Wahnström, and Y. Yourdshahyan, “Density-functional bridge between surfaces and interfaces,” *Surface Science*, vol. 493, pp. 253–270, Nov. 2001.
- [319] S. B. Sinnott and E. C. Dickey, “Ceramic/metal interface structures and their relationship to atomic- and meso-scale properties,” *Materials Science and Engineering: R: Reports*, vol. 43, pp. 1–59, Dec. 2003.
- [320] F. Ercolessi and J. B. Adams, “Interatomic potentials from first-principles calculations: The force-matching method,” *Europhysics Letters (EPL)*, vol. 26, pp. 583–588, June 1994.
- [321] A. Jaramillo-Botero, S. Naserifar, and W. A. Goddard, “General multiobjective force field optimization framework, with application to reactive force fields for silicon carbide,” *Journal of Chemical Theory and Computation*, vol. 10, pp. 1426–1439, Apr. 2014.
- [322] M. Avinun, N. Barel, W. D. Kaplan, M. Eizenberg, M. Naik, T. Guo, L. Y. Chen, R. Mosely, K. Littau, S. Zhou, and L. Chen, “Nucleation and growth of CVD Al on different types of TiN,” *Thin Solid Films*, vol. 320, pp. 67–72, May 1998.
- [323] J.-S. Chun, P. Desjardins, C. Lavoie, C.-S. Shin, C. Cabral, I. Petrov, and J. E. Greene, “Interfacial reactions in epitaxial Al/TiN(111) model diffusion barriers: Formation of an impervious self-limited wurtzite-structure AlN(0001) blocking layer,” *Journal of Applied Physics*, vol. 89, no. 12, pp. 7841–7845, 2001.
- [324] L. M. Liu, S. Q. Wang, and H. Q. Ye, “Adhesion of metal-carbide/nitride interfaces: Al/TiC and Al/TiN,” *Journal of Physics: Condensed Matter*, vol. 15, no. 47, pp. 8103–8114, 2003.

BIBLIOGRAPHY

- [325] L. M. Liu, S. Q. Wang, and H. Q. Ye, “First-principles study of polar Al/TiN(111) interfaces,” *Acta Materialia*, vol. 52, no. 12, pp. 3681–3688, 2004.
- [326] L. M. Liu, S. Q. Wang, and H. Q. Ye, “First-principles study of the effect of hydrogen on the metal-ceramic interface,” *Journal of Physics: Condensed Matter*, vol. 17, no. 35, pp. 5335–5348, 2005.
- [327] J. Song and D. J. Srolovitz, “Adhesion effects in material transfer in mechanical contacts,” *Acta Materialia*, vol. 54, no. 19, pp. 5305–5312, 2006.
- [328] H. Z. Zhang, L. M. Liu, and S. Q. Wang, “First-principles study of the tensile and fracture of the Al/TiN interface,” *Computational Materials Science*, vol. 38, no. 4, pp. 800–806, 2007.
- [329] H. Z. Zhang and S. Q. Wang, “The effects of Zn and Mg on the mechanical properties of the Al/TiN interface: A first-principles study,” *Journal of Physics: Condensed Matter*, vol. 19, no. 22, p. 226003, 2007.
- [330] J. Song and D. J. Srolovitz, “Mechanism for material transfer in asperity contact,” *Journal of Applied Physics*, vol. 104, no. 12, p. 124312, 2008.
- [331] S. K. Yadav, R. Ramprasad, A. Misra, and X.-Y. Liu, “First-principles study of shear behavior of Al, TiN, and coherent Al/TiN interfaces,” *Journal of Applied Physics*, vol. 111, no. 8, p. 083505, 2012.
- [332] S. K. Yadav, R. Ramprasad, J. Wang, A. Misra, and X.-Y. Liu, “First-principles study of Cu/TiN and Al/TiN interfaces: Weak versus strong interfaces,” *Modelling and Simulation in Materials Science and Engineering*, vol. 22, p. 035020, Apr. 2014.
- [333] H. J. Monkhorst and J. D. Pack, “Special points for Brillouin-zone integrations,” *Physical Review B*, vol. 13, pp. 5188–5192, June 1976.
- [334] P. E. Blöchl, O. Jepsen, and O. K. Andersen, “Improved tetrahedron method for Brillouin-zone integrations,” *Physical Review B*, vol. 49, pp. 16223–16233, June 1994.

BIBLIOGRAPHY

- [335] M. Methfessel and A. Paxton, “High-precision sampling for Brillouin-zone integration in metals,” *Physical Review B*, vol. 40, pp. 3616–3621, Aug. 1989.
- [336] M. Marlo and V. Milman, “Density-functional study of bulk and surface properties of titanium nitride using different exchange-correlation functionals,” *Physical Review B*, vol. 62, pp. 2899–2907, July 2000.
- [337] X.-G. Wang, W. Weiss, S. Shaikhutdinov, M. Ritter, M. Petersen, F. Wagner, R. Schlögl, and M. Scheffler, “The hematite (α -Fe₂O₃) (0001) surface: Evidence for domains of distinct chemistry,” *Physical Review Letters*, vol. 81, no. 5, pp. 1038–1041, 1998.
- [338] K. Reuter and M. Scheffler, “Composition, structure, and stability of RuO₂(110) as a function of oxygen pressure,” *Physical Review B*, vol. 65, no. 3, p. 035406, 2001.
- [339] C.-W. Lee, R. K. Behera, E. D. Wachsman, S. R. Phillpot, and S. B. Sinnott, “Stoichiometry of the LaFeO₃ (010) surface determined from first-principles and thermodynamic calculations,” *Physical Review B*, vol. 83, p. 115418, Mar. 2011.
- [340] M. W. Chase, *NIST-JANAF Thermochemical Tables*. College Park, MD: American Institute of Physics, 4th ed., Aug. 1998.
- [341] C. Wang, Y. Dai, H. Gao, X. Ruan, J. Wang, and B. Sun, “Surface properties of titanium nitride: A first-principles study,” *Solid State Communications*, vol. 150, pp. 1370–1374, Aug. 2010.
- [342] J. Neugebauer and M. Scheffler, “Adsorbate-substrate and adsorbate-adsorbate interactions of Na and K adlayers on Al(111),” *Physical Review B*, vol. 46, no. 24, pp. 16067–16080, 1992.
- [343] R. W. G. Wyckoff, *Crystal Structures*. Interscience, New York, 2nd ed., 1971.
- [344] T. Kundu, *Ultrasonic and Electromagnetic NDE for Structure and Material Characterization: Engineering and Biomedical Applications*. Boca Raton, FL: CRC Press, 2012.

BIBLIOGRAPHY

- [345] J. M. Howe, “Bonding, structure, and properties of metal/ceramic interfaces: Part 2 Interface fracture behaviour and property measurement,” *International Materials Reviews*, vol. 38, pp. 257–271, Jan. 1993.
- [346] F. Ernst, “Metal-oxide interfaces,” *Materials Science and Engineering: R: Reports*, vol. 14, pp. 97–156, Apr. 1995.
- [347] G. Feldbauer, M. Wolloch, P. O. Bedolla, P. Mohn, J. Redinger, and A. Vernes, “Adhesion and material transfer between contacting Al and TiN surfaces from first-principles,” *Physical Review B*, 2015. accepted.
- [348] C. Vargel, *Corrosion of aluminium*. Amsterdam: Elsevier, 2004.
- [349] D. Jennison, C. Verdozzi, P. Schultz, and M. Sears, “Ab initio structural predictions for ultrathin aluminum oxide films on metallic substrates,” *Physical Review B*, vol. 59, pp. R15605–R15608, June 1999.
- [350] Y. Li, F. Qian, J. Xiang, and C. M. Lieber, “Nanowire electronic and optoelectronic devices,” *Materials Today*, vol. 9, pp. 18–27, Oct. 2006.
- [351] P. Sony, P. Puschnig, D. Nabok, and C. Ambrosch-Draxl, “Importance of van der Waals interaction for organic molecule-metal junctions: Adsorption of thiophene on Cu(110) as a prototype,” *Physical Review Letters*, vol. 99, p. 176401, Oct. 2007.
- [352] G. Li, I. Tamblyn, V. R. Cooper, H.-J. Gao, and J. B. Neaton, “Molecular adsorption on metal surfaces with van der Waals density functionals,” *Physical Review B*, vol. 85, p. 121409, Mar. 2012.
- [353] H. Knözinger and K. Kochloeff, “Heterogeneous catalysis and solid catalysts,” in *Ullmann’s Encyclopedia of Industrial Chemistry*, Weinheim, Germany: Wiley-VCH Verlag GmbH & Co. KGaA, Jan. 2003.
- [354] J. K. Nørskov, T. Bligaard, J. Rossmeisl, and C. H. Christensen, “Towards the computational design of solid catalysts,” *Nature Chemistry*, vol. 1, pp. 37–46, Apr. 2009.

- [355] P. Błoński and N. López, “On the adsorption of formaldehyde and methanol on a water-covered Pt(111): A DFT-D study,” *The Journal of Physical Chemistry C*, vol. 116, pp. 15484–15492, June 2012.
- [356] P. Tereshchuk and J. L. F. Da Silva, “Density functional investigation of the adsorption of ethanol-water mixture on the Pt(111) surface,” *The Journal of Physical Chemistry C*, vol. 117, pp. 16942–16952, July 2013.
- [357] IEA, *Tracking Clean Energy Progress 2013*. Paris: International Energy Agency, 2013.
- [358] H. Takahashi, S. Hisaoka, and T. Nitta, “Ethanol oxidation reactions catalyzed by water molecules: $\text{CH}_3\text{CH}_2\text{OH} + n\text{H}_2\text{O} \rightarrow \text{CH}_3\text{CHO} + \text{H}_2 + n\text{H}_2\text{O}$ ($n=0,1,2$),” *Chemical Physics Letters*, vol. 363, pp. 80–86, Sept. 2002.
- [359] A. Haryanto, S. Fernando, N. Murali, and S. Adhikari, “Current status of hydrogen production techniques by steam reforming of ethanol: A review,” *Energy & Fuels*, vol. 19, pp. 2098–2106, Sept. 2005.
- [360] S. Duan and S. Senkan, “Catalytic conversion of ethanol to hydrogen using combinatorial methods,” *Industrial & Engineering Chemistry Research*, vol. 44, pp. 6381–6386, Aug. 2005.
- [361] A. Kowal, M. Li, M. Shao, K. Sasaki, M. B. Vukmirovic, J. Zhang, N. S. Marinkovic, P. Liu, A. I. Frenkel, and R. R. Adzic, “Ternary Pt/Rh/SnO₂ electrocatalysts for oxidizing ethanol to CO₂,” *Nature Materials*, vol. 8, pp. 325–330, Apr. 2009.
- [362] M. Ni, D. Y. C. Leung, and M. K. H. Leung, “A review on reforming bio-ethanol for hydrogen production,” *International Journal of Hydrogen Energy*, vol. 32, pp. 3238–3247, Oct. 2007.
- [363] S. Ilincic, A. Vernes, G. Vorlaufer, H. Hunger, N. Dörr, and F. Franek, “Numerical estimation of wear in reciprocating tribological experiments,” *Proceedings of the Institution of Mechanical Engineers, Part J: Journal of Engineering Tribology*, vol. 227, pp. 510–519, May 2013.

- [364] P. Tereshchuk and J. L. F. Da Silva, “Ethanol and water adsorption on close-packed 3d, 4d, and 5d transition-metal surfaces: A density functional theory investigation with van der Waals correction,” *The Journal of Physical Chemistry C*, vol. 116, pp. 24695–24705, Nov. 2012.
- [365] R. R. Q. Freitas, R. Rivelino, F. de Brito Mota, and C. M. C. de Castilho, “Dissociative adsorption and aggregation of water on the Fe(100) surface: A DFT study,” *The Journal of Physical Chemistry C*, vol. 116, pp. 20306–20314, Sept. 2012.
- [366] M. Eder, K. Terakura, and J. Hafner, “Initial stages of oxidation of (100) and (110) surfaces of iron caused by water,” *Physical Review B*, vol. 64, p. 115426, Aug. 2001.
- [367] S. C. Jung and M. H. Kang, “Adsorption of a water molecule on Fe(100): Density-functional calculations,” *Physical Review B*, vol. 81, p. 115460, Mar. 2010.
- [368] F. Karlický, P. Lazar, M. Dubecký, and M. Otyepka, “Random phase approximation in surface chemistry: Water splitting on iron,” *Journal of Chemical Theory and Computation*, vol. 9, pp. 3670–3676, Aug. 2013.
- [369] P. Lazar and M. Otyepka, “Dissociation of water at iron surfaces: Generalized gradient functional and range-separated hybrid functional study,” *The Journal of Physical Chemistry C*, vol. 116, pp. 25470–25477, Nov. 2012.
- [370] A. Govender, D. Curulla Ferré, and J. W. Niemantsverdriet, “The surface chemistry of water on Fe(100): A density functional theory study,” *ChemPhysChem*, vol. 13, pp. 1583–1590, Feb. 2012.
- [371] E. D. Murray, K. Lee, and D. C. Langreth, “Investigation of exchange energy density functional accuracy for interacting molecules,” *Journal of Chemical Theory and Computation*, vol. 5, pp. 2754–2762, Oct. 2009.
- [372] A. D. Becke and K. E. Edgecombe, “A simple measure of electron localization in atomic and molecular systems,” *The Journal of Chemical Physics*, vol. 92, no. 9, pp. 5397–5403, 1990.

BIBLIOGRAPHY

- [373] B. Silvi and A. Savin, “Classification of chemical bonds based on topological analysis of electron localization functions,” *Nature*, vol. 371, pp. 683–686, Oct. 1994.
- [374] E. V. Anslyn and D. A. Dougherty, *Modern Physical Organic Chemistry*. Sausalito, CA: University Science Books, 2006.
- [375] D. J. Dwyer, S. R. Kelemen, and A. Kaldor, “The water dissociation reaction on clean and oxidized iron (110),” *The Journal of Chemical Physics*, vol. 76, pp. 1832–1837, Feb. 1982.
- [376] U. Bergmann, A. Di Cicco, P. Wernet, E. Principi, P. Glatzel, and A. Nilsson, “Nearest-neighbor oxygen distances in liquid water and ice observed by X-ray raman based extended X-ray absorption fine structure,” *The Journal of Chemical Physics*, vol. 127, p. 174504, Nov. 2007.
- [377] S. Kirkpatrick, C. D. Gelatt, and M. P. Vecchi, “Optimization by simulated annealing,” *Science*, vol. 220, pp. 671–680, May 1983.
- [378] V. Černý, “Thermodynamical approach to the traveling salesman problem: An efficient simulation algorithm,” *Journal of Optimization Theory and Applications*, vol. 45, pp. 41–51, Jan. 1985.

Acknowledgements

First, I acknowledge the support from the Austrian Science Fund (FWF) within F4109 SFB ViCoM, the Austrian Research Promotion Agency (FFG) via the Austrian COMET-Program (project K2 XTribology, No. 824187 and 849109), the AC2T research GmbH and the Center for Computational Materials Science (CMS) at the Vienna University of Technology. I further appreciate the ample support of computer resources provided by the Vienna Scientific Cluster (VSC). Such financial and technological support was necessary but not sufficient for creating this thesis. This final pile of paper (or the PDF file), summarizing about three years of work, was only possible because of the help, support, friendship and love of many people, who I want to express my gratitude in the following, truly more important part of this acknowledgements. In particular, I want to thank the following people:

My supervisors, Peter Mohn, Josef Redinger and András Vernes for all their help, support, guidance, effort, ideas and many more things. To name a few, Peter for creating such a great working environment at the CMS, giving me the freedom to do my thing but also being there when needed and all the conversations we had. Sepp for his critical mind, the IT support, his sense of humour, several nice evenings at conferences involving beer and for opening the door to the next chapter of my life. András for his ideas that are the basis of my thesis and the always very detailed feedback. I also want to thank Georg Vorlaufer and Florian Mittendorfer for fruitful discussions. Furthermore, many thanks to Raimund Podloucky who kindly agreed to serve as the second referee of my thesis and on my doctoral committee, while already being “in the so-called state-of-retirement”.

Special thanks belong to Maria Steiner who was a great help with all the administrative challenges, which made my life much easier and for her kind personality.

My colleagues at the CMS: Andi, Christoph, Jacky, Michi, Pedro, Robert, Roland, Stefan and Wernfried who made my life much easier and more enjoyable. It was just a pleasure

to work and “live” with you guys (I have spent quite some time at the Makartvilla during the last three and a half years). Also all the conferences, workshops, schools and the last years in general would not have been the same without you.

All employees at AC2T who helped, worked and collaborated with or just shared fun moments with me. Although I have not spent that much time in Wiener Neustadt, I really appreciate the support. Especially, I thank the members of the SIM group, who I spent most time with when I was at AC2T.

My family and relatives, especially my parents and my brother, for always loving, supporting and believing in me. My parents gave me the opportunity of a rather carefree childhood, youth and education, which I greatly appreciate. Special thanks also to Peter and Helma for all the excellent dinners, great conversations and splendid wines. Also the family of my girlfriend for warmly welcoming me in their midst and for providing me with a second family in Vorarlberg.

All my friends, to name a few of all the names that are popping up in my mind: Philipp, Reini, Christoph, Nici, Lukas, Dominik, Anna, Mathias, Susi, Peter, Javi, Julia, Max, Ivo, Vali, Flo, ... (some names actually refer to more than one person). My life would not be the same without you. To all my friends ...

Finally and most importantly, Ramona for being the best girlfriend, for loving and supporting me. For just making the last years we have spent together the best time of my life. To our future, I love you!

Curriculum Vitae

Personal Data

Date of Birth 16.06.1985
Place of Birth Vöcklabruck, Austria
Nationality Austrian
Home address Obere Weißgerberstraße 11/1/21
1030 Wien, Austria
E-mail gregor_feldbauer@yahoo.de

Education

- 10/2011–04/2015 **Doctoral studies in Technical Sciences**, *Vienna University of Technology*, Institut of Applied Physics, Center for Computational Materials Science, 1040 Wien, Austria.
○ Thesis: “First-principles simulations of tribologically relevant nanoscopic interfaces”
○ Supervisors: Peter Mohn, Josef Redinger, András Vernes
- 10/2004–06/2011 **Diploma studies in Technical Physics**, *Vienna University of Technology*, 1040 Wien, Austria.
○ Diploma thesis: “Extraction methods for the MedAustron Synchrotron” at CERN, Geneva, CH
○ Supervisor: Michael Benedikt
- 08/2009–12/2009 **Semester abroad**, *City College of New York*, New York, USA.
- 09/1995–06/2003 **BRG Schloss Wagrain**, *Secondary school*, 4840 Vöcklabruck, Austria.

Publications

- [1] S. J. Eder, G. Feldbauer, D. Bianchi, U. Cihak-Bayr, G. Betz, and A. Vernes, "Applicability of macroscopic wear and friction laws on the atomic length scale," *Physical Review Letters*, 2015. under review.
- [2] M. Wolloch, G. Feldbauer, P. Mohn, J. Redinger, and A. Vernes, "Ab-initio calculation of the real contact area on the atomic scale," *Physical Review B*, 2015. under review.
- [3] G. Feldbauer, M. Wolloch, P. O. Bedolla, P. Mohn, J. Redinger, and A. Vernes, "Adhesion and material transfer between contacting Al and TiN surfaces from first-principles," *Physical Review B*, 2015. accepted.
- [4] M. Wolloch, G. Feldbauer, P. Mohn, J. Redinger, and A. Vernes, "Ab initio friction forces on the nanoscale: A density functional theory study of fcc Cu(111)," *Physical Review B*, vol. 90, p. 195418, Nov. 2014.
- [5] P. O. Bedolla, G. Feldbauer, M. Wolloch, C. Gruber, S. J. Eder, N. Dörr, P. Mohn, J. Redinger, and A. Vernes, "Density functional investigation of the adsorption of isooctane, ethanol, and acetic acid on a water-covered Fe(100) surface," *The Journal of Physical Chemistry C*, vol. 118, pp. 21428–21437, Sept. 2014.
- [6] P. O. Bedolla, G. Feldbauer, M. Wolloch, S. J. Eder, N. Dörr, P. Mohn, J. Redinger, and A. Vernes, "Effects of van der Waals interactions in the adsorption of isooctane and ethanol on Fe(100) surfaces," *The Journal of Physical Chemistry C*, vol. 118, pp. 17608–17615, July 2014.
- [7] G. Feldbauer, U. Dorda, and M. Benedikt, "Simulations of Various Driving Mechanisms for the 3rd Order Resonant Extraction from the MedAustron Medical Synchrotron," in *Proc. IPAC 2011*, Sept. 2011.

Conference contributions

- [1] G. Feldbauer, P. O. Bedolla, M. Wolloch, P. Mohn, J. Redinger, and A. Vernes, "Adsorption of organic molecules on a water-covered Fe(100) surface from first-principles." Talk, 79th Annual Meeting of the DPG and DPG Spring Meeting (SKM), Berlin, Germany, Mar. 2015.
- [2] G. Feldbauer, P. O. Bedolla, M. Wolloch, P. Mohn, J. Redinger, and A. Vernes, "Adsorption of organic molecules on a bcc Fe(100) surface from first principles." Talk, ECOS30 (European Conference on Surface Science), Antalya, Turkey, Sept. 2014.
- [3] G. Feldbauer, M. Wolloch, P. Mohn, J. Redinger, and A. Vernes, "Effects of oxidation on adhesion and material transfer between contacting Al and TiN surfaces from first principles." Poster, The First European Workshop on Understanding and Controlling Nano and Mesoscale Friction, Can Picafort, Spain, May 2014.
- [4] G. Feldbauer, M. Wolloch, P. Mohn, J. Redinger, and A. Vernes, "Ab-initio study of van der Waals forces in metallo-organic interfaces." Poster, ViCoM (Vienna Computational Materials Laboratory) conference "From electrons to phase transitions", Vienna, Austria, Apr. 2014.
- [5] G. Feldbauer, M. Wolloch, P. Mohn, J. Redinger, and A. Vernes, "Adhesion and material transfer between contacting Al and TiN surfaces from first principles." Talk, DPG Spring Meeting (SKM), Dresden, Germany, Apr. 2014.
- [6] M. Wolloch, G. Feldbauer, P. Mohn, J. Redinger, and A. Vernes, "Ab-initio modelling of energy dissipation in nanotribological systems. A DFT study of fcc Cu(111)." Talk, DPG Spring Meeting (SKM), Dresden, Germany, Apr. 2014.
- [7] G. Feldbauer, M. Wolloch, P. Mohn, J. Redinger, and A. Vernes, "Ab-initio simulations on adhesion and material transfer between contacting Al and TiN surfaces." Talk, APS March Meeting, Denver, USA, Mar. 2014.
- [8] G. Feldbauer, M. Wolloch, P. Mohn, J. Redinger, and A. Vernes, "Ab-initio study of van der Waals forces in metallo-organic interfaces." Poster, ViCoM (Vienna Computational Materials Laboratory) Young Researchers Meeting, Vienna, Austria, Feb. 2014.
- [9] G. Feldbauer, U. Dorda, and M. Benedikt, "Simulations of various driving mechanisms for the 3rd order resonant extraction from the MedAustron Medical Synchrotron." Poster, IPAC (International Particle Accelerator Conference) 2011, San Sebastian, Spain, Sept. 2011.